Title
Evaluation of the Near Source Air Quality Impact of Distributed Generation

Authors
Venkatram, Akula
Lee, Sang-Mi
Jing, Qiguo
et al.

Publication Date
2010

Arnold Schwarzenegger
Governor

EVALUATION OF THE NEAR SOURCE AIR QUALITY IMPACT OF DISTRIBUTED GENERATION

PIER FINAL PROJECT REPORT

Prepared For:
California Energy Commission
Public Interest Energy Research Program

Prepared By:
University of California, Riverside

Prepared By:
University of California, Riverside

Akula Venkatram
Sang-Mi Lee
Qiguo Jing
Wenjun Qian

Riverside, CA 92507
Commission Contract No. MAQ-07-03

Prepared For:
Public Interest Energy Research (PIER)
California Energy Commission

Marla Mueller
Contract Manager

Linda Spiegel
Program Area Lead
Energy-Related Environmental Research

Mike Gravely
Office Manager
Energy Systems Research

Thom Kelly, Ph.D.
Deputy Director
ENERGY RESEARCH & DEVELOPMENT DIVISION

Melissa Jones
Executive Director

PREFACE

The California Energy Commission's Public Interest Energy Research (PIER) Program supports public interest energy research and development that will help improve the quality of life in California by bringing environmentally safe, affordable, and reliable energy services and products to the marketplace.

The PIER Program conducts public interest research, development, and demonstration (RD&D) projects to benefit California.

The PIER Program strives to conduct the most promising public interest energy research by partnering with RD&D entities, including individuals, businesses, utilities, and public or private research institutions.

PIER funding efforts are focused on the following RD&D program area:

- Buildings End-Use Energy Efficiency
- Energy Innovations Small Grants
- Energy-Related Environmental Research
- Energy Systems Integration
- Environmentally Preferred Advanced Generation
- Industrial/Agricultural/Water End-Use Energy Efficiency
- Renewable Energy Technologies
- Transportation

The final report entitled *"Evaluation of the Near Source Air Quality Impact of Distributed Generation"* summarizes the results obtained in fulfilling the objectives of Contract Number MAQ-07-03 awarded to the University of California, Riverside. The information from this project contributes to PIER's Energy-Related Environmental Research Program.

For more information about the PIER Program, please visit the Energy Commission's website at http://www.energy.ca.gov/contracts/pier.html or contract the Energy Commission at 916-654-6164.

Table of Contents

List of Figures

List of Tables

Abstract

Distributed generation (DG) has been adopted in California because of its potential to supply a significant fraction of increased power demand in the future. DG offers several advantages over conventional centralized power plants. The relatively small size of a DG unit (usually less than 5 MW) allows location of the unit in the immediate vicinity of the area that requires the power. This independence from a large power supplier results in 1) reliability of power supply, 2) potential cost control because the DG unit is tied to the community that it services, 3) reduction of transmission losses, and 4) increased efficiency when waste heat is utilized for local heating and cooling needs. However, the emissions from a DG unit can impact the air quality in the populated area where it is located. This report summarizes the results from a project designed to estimate the local air quality impact of DG growth in the South Coast Air Basin.

This project takes advantage of emission inventories developed by UCI (Samuelsen et al., 2005), for several DG growth scenarios in the South Coast Air Basin (SoCAB). We first developed and applied a systematic method to allocate the 5 km by 5 km gridded emission inventory from UCI to individual DG units within each grid. Then, a state of the art dispersion model, AERMOD (Cimorelli et al., 2005) was used to examine the air quality impact of the DG units in these emission inventories. The meteorological inputs for AERMOD were constructed from observations made at 26 meteorological stations maintained by the South Coast Air Quality Management District (AQMD). Finally, we examines the air quality impact of using distributed generation (DG) to satisfy future growth in power demand in the South Coast Air Basin, relative to the impact when the same power is supplied by expanding current central generation (CG) units. In these two scenarios, the emission factors for both the DGs and the CGS are assumed to meet the California standard for new sources. The impact of decreasing boiler emissions by capturing the waste heat from DGs is not examined. The impact from some micro turbines and fuel cells, which are located on the ground but have relative low emissions, is not examined either.

The results from this study indicate that 1) Meteorology plays a major role in determining both the maximum hourly as well as annually averaged concentrations associated with DG units, 2) Because of the interaction between buoyant plume rise and meteorology, ground-level impact does not always increase with size of the DG: a 10 MW unit can have a smaller air quality impact than a 1 MW unit. These results suggest that siting of DG units has to pay attention to meteorology to reduce air quality impact.

Simulations with AERMOD suggest that DG growth in the SoCAB is likely to have its greatest impact on NO_2 and PM levels, which are already close to or exceed either NAAQS or CAAQS in several areas in the SoCAB in 2007. Areas near Central LA meteorological station will exceed the California NO_2 annual standard if any future generating capacity is located in the area.

The air quality impacts of the two alternate scenarios indicate that the shift to DGs has the potential for decreasing maximum hourly impacts of power generation in the vicinity of the power plants. The maximum impact on hourly concentrations is reduced from 24.5 ppb to 6 ppb if DGs rather than CGs are used to generate power. However, the annually averaged concentrations are likely to be higher than the scenario in which existing CGs are used to satisfy power demand growth. Future DG penetration will add an annual average of 0.1 ppb to the

current basin average of 20 ppb, while expanding existing CGs will add 0.05 ppb to the existing level.

Keywords: Distributed generation (DG), DG allocation and placing, air quality impacts, dispersion model, AERMOD, South California Air Basin

Executive Summary

Introduction

Distributed generation (DG) has the potential to meet a significant portion of increased power demand in California because of the following advantages: 1) reduction in electricity transmission losses because DG units are located in the area they service, 2) flexibility in size tailored to local power demand; 3) increase in efficiency and decrease in emissions by replacing boilers by Combined Heat and Power (CHP) systems. The main disadvantage of DG is that emissions from DG units can affect the air quality in local populated areas.

Several studies have examined the impact of distributed generation (DG) on air quality at urban and regional scales. Allison and Lents (2002) found that realistic DG scenarios were likely to lead to net increases in emissions in urban areas. However, their analysis focused on aggregated emissions and did not relate these emission changes to air quality impacts. Heath et al. (2003) found that the air quality impact of DG units, quantified in terms of intake factors - the mass of pollutant inhaled normalized by the electricity delivered, could be several times that of central generating (CG) stations. The intake factor used to estimate the relative impacts of the DG and CG stations normalizes the concentrations by the emission rates, which means that comparison of the relative impacts is effectively a comparison of the dispersive abilities of tall CG stacks with much shorter DG stacks no matter which technique DG uses. A more realistic comparison has to account for the fact that CG stations have much higher emission rates than DG stations. Thus, these conclusions do not directly address the impact of DG emissions on ambient concentrations under realistic emission scenarios. Carreras et al. (2004) have performed a detailed examination of the impact of DG emissions on ambient concentrations of both primary and secondary pollutants in the South Coast Air Basin (SoCAB) using a regional grid model. Their results show that DG penetration, amounting to as much as 20% of energy growth until 2010, results in the total increase of primary pollutants of less than 1% with respect to the baseline, and has little effect on secondary pollutants such as ozone and $PM_{2.5}$ concentrations. However, this study did not provide results on the impact of primary DG emissions on scales of less than 5 km because the comprehensive air quality model uses a 5 km by 5 km grid resolution.

This report describes results from a study to estimate the air quality impacts of DG units at distances of tens to hundreds of meters from the DG, which focuses on the impacts of DG penetration in the South Coast Air Quality Basin (SoCAB) for several scenarios developed by UCI (Samuelson et al., 2005) for the year, 2010. This study makes a direct comparison between the relative impacts of DG and CG explicitly accounting for their differences in stack characteristics and emission rates.

Methods

The evaluation of the near source air quality impact of DG penetration was carried out using a state of the art dispersion model, AERMOD (Cimorelli et al., 2005). The inputs consisted of DG emission inventories and meteorology derived from 26 meteorological stations in the SoCAB. The study was conducted in four phases. The first phase developed a set of emission inventories of primary pollutants for SoCAB from the gridded emissions constructed by UCI.

UCR developed and applied a method to distribute the emissions in each 5 km by 5 km grid to DG units with capacities dependent on land use within each grid. The emissions were distributed among DG units consisted of three sizes, 625 kW, 2.5 MW, and 12.5 MW, which represent small, medium, and large DG units.

Phase II consisted of sensitivity studies with AERMOD to understand the interaction between DG plant size and meteorological variables in determining ground-level concentrations. As part of this phase, AERMOD was validated with tracer data collected in a field study conducted in the vicinity of a DG unit driven by a 650 KW gas fired IC engine with heat recovery, in Palm Springs, CA, in 2008.

In phase III, AERMOD was applied to estimate the air quality impact of the DG units in the emission inventories of two scenarios developed by UCI. The latest available meteorological inputs obtained from AQMD were used. Both hourly as well as annually averaged concentrations of CO, NO_2, SO_2, and PM were calculated over the SoCAB at distances ranging from ten meters to several kilometers from DG units in each grid. These concentrations were then compared to existing levels at each of the grid squares to evaluate the potential for DG penetration to affect violation of NAAQS and CAAQS.

In phase IV, we compare the relative impacts of CG and DG using the measures: 1) the maximum hourly ground-level NO_x concentration, which is of regulatory significance, and 2) the annually averaged NO_x concentration as a function of distance from the source, which we will see later is an estimate of the pollution exposure of a person who travels within the specified distance. Comparison of an individual CG to a DG is conducted. The more relevant comparison is conducted, in which the projected increase in distributed power generation is replaced by central generation.

Results

This project has resulted in:

- Detailed emission inventories for several DG penetration scenarios in SoCAB corresponding to 2010.
- A modeling system to estimate near source concentrations of primary pollutants caused by emissions from DG units placed in the SoCAB. The system can be readily adapted to other domains.
- A preliminary evaluation of the performance of AERMOD in explaining tracer concentrations associated with releases from a small DG unit.
- A quantitative understanding of the interaction between DG plant characteristics and meteorology in determining ground-level concentrations.
- Estimates of hourly and annually averaged near source concentrations of primary pollutants associated with DG penetration scenarios for 2010 developed by UCI.
- Comparison of the relative impacts of distributed and centralized generation of electricity on local air quality in SoCAB.

Conclusions

The study on the interaction between DG plant characteristics and meteorology in determining ground-level concentrations results in the following major conclusions:

- The hourly averaged ground-level concentration and the grid maximum annually averaged ground-level concentrations are determined by the interaction of meteorology and the physical characteristics of the DG unit rather than only the total power output of the DG. A DG unit located in urban area emits its hot exhaust gases through relatively short stacks mounted on buildings that rarely exceed 10 m. The ground-level concentrations associated with the emissions are governed by plume rise of the buoyant exhaust, and the effects of the building wake on the emissions: these ground-level concentrations increase with wind speed because plume rise decrease and downwash effects increase with wind speed. Heat recovery from exhaust gases has the potential of magnifying these effects by decreasing plume buoyancy. Thus, ground-level concentrations do not necessarily increase with power plant capacity.
- Modeling the air quality impact of DGs requires careful considerations of a number of interacting processes such as building enhanced turbulent levels, building downwash, micrometeorology and exhaust gas characteristics, in addition to emissions.
- The maximum hourly and annually averaged concentrations from a DG unit increase with wind speeds. However, annually averaged increases of concentrations averaged over a grid cell are proportional to the total power output due to DG deployment in that grid cell.
- The maximum concentrations from the DG units considered in this study occur within hundred meters from the source.

The comparison of the relative impacts of distributed and centralized generation of electricity on local air quality yields the following major conclusions:

- Although the hourly maximum NO_x dilution from CGs is at least a factor of ten higher than that of DGs, the hourly maximum NO_x nominal concentration associated with most CGs is at least a factor of two higher than those of DGs because of the much higher emissions from CGs. The maximum impact on hourly concentrations in the basin can be reduced from 24.5 ppb to 6.0 ppb if DGs rather than CGs are used to generate power. This result is important in view of the recently promulgated 1 hour NO_2 standard.
- The grid averaged annual concentrations (long-term exposure from the DG scenario) are generally higher than those from the CG scenario over most of the basin. Over half of the basin, the annually air quality impact of the DG scenario is about a factor of two larger than that of the CG scenario. Future DG penetration into the SoCAB will add an annual average of about 0.1 ppb to the existing level of about 20 ppb in the basin while expanding existing CGs will add about 0.05 ppb to the existing level. The impact of DG penetration is likely to be smaller if their emissions are offset by the decrease in boiler emissions if waste heat from the DGs is captured.
- The area near Central LA station will exceed the California NO_2 annual standard if any generating capacity is located in the area.

The comparison of the relative impacts of distributed and centralized generation of electricity on local air quality also yields the following secondary conclusions:

- The personal exposure due to both DGs and CGs is insensitive to the effective stack height. It increases with the increase of the power and the decrease of the mean wind speed. The personal exposure due to most individual CGs is at least a factor of twenty higher than that due to DGs because of much higher emissions from CGs.

- Waste heat recovery is likely to increase the maximum ground-level concentrations in the vicinity of a DG especially when the average winds are low. This conclusion is relevant to locating DGs in urban areas where wind speeds are typically low because of sheltering by buildings.

The EHP and PW2010 scenario studies yield the following hourly and annual concentrations of four primary criteria pollutants.

- After DGs are deployed, the maximum hourly averaged increase of CO is 117 ppb for both EHP and PW2010 scenarios occurring near Riverside. Those of NO_x, SO_2 and PM are 19 ppb, 0.5 ppb, and 8 $\mu g/m^3$ respectively for both scenarios occurring near Fontana.
- After DGs are deployed, the highest grid maximum annually averaged increases of CO, NO_x, SO_2 and PM are 13 ppb, 1.9 ppb, 47 ppt, and 0.7 $\mu g/m^3$ respectively for EHP scenario occurring close to Banning, and are 11 ppb, 1.6 ppb, 38 ppt and 0.6 $\mu g/m^3$ respectively for PW2010 scenario occurring close to Banning.
- After DGs are deployed, the maximum grid-averaged annually averaged increases of CO, NO_x, SO_2 and PM for both scenarios occur near Lynnwood where the highest increase of power is met by DG, and they are 6.1 ppb, 1.3 ppb, 34 ppt, and 0.5 $\mu g/m^3$ respectively for EHP scenario and 1.4 ppb, 0.3 ppb, 8 ppt and 0.1 $\mu g/m^3$ respectively for PW2010 scenario.
- The annual exposure level can be represented by grid averaged annual averages of pollutants. The highest resulting grid-averaged annual averages of NO_2 are 32.7 ppb for EHP and 32.0 ppb for PW2010 occurring near Pomona, where the 2007 level was 31.8 ppb. Areas near Central LA are above California annual NO_2 standard after DG being deployed, which were under the standard in 2007. The impacts of DG on PM_{10} are negligible because the grid maximum increases are much smaller than 2007 levels.

Recommendations

- The near field impact of a DG unit is governed by the interaction of plume rise with the flow fields induced by the building housing the generator as well by buildings in the vicinity of the DG. A recent paper by Olesen *et al*. (2009) indicates that current regulatory models perform poorly in estimating building effects. As far as we know, none of the models deal with the effects of multiple buildings on plume rise and dispersion. We recommend that adequate models be developed for such situations because of the regulatory concern with risks posed by emissions of toxics in urban areas.
- We recommend that future modeling improvements address concentrations at scales ranging from scales of few meters to hundreds of kilometers by combining large scale grid models with short range dispersion models, such as AERMOD. Although progress has been made in this area (Stein *et al*. 2007; Isakov *et al*. 2007), there are still unresolved issues related to combining concentrations and the associated chemistry at vastly different scales.
- The near source air quality impact of DG estimated in this study does not account for the replacing of boilers by CHP. We recommend that future work consider the impact of this replacement.

Benefits to California

This research provides estimates of the near field impact on primary emissions associated with DG penetration in the South Coast Air Basin in 2010. The study has also identified the principal factors that govern the ground-level concentrations associated with primary emissions from DG units of various sizes. This information can be used to develop to optimum strategies for DG placement.

1.0 Introduction

Several studies have examined the impact of distributed generation (DG) on air quality at urban and regional scales. Allison and Lents (2002) examined the tradeoff between the increase in emissions associated with urban DG emissions and the decrease in emissions by replacing heating plants with waste heat generated from DG plants. They found that realistic DG scenarios were likely to lead to net increases in emissions in urban areas. Their relatively simple analysis focused on aggregated emissions and did not relate these emission changes to air quality.

Heath et al. (2003) examined the air quality impact of DG units relative to central generating stations. They found that the air quality impact of DG units, quantified in terms of intake factors, could be several times that of central generating (CG) stations because a) the ground-level concentrations from the elevated emissions of a CG plant are much smaller than those associated with the near surface emissions from DG units, such as microturbines, and b) CG plants are likely to be located far from urban centers, while DG units are located in urban areas close to energy consumers. These conclusions are based on a simple Gaussian model applied to idealized emission scenarios that do not account for existing emissions. Thus, the results from Heath et al. (2003) do not directly address the impact of DG emissions on ambient concentrations under realistic emission scenarios.

Carreras et al. (2004) have performed a detailed examination of the impact of DG emissions on ambient concentrations of both primary and secondary pollutants in the South Coast Air Basin (SoCAB). A major part of their effort was the construction of detailed emission inventories for the year 2010. These inventories accounted for growth in energy demand as well as likely DG penetration scenarios. The DG emissions were spatially allocated in the South Coast Air Basin in California using demographic and land-use information. The regional air quality impacts of DG were examined by running a comprehensive photochemical model using these emission scenarios as inputs. Because DG emissions contribute less than 3% to the total projected NO_x emissions in the South Coast Air Basin in California, and less to the VOC emissions, ambient concentrations of ozone, NO_2, and PM are changed by relatively small amounts. The maximum concentrations show almost no change, while the largest changes of about 5% occur during nighttime conditions. These results show that DG penetration, amounting to as much as 20% of energy growth until 2010, has little effect on secondary pollutants such as ozone and $PM_{2.5}$ concentrations. However, this study did not provide results on the impact of primary DG emissions on scales of less than 5 km because the comprehensive air quality model uses a 5 km by 5 km grid resolution. Thus, emissions are instantaneously mixed through a box that is 5 km by 5 km by 10 m. While this approximation might be valid for estimating secondary pollutants, it cannot provide realistic concentration estimates of primary pollutants at neighborhood scales of meters to kilometers.

This report describes the results of a project to estimate the short-range air quality impact of distributed generation of electricity at distances of tens of meters from the source. The impact has been estimated using a state-of-the-art dispersion model, AERMOD (Cimorelli et al., 2005), which incorporates the latest developments in micrometeorology and dispersion. The model has been evaluated with results of tracer study conducted in Palm Springs, CA, in the vicinity of a 650 kW power plant. The evaluation has been used to estimate the uncertainty associated with the modeling results presented in this report.

The goal of this work is to develop methods to estimate the air quality impact of distributed generation of electricity. We estimated both hourly and annually averaged concentrations by running AERMOD for 2007. The procedures for creating AERMOD-ready emissions inputs from University of California at Irvine (UCI) emissions inventory are described in section two. The simplified dispersion model is presented in section two, providing the basic knowledge of several key factors governing the impact of emissions from DG on local air quality. The AERMOD simulations and results for distributed generation (DG) are described in section four, including the evaluation of the model, sensitivity studies and the hourly and annually averaged concentrations of primary criteria pollutants.

2.0 Emissions

2.1. Introduction

The objective of this task is to develop a set of emission inventories for SO_2, NO_x, particulate matter (PM), and CO for the South Coast Air Basin in California that reflects possible scenarios of distributed generation (DG) penetration by the year 2010. The required spatial resolution is 50 m so as to allow the application of short range dispersion models, such as AERMOD, to assess the near field impact of DG emissions. The starting point for this task is an emission inventory developed by UC Irvine under the sponsorship of the CEC (Samuelsen et al., 2005). The emission inventory developed by UCI uses a 5 km by 5 km grid, which is compatible with the photochemical model used in UCI's analysis. In this task, we developed and applied a method to convert the 5 km by 5 km grid inventory to a 50 m by 50 m grid. We provide a brief description of the UCI inventory in Section 2. Section 3 describes the Geographical Information System (GIS) based method to derive the high resolution inventory. Section 4 describes the program developed to locate DG units. Lastly, section 5 discusses the application of this program.

2.2. UCI's DG emission inventory

DG emission scenarios for the year 2010 were developed by Samuelsen et al. (2005) in order to investigate the air quality impacts of DG in the South Coast Air Basin in California. Their inventory covers an area that extends 250 km in the east-west direction and 115 km in the north-south direction. The inventory includes most of the criteria pollutants and other species required by the Caltech Atmospheric Chemical Mechanism (CACM) (photochemical mechanism: NO, NO_2, SO_2, SO_3, 23 specific volatile organic compounds, and 18 types of particulate matter (Carreras et al., 2004)). The inventory also incorporates various DG implementation scenarios including a realistic scenario and spanning scenarios.

The realistic scenario is based on a set of DG technologies that are likely to be dominant in certain market segments because their capacity and operating properties are best suited to the energy demands of that segment. The spanning scenario, developed for the determination of potential impacts of unexpected outcomes, is suitable for the investigation of a high DG penetration case. We applied the method to derive the high resolution inventory to a spanning scenario. The spatial distributions of CO, NO and SO_2 emissions of the UCI inventory are shown in Figure 1-1. Most of the emissions are located in highly populated areas near the coast. The spatial distributions of the different species are similar to each other. Table 1-1 lists the grid cells with the ten largest DG capacities together with the emissions of chemical species that are likely to have their highest concentrations close to their emission points. Because a typical DG has a capacity of less than 1 MW (Heath et al., 2003), the DG capacities presented in the table consist of multiple DGs within the 5 km by 5 km area of each grid cell. The next section describes how DG capacities and emissions of a large grid were assigned to a small high-resolution grid.

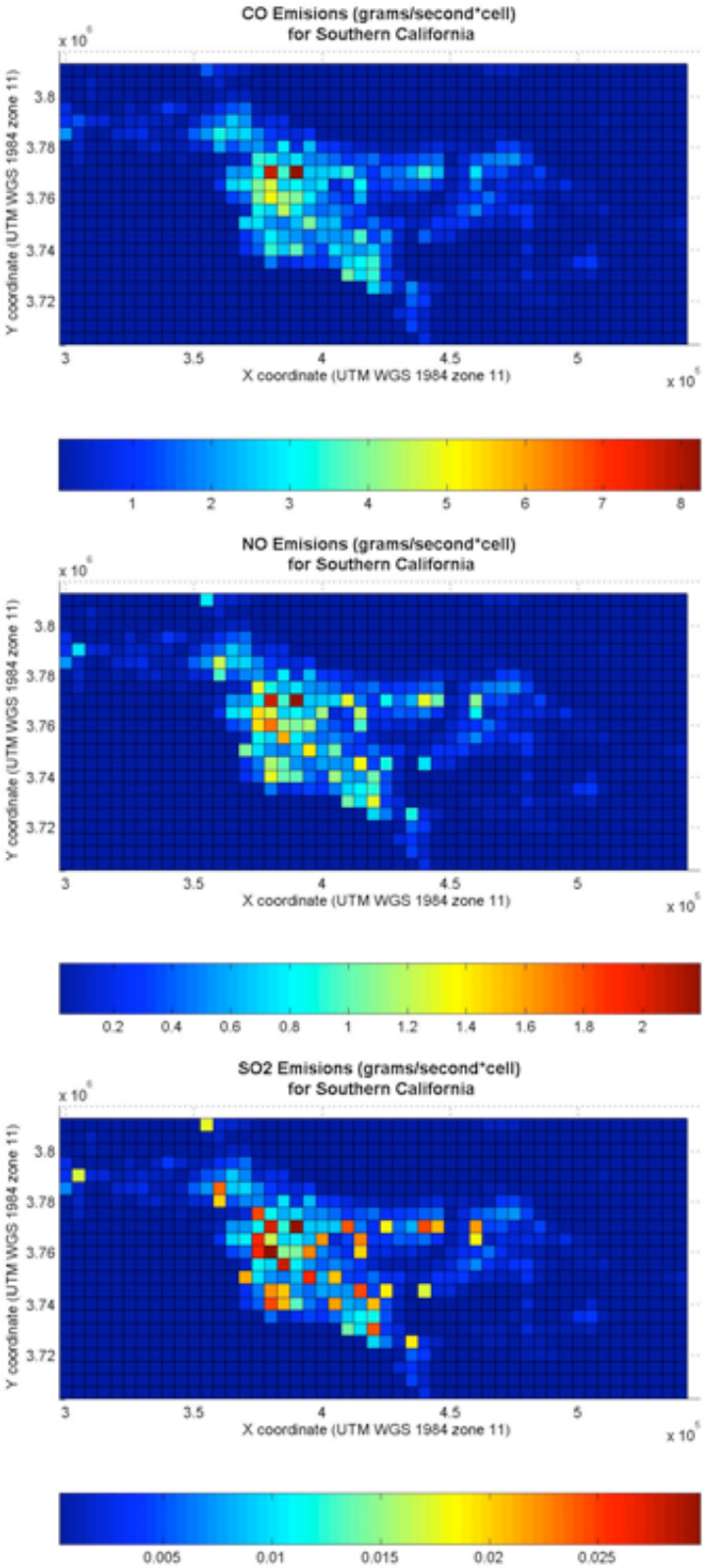
CO Emisions (grams/second*cell)
for Southern California
x 10^6
Y coordinate (UTM WGS 1984 zone 11)
3.8
3.78
3.76
3.74
3.72
3
3.5
4
4.5
5
X coordinate (UTM WGS 1984 zone 11)
x 10^5
1
2
3
4
5
6
7
8
NO Emisions (grams/second*cell)
for Southern California
x 10^6
Y coordinate (UTM WGS 1984 zone 11)
3.8
3.78
3.76
3.74
3.72
3
3.5
4
4.5
5
X coordinate (UTM WGS 1984 zone 11)
x 10^5
0.2
0.4
0.6
0.8
1
1.2
1.4
1.6
1.8
2
SO2 Emisions (grams/second*cell)
for Southern California
x 10^6
Y coordinate (UTM WGS 1984 zone 11)
3.8
3.78
3.76
3.74
3.72
3
3.5
4
4.5
5
X coordinate (UTM WGS 1984 zone 11)
x 10^5
0.005
0.01
0.015
0.02
0.025

Figure 2-1. DG emissions of (a) CO, (b) NO and (c) SO_2 projected for year 2010 in the The South Coast Air Basin in California. The horizontal size of a grid square is 5 km X 5 km.

Table 2-1. The Highest Ten DG Emission Rates and Their Locations.

Rank	UTM Easting (m)	UTM Northing (m)	DG Capacity (MW)	CO Emissions g/s	NO Emissions g/s	SO_2 Emissions g/s
1	382500	3762500	87.45	5.02	1.60	0.05
2	392500	3772500	84.27	8.27	2.07	0.07
3	387500	3757500	81.39	4.43	1.45	0.05
4	382500	3772500	78.21	7.68	1.92	0.07
5	377500	3767500	76.59	3.95	1.33	0.05
6	377500	3762500	76.48	3.94	1.33	0.05
7	397500	3752500	75.96	3.89	1.32	0.05
8	417500	3747500	72.40	3.54	1.23	0.04
9	442500	3772500	71.88	3.49	1.22	0.04
10	377500	3777500	71.69	3.47	1.21	0.04

2.3. Fine scale allocation of DG emission inventory

In order to maintain a consistency with the UCI inventory, we re-grouped 36 EPA land use into 6 categories that UCI used. The Land Use and Land Cover (LULC) data describe the vegetation, water, natural surface, and cultural features on the land surface. The United States Geological Survey (USGS 1990) provides these data sets and associated maps as a part of its National Mapping Program. There are two sources of LULC coverages available through the Internet. The USGS provides these coverages, in a Geographic Information Retrieval Analysis System (GIRAS) format. These coverages are projected in a "modified" Universal Transverse Mercator (UTM) system. The second source is through the EPA. These coverages are the same as the USGS, but they are projected in an Albers projection. We acquired land use data from EPA.

The LULC data consist of historical land use and land cover classification data that was primarily based on the manual interpretation of 1970's and 1980's aerial photography. Secondary sources included land use maps and surveys. The spatial resolution of the data is 30 m. Land use was mapped and coded using the Anderson classification system (Anderson et al., 1976) which is a hierarchical system of general (level 1) to a more specific (level 2) characterization. The Anderson land-use codes are given in Table 2-2.

Table 2-2. The Anderson Land-Use codes used in EPA database and their re-classification into UCI codes.

Level 1 Code	Level 2 Code	Description	UCI Code
1		**Urban or built-up land**	
	11	Residential	1
	12	Commercial and services	3
	13	Industrial	4

	14	Transportation, communication, utilities	6
	15	Industrial and commercial complexes	4
	16	Mixed urban or built-up land	2
	17	Other urban or built-up land	2
2		**Agricultural land**	
	21	Cropland and pasture	5
	22	Orchards, groves, vineyards, nurseries, and ornamental horticultural	5
	23	Confined feeding operations	5
	24	Other agricultural land	5
3		**Rangeland**	
	31	Herbaceous rangeland	0
	32	Shrub and brush rangeland	0
	33	Mixed rangeland	0
4		**Forest land**	
	41	Deciduous forest land	0
	42	Evergreen forest land	0
	43	Mixed forest land	0
5		**Water**	
	51	Streams and canals	0
	52	Lakes	0
	53	Reservoirs	0
	54	Bays and estuaries	0
6		**Wetland**	
	61	Forested wetland	0
	62	Nonforested wetland	0
7		**Barren land**	
	71	Dry salt flats	0
	72	Beaches	0
	73	Sandy areas not beaches	0
	74	Bare exposed rock	0
	75	Strip mines, quarries, gravel pits	0
	76	Transitional areas	0
8		**Tundra**	
	81	Shrub and brush tundra	0
	82	Herbaceous tundra	0
	83	Bare ground	0
	84	Wet tundra	0
	85	Mixed tundra	0
9		**Perennial snow or ice**	
	91	Perennial snowfields	0
	92	Glaciers	0

The EPA LULC re-grouped into 6 categories that were used in the UCI inventory (Table 2-3). Category 0 was assumed to adopt zero DG power (Samuelsen et al., 2005).

Table 2-3. Land-Use categories used in UCI emission inventory (Samuelsen et al., 2005)

UCI Code	Description
1	low density residential
2	medium and high density residential
3	Commercial
4	Industrial
5	Agricultural
6	Others
0	The rest

The second step was to determine land-use dependent split factors, which were adopted from the procedures used in the UCI inventory. Adoption Rate Relative Intensity factors accounts for the fact that a certain amount of land that is occupied by a certain economic sector will adopt DG technology at a rate that differs from that of other sectors. Though Samuelson et al. (2005) treated the factor as a function of both land-use sector and DG plant size category; we did not distinguish DG plant size, but only the land use category. The relative intensity adoption rate of each land-use sector is summarized in Table 2-4.

Table 2-4. Adoption rate relative intensity factors per land-use category (Samuelson et al., 2005)

UCI Code	Description	Adoption Rate Relative Intensity Factors
1	low density residential	0.4
2	medium and high density residential	9.2
3	Commercial	21.5
4	Industrial	60.4
5	Agricultural	0.8
6	Others	7.6
0	The rest	0

The factors are interpreted as follows: if the DG power penetration within a 5 km by 5 km grid square is 100 MW, 21.5 MW are used by the commercial sector and 60.4 MW are used by the industrial sector.

Detailed specifications of an exhaust stack are necessary input information for dispersion modeling. They are the location, physical height, the inner diameter of an exhaust stack, the temperature and the vertical velocity of exhaust plume at stack tip. We, first, determined the size of a DG unit that would be most likely adopted in each land-use sector. Then, based on the size of a plant, detailed stack specifications were assigned. Since no literature clearly defines the representative size of a DG unit, we assigned it in each sector based on our best knowledge and intuitions. Though the size of a representative DG unit is in proximity of the dominant size of each land-use sector defined in the UCI analysis, we adjusted it in a way to avoid unreasonably

excessive number of DG units located in a small area. Note that UCI inventory (Samuelson et al., 2005) has 5 size categories per each land-use sector and the dominant size of a DG unit of each sector was used as the first guess value in our analysis. See Table 2-5 for the representative capacity of a DG unit in each sector determined in the present work.

Table 2-5. The representative size of a DG unit in each land-use sector

Land-Use Code	Description	DG capacity (KW)
1	Low Density Residential	250
2	Medium & High Density Residential	500
3	Commercial	2,500
4	Industrial	12,500
5	Agricultural	625
6	Others	12,500

The stack specifications were collected from vendors listed in "California Distributed Energy Resources Guide" (CEC, 2006). As shown in Figure 2-2, the temperature at the tip of an exhaust stack appears to be constant regardless to a plant capacity. Therefore, we applied 500 ^{o}C of exhaust temperature unanimously to all DG units. On the contrary, exhaust mass flow rate shows a clear correlation with the size of a power plant, which is

$$Mass\ Rate = 3.37 \cdot Capacity + 3.15 \qquad (2.1)$$

The units for the Mass Rate and the Capacity are kg/s and MW, respectively. The correlation coefficient of the linear regression is 0.99. Mass flow rate was converted to exit velocity from given exhaust temperature and exhaust stack diameter by means of the ideal gas law. The diameter and the physical stack height of an exhaust stack were also assigned based on our best knowledge and intuitions (Table 2-6).

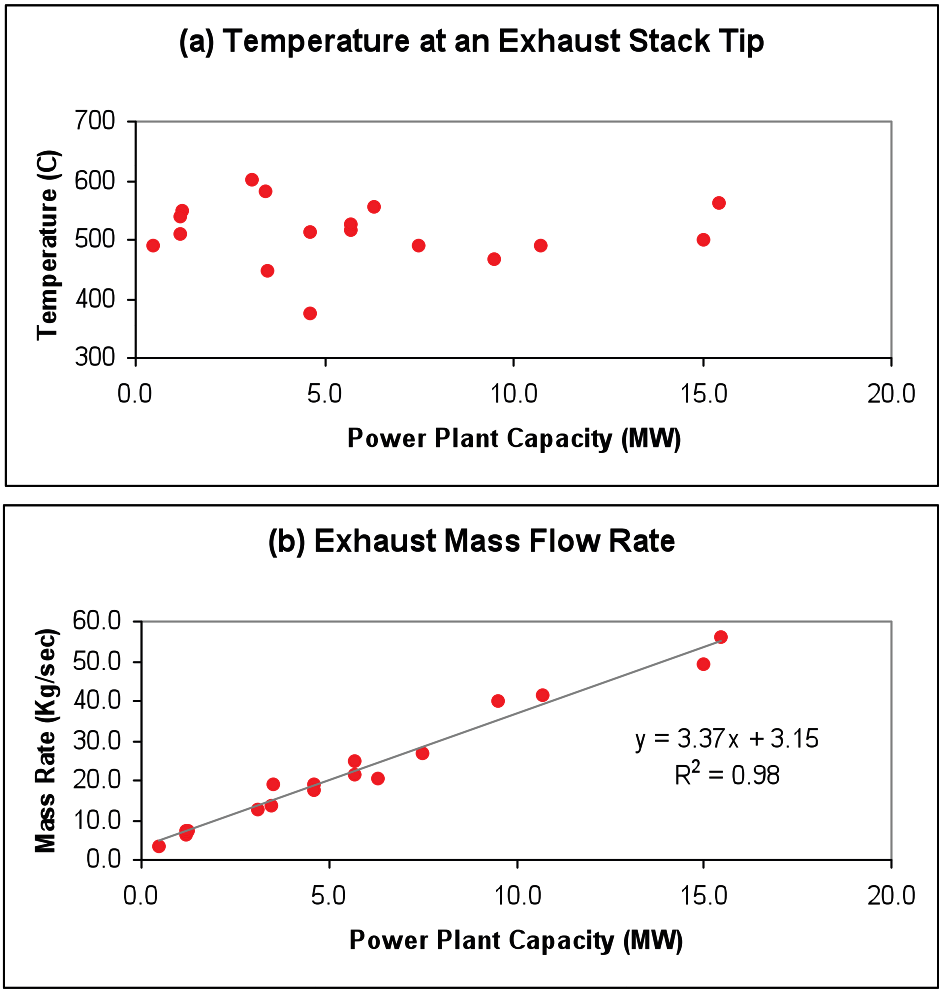

Figure 2-2. (a) Stack exhaust temperature vs. a power plant capacity, and (b) mass flow rate from an exhaust stack vs. a plant capacity. The data given in the figures were surveyed from vendors listed in "California Distributed Energy Resources Guide" (CEC, 2006).

Table 2-6. Stack specifications of DG units selected in the present analysis

DG capacity (KW)	Exit Temperature (° C)	Mass Rate (kg/s)	Exit Velocity (m/s)	Stack Tip Diameter (m)	Physical Stack Height (m)
12500	500	45.23	18.65	2.60	11.3
5000	500	19.98	13.92	2.00	10.5
1000	500	6.52	8.07	1.5	9.5
250	500	3.99	9.20	1.1	8.3

2.4. DG location program

MatLab and C were used to create a DG location program. MatLab was used to run the main looping function while C was used for tasks that required heavy computational resources. The current method of DG location finds the total number of stacks using EPA land use data and EHP and PW2010 scenarios for each UCI category, finds the number of units for each cell, finds

the unit insides the cell, and then finally outputs the results into an AERMOD ready file. The details of these two scenarios will be presented in section 4, here we just report how we calculate the DG units and how we locate them into grids. A flow diagram of the program is presented in Figure 2-3. The residential areas (LU 1 and 2) were expected to have advanced technologies to reduce emissions. Therefore, we assumed that emissions from residential sectors were negligible compared to those from other land use sectors.

The EHP/PW2010 and EPA land use data were originally examined on a 5 km by 5 km grid basis, but due to discrepancies in the data, the method led to high DG count in residential areas. A modified method accounts for discrepancies in the data by forcing the residual DG of each LU category to be almost 0.

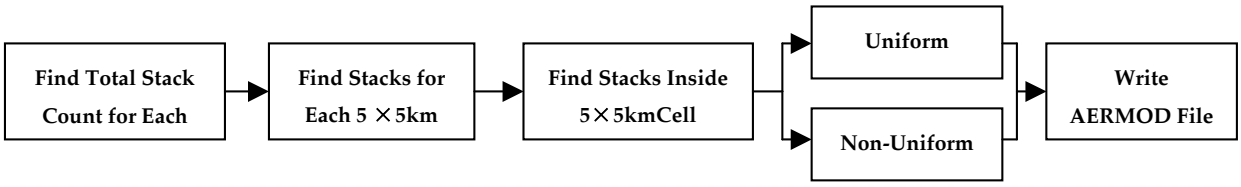

Figure 2-3. Flow Diagram for the DG siting algorithm

2.4.1. Finding total unit count for each LU category

The number of DG units for each LU category on the whole domain was computed based on EPA land use data, EHP/PW2010 DG requirement, and EHP/PW2010 adoption rate. The EPA land use data was converted to the UCI land use data. The percent area of each land use category was recorded. The EHP/PW2010 DG requirement of the whole domain was found by totaling the DG requirement of each cell in 5x5km cell. The total DG unit requirements over the whole Southern California domain are 5781 MW and 1101 MW for EHP and PW2010 scenarios respectively. The unit count can be found by:

$$\#\text{unit}_i = \frac{\text{DG}_{\text{EHP/PW2010}} * R_i * A_i}{\text{unitSize}_i * \sum_{j=1}^{6} R_j * A_j} \qquad (2.2)$$

where $\text{DG}_{\text{EHP/PW2010}}$ is the total DG need found from EHP/PW2010 data, R_i is the adoption rate of land use category *i*, unitSize_i is the unit size for land use *i*, A_i is the area of land use category *i* over the whole domain, and *A* is the area of all non-zero category land use. The final unit count for each land use category is resented in table 2-7.

Table 2-7. Parameters used to compute the number of stacks in each LU category and the final number of stacks.

UCI Land Use	DG Power Type	DG Size (MW)	Area (A_i) (%)	Adoption Rate (R_i)	$A_i.R_i$	$A_i.R_i$ (%)	Expected DG Capacity per LU sector (MW)		Expected Number of DG units per LU sector	
							EHP	PW2010	EHP	PW2010
1	Fuel Cell	0.25	41.21	0.40	16.48	2.37	137.14	26.12	549	104
2	Fuel Cell	0.50	5.06	9.20	46.55	6.70	387.36	73.77	775	148
3	AGT	2.50	11.23	21.50	241.49	34.76	2009.33	382.68	804	153
4	CGT	12.50	5.60	60.40	338.52	48.72	2816.69	536.44	225	43
5	AGT	0.63	33.63	0.80	26.90	3.87	223.86	42.63	358	68
6	CGT	12.50	3.27	7.60	24.83	3.57	206.62	39.35	17	3

The benefit of finding the number of DG units over the whole South Coast Air Basin in California domain is that this method forces the residual DG capacity for each LU type to be almost 0. In previous attempts at DG location the residual DG power for the different LU types was no regulated.

2.4.2. Unit count for each LU category for each 5x5km grid

Once the number of units of the modeling whole domain is known, the next step is to locate the units into each land use category within a 5x5km grid. The average size of an area that a unit represents for is determined by the size of each LU category and number of units of the LU category. I.e., the area per stack was computed by:

$$As_i = A_i / \#units_i \tag{2.3}$$

where As_i is the average area for a stack of a LU category *i*. Another variable we introduced is '*unitneed*', which is defined as below.

$$unitneed = (Agrid_i / As_i) - unitsplaced \tag{2.4}$$

where $Agrid_i$ represents the area of LU category *i* in a grid. The '*unitneed*' has a first guess value of 0. If the '*unitneed*' of a grid is greater than one, this signifies the grid that requires more than one DG unit. After a unit is assigned within a grid of which '*unitneed*' is equal to or greater than 1, the '*unitneed*' is re-calculated. Units are assigned in the grids with the largest unit need until the correct number of units is assigned.

2.4.3. Placing DG units inside grid

There are two techniques used to place DGs inside a 5x5km grid based on EPA LU data: non-uniform placing based on land use shape, and uniform honeycomb shaped distribution. A non-uniform distribution was used for a grid with small number of DG units. The non-uniform distribution uses the shape of the land use in the cell in order to place the units. The uniform

distribution uses honeycomb patterns to place units. The uniform distribution can place up to around 100 to 150 units in a 5x5km grid.

Non-Uniform DG placing

For cells with the number of DG units less than 5 per land use category, we used a non-uniform distribution based on the shape of the land use category of a grid. The DG unites are arranged in a way to minimize the distance squared of the units to the land use that they are supplying. The non-uniform calculations are the most stressful on computation time, so the program was written in C language in order to reduce the time computation time of the program. The program analyzes the grid by the different LU categories. In order to integrate the C program into the MatLab interface, the MatLab program outputs the EPA land use data into 6 text files (one text file for each land use category) which can be read by the C program. Using the MatLab DOS function, the C program can have arguments passed, such as the location of the text file and the stack count. The output of the C program is received as a string. The string file contains the resulting DG location of the found by the C program.

Once the land use data and unit count are passed to the C program, the program goal of the program is to find the most efficient unit location using the least computation time. For the most accurate results a brute technique can be used, but a brute technique also requires the longest computational time. The technique chosen is where the position of the DG unit is arbitrarily placed in the grid and then "shook" until placed to the most efficient position is found. The first step is where the correct number of units is placed inside the grid. To reduce the computation time, the points are placed near desired DG location. The distance squared of each land use point to the closest unit is calculated and summed. This is considered to be the score of this specific unit arrangement. The units are then "shook". Each unit is moved up, down, left, and right a large distance. The sum of the distance square is again calculated for everyone combination and the combination with the lowest score are considered the best. Figure 2-4 shows an example of grid which has 2 units to be placed. The red area is the desired area of the units and the blue area is everything else.

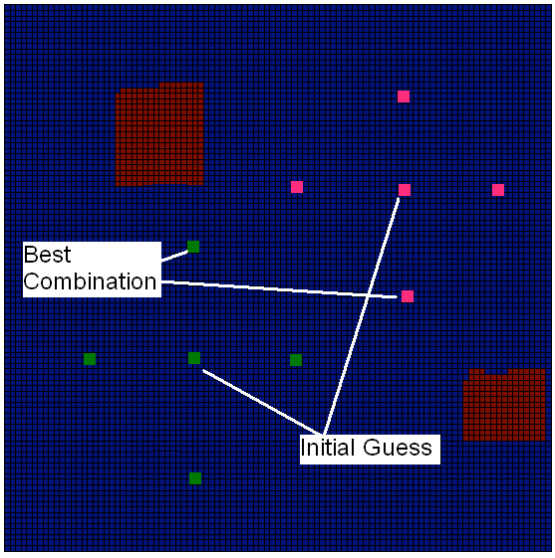

Figure 2-4. 1st Iteration of Non-Uniform DG placement

The number of unit combinations is approximately the power n^{th} order. This is extremely computational expensive.

$$Stack\ Combinations\ \alpha\ 5\hat{}\ Stack\ Count \quad (2.5)$$

The process is repeated with the new unit arrangement as the initial guess. The new configuration is shook again. The distance is minimized for the best combination of unit locations. Figure 2-5 shows the 2nd iteration of shaking.

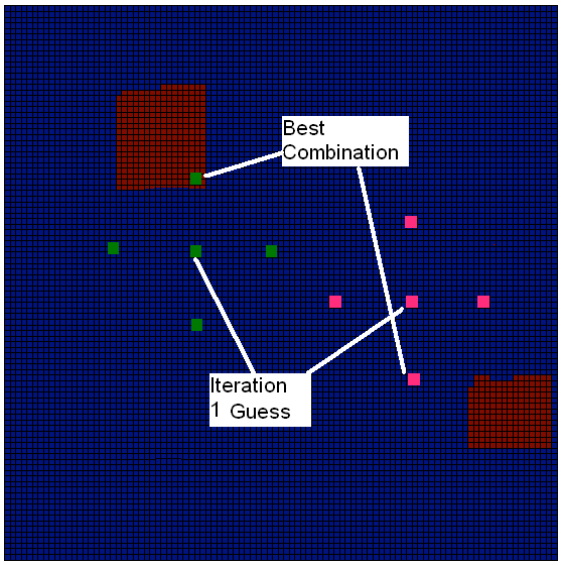

Figure 2-5. 2nd Iteration of Non-Uniform DG placement

This process is repeated until the distance the unit is moved is less than the 50m, which is the resolution of LU data. This technique of placing DGs can be thought of as a board with hills and valleys. The valleys are the points of low energy states. The point is arbitrarily placed on the terrain and shook. The final result should be the lowest energy state. The computation time of this technique is proportional the power of the number of units. The computation time of placing 5 units is roughly 10 seconds, while placing 6 units is around 1 minute. Placing 7 units in a cell takes roughly 30 minutes.

Uniform DG placing

For cells with DG counts larger than 5 per a UCI land use category, the computational time for non-uniform DG placing is too large. Therefore, a uniform, honeycomb, pattern is used. Like the non-uniform each grid is examined one land use category at a time. The process starts by creating a uniform hexagonal pattern across the cell. The uniform pattern can be rotated using polar coordinates or shift in Cartesian coordinates. The uniform hexagon pattern can be seen in Figure 2-6.

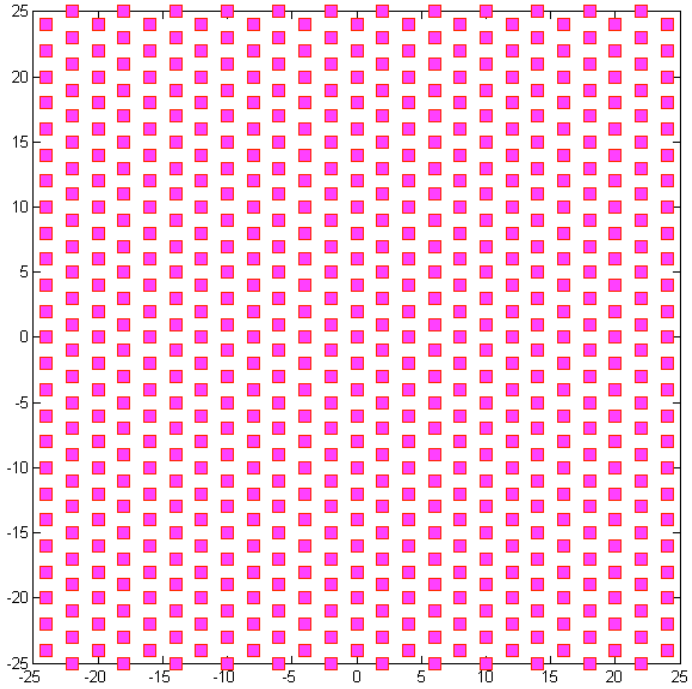

Figure 2-6. Hexagon grid used in the uniform locating method

The uniform hexagonal grid is superimposed onto the 5 km by 5 km cell. The 5 km by 5 km cell is converted to areas that DG can be placed (red) and areas the DG can not be placed (blue) as seen in Figure 2-7.

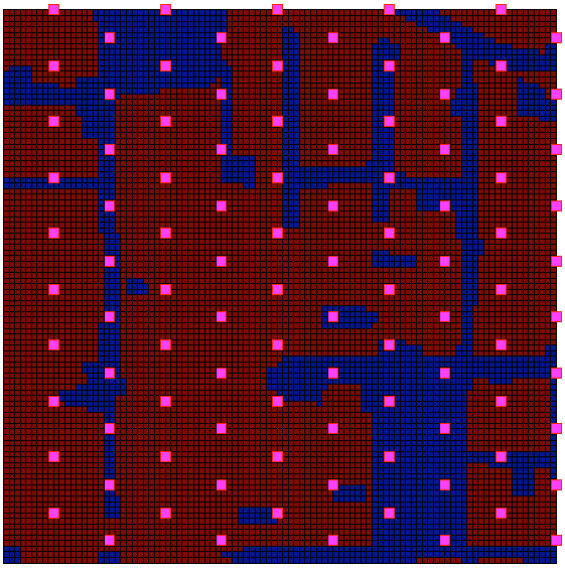

Figure 2-7. Uniform grid over-lapped onto land-use. The red represents the area that DG units are supplying to, and the blue represents the rest.

All points that do not lie within the desired region are removed. Points close to the undesired region of the edge are also removed. If the distance of the point is half the distance between the hexagon the point is removed. The number of grid points remaining is then compared to the desired DG count. If the number of grid points is more than the desired DG count, the grid spacing is increased. If the number of grid points is less than the desired DG count, the grid spacing is reduced. The grid spacing is also rotated if a solution is not possible. The hexagonal pattern with the largest grid spacing is selected to be the final answer.

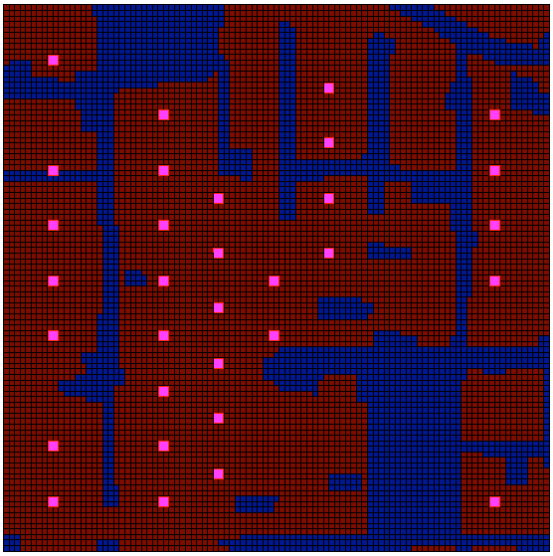

Figure 2-8. Final output of the Uniform distributing method.

This technique can be repeated for the different LU categories in a single cell as seen in Figure 2-9.

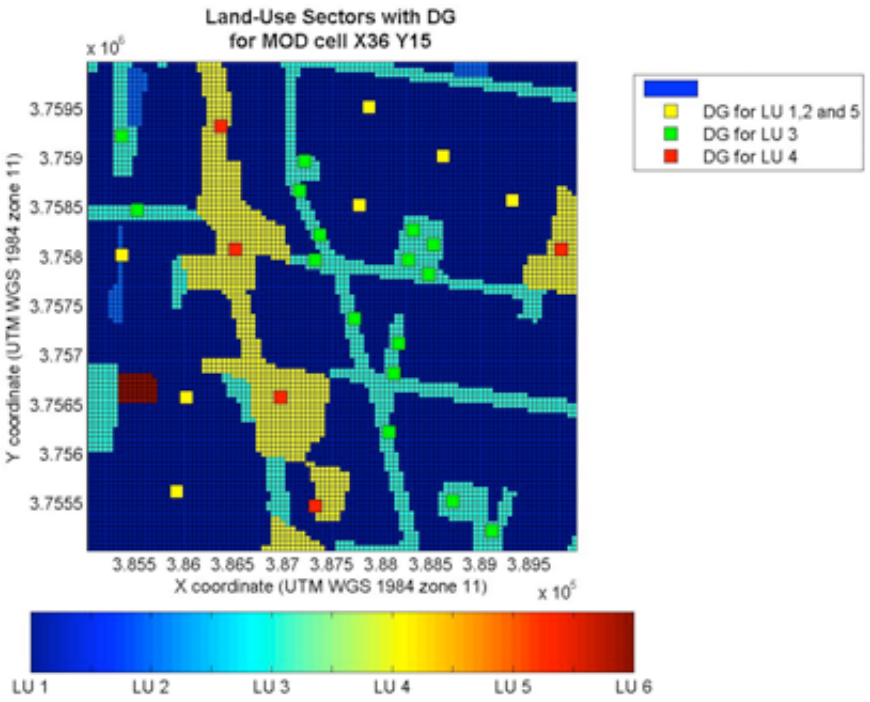

Figure 2-9. Uniform Distribution for All LU.

2.4.4. Output to AERMOD compatible file

Once the location of all the DG units is known in a cell, the stack information is output into an AERMOD ready file. AERMOD allows for lists of stack information to be imported through text files. The following is the syntax of an AERMOD ready file:

AERMOD Export:

Srcid Srctyp Xs Ys Zs Ptemis Stkhgt Stktmp Stkvel Stkdia

Srcid: This is the Source ID (up to 8 characters)

Srctyp: This is the source type which is identified by the POINT keyword.

Xs: This is the X coordinate of the source location in meters

Ys: This is the Y coordinate of the source location in meters

Zs: This is the source elevation location in meters or feet. This parameter is optional and can be omitted. If this parameter is omitted, then you need to uncheck the Base Elevation (Zs) box in the Sources Import dialog box.

Ptemis: This is the point emission rate in g/s.

Stkhgt: This is the release height above ground in meters.

Stktmp: This is the stack gas exit temperature in degrees K.

Stkvel: This is the stack gas exit velocity in m/s.

Stkdia: This is the stack inside diameter in meters.

An example of an AERMOD ready file with 7 stacks is given below.

```
LU3_001 POINT 379725 3766125 0 3.635178e-001 6.5 733 9.95 1.80
LU3_002 POINT 379325 3765875 0 3.635178e-001 6.5 733 9.95 1.80
LU3_003 POINT 377675 3765375 0 3.635178e-001 6.5 733 9.95 1.80
LU3_004 POINT 377325 3765575 0 3.635178e-001 6.5 733 9.95 1.80
LU3_005 POINT 376975 3765825 0 3.635178e-001 6.5 733 9.95 1.80
LU3_006 POINT 379775 3766625 0 3.635178e-001 6.5 733 9.95 1.80
LU3_007 POINT 375775 3765575 0 3.635178e-001 6.5 733 9.95 1.80
```

2.4.5. Original method for placing DG in 5x5km cells

In previous methods for placing DG units, the EHP/PW2010 and EPA land use data was used to examine the domain on a cell by cell basis for determining the total unit count. The unit count was found by:

$$\#\text{Stack}_i = \text{DG}_{\text{EHP,cell}} * \frac{\sum \text{R}_i * \text{A}_{\text{i,cell}}}{\text{A}_{\text{cell}}} \qquad (2.6)$$

where $DG_{EHPcell}$ is the DG requirement of the grid, R_i is the adoption factor, $A_{i,cell}$ is the area of land use *i*, and A_{cell} is the are of non-zero land use category. The unit count is then rounded to the nearest whole number. The DG requirement of the cell was then compared to the DG from the units. Because of rounding of the unit count, the DG requirement of the cell differs from the DG generated from the rounded values of the units. Units were added and removed to create the least residual DG for each cell.

Because of discrepancies in the data, this technique did not work for the cells with high DG requirement. The EHP/PW2010 and EPA data are most likely slightly misaligned. For areas of high EHP/PW2010 DG requirement, the EPA data does not have industry sectors. Instead commercial and residential sectors are present. This creates a spike in the for commercial and residential DG count while reducing the industry sector.

2.5. Summary

Using the finer resolution EPA land use data the emission data from the emission data from the EHP/PW2010 prediction was converted from a 5x5km resolution to a 50x50m resolution. This allows for the use of short range dispersion models, such as AERMOD, to model the emissions from expected DG penetration in 2010. The output of this program is the unit point locations and emission rates on a 50m resolution under extra high penetration. The emission rate is not

time dependant. For further modeling of air emissions, the 24 hour time dependant emissions can be modeled. Using 24 emission data, the emissions from the different unit types can be found as a function of time. The time dependant point emissions can then be modeled in a dispersion simulator.

3.0 Modeling

The impact of emissions from distributed generators (DG) on local air quality is governed by several factors. First, DGs are generally located in urban areas surrounded by buildings that enhance turbulence levels above those in surrounding rural areas. These relatively high turbulence levels increase dispersion of emissions, thus reducing ground-level concentrations. At the same time, enhanced turbulence can reduce the rise of buoyant emissions from DGs and thus increase ground-level concentrations. Emissions from distributed generators are generally vented into the atmosphere from short stacks located on buildings less than 10 meters high. Thus, these emissions have the potential of being drawn into the wake of the building and causing high ground-level concentrations, especially when the wind speeds are high. High

exhaust temperatures, common in gas turbine powered DGs, can reduce this downwash problem, but heat recovery to increase the overall efficiency of the DG can reduce the plume buoyancy required to avoid downwash. These interacting processes have to be accounted for in an examination of the air quality impact of DGs. AERMOD (Cimorelli et al., 2005) incorporates these processes, and has been used to estimate the air quality impact of distributed generation in the South Coast Air Basin (SCAB). Before presenting results from AERMOD, we will examine the effects of these processes through a simplified dispersion model. Results of sensitivity studies conducted with this model can be used to interpret the results from the much more complicated AERMOD, presented later. The model is described next.

3.1. Dispersion model

The simplified dispersion model is based on that used by the Danish National Research Institute (Olesen et al., 2007). We chose this model because it is well documented and its description of the major processes that affect dispersion allow for ready interpretation of their effects. It is based on the Gaussian dispersion formulation:

$$C(x,0) = \frac{Q}{\pi U \sigma_y \sigma_z} exp\left(-\frac{h_{eff}^2}{2\sigma_z^2}\right) \quad (3.1)$$

where $C(x,0)$ is the ground-level concentration along the plume centerline, Q is the emission rate, U is the mean wind speed, σ_y and σ_z are the plume spreads in the horizontal and vertical directions, and h_{eff} is the effective stack height, given by

$$h_{eff} = h_s + \Delta h \quad (3.2)$$

In Equation (3.2), h_s is the physical stack height, and Δh is the plume rise associated with the buoyancy and momentum of the exhaust gases.

The effects of buildings on ground-level concentrations are included through modifications to plume rise and plume spread. These are addressed next.

3.2. Plume rise

Plume rise is described by the equation (Briggs, 1984):

$$wr^2U = F_B t + F_M \quad (3.3)$$

where r is the effective radius of the plume, w is the vertical velocity of the rising plume, and t is the travel time, x/U. The buoyancy parameter, F_B, of the plume is

$$F_B = \frac{g}{T_s} v_s r_s^2 \left(T_s - T_a\right) \quad (3.4)$$

where g is the acceleration due to gravity, T_s is the exit gas temperature, v_s is the exit gas velocity, r_s is the stack radius, and T_a is the ambient temperature. The momentum parameter, F_M is given by

$$F_M = v_s^2 r_s^2 \quad (3.5)$$

If z is the plume rise, then the vertical velocity of the plume $w = dz/dt$. As is Briggs (1984), the radius of the plume is taken to be

$$r_p = r_0 + \beta z \tag{3.6}$$

where r_0 is the initial radius of the plume, and □ is the entrainment parameter taken to be 0.6.

Substituting this expression into Equation (3.3) and integrating we obtain

$$z = \left[\frac{3}{2\beta^2} \left(F_M t + \frac{F_B t^2}{2} \right) + \left(\frac{r_0}{\beta} \right)^3 \right] - \frac{r_0}{\beta} \tag{3.7}$$

We also account for the penetration of the buoyant plume into the stable layer above the mixed layer using the formulation described by the Olesen et al. (2007).

3.2.1. Downwash

The effects of downwash on plume rise are accounted for by modifying the initial radius, r_0, as follows. Assume that the height of the building is h_0. Based on observations summarized by Schulman and Scire (1980), the plume rise at a distance of $2h_0$ downwind of the building is used to determine the effects of the building on r_0. Denote the plume rise at this distance by z_b, computed using Equation (3.7) by setting $r_0=r_s$. Then, the ratio, r_b, of the effective stack height, $h_b=h_s+z_b$, to the building height, h_0, is used to compute the horizontal and vertical radius of the plume, r_{0y} and r_{0z}. If this ratio is greater than 3, the building does not affect r_{0z}. At smaller values,

$$\begin{aligned} r_{0z} &= h_0 \ \ when\ r_b \le 1 \\ &= max\left(h_0 \frac{(3 - r_b)}{2}, 0 \right) \end{aligned} \tag{3.8}$$

The plume radius, r_{0z}, has a maximum value of h_0 when $r_b \le 1$, and then goes linearly to zero at $r_b=3$.

On the other hand, the horizontal plume radius, r_{0y}, has a maximum value of $0.5h_0$ when $r_b \le 1$, and then goes linearly to zero at $r_b=1.2$,

$$\begin{aligned} r_{0y} &= 0.5 h_0 \ \ when\ r_b \le 1 \\ &= max\left(0.5 h_0 \left(6 - 5 r_b \right), 0 \right) \end{aligned} \tag{3.9}$$

Then, the plume rise at any distance, x, is recalculated using Equation (3.7) by setting $r_0=r_{0z}$. The plume contributions to the horizontal and vertical plume spreads are taken to be

$$\begin{aligned} \sigma_{zp} &= \left(r_{0z} + \beta z \right) / \sqrt{2} \\ \sigma_{yp} &= \left(r_{0y} + \beta z \right) / \sqrt{2} \end{aligned} \tag{3.10}$$

The $\sqrt{2}$ in Equation (3.10) arises from the assumption that the concentration distribution is taken to be uniform across the plume. This factor makes it consistent with the Gaussian distribution of Equation (3.1).

3.2.2. Plume spread

We assume that the turbulent plume spreads are given by the formulations:

$$\sigma_{yt} = \frac{\sigma_v x}{U}$$
$$\sigma_{wt} = \frac{\sigma_w x}{U} \tag{3.11}$$

where σ_w and σ_v are the standard deviations of the vertical and horizontal velocity fluctuations. These are calculated from

$$\sigma_w = 1.3\left(u_*^3 + u_f^3\right)^{1/3}$$
$$\sigma_v = \left((2.5u_*)^3 + (0.6w_*)^3\right)^{1/3} \tag{3.12}$$

where the surface friction velocity, u_*, is estimated from the neutral equation,

$$u_* = \frac{kU}{ln\left(z_r / z_0\right)} \tag{3.13}$$

In Equation (3.13), k is the Von-Karman constant, taken to be 0.4, z_r is the height at which U is measured, and z_0 is the roughness length. The free convection velocity scale, u_f, is

$$u_f = \left(\frac{g}{T_0} Q_0 z_r\right)^{1/3} \tag{3.14}$$

where Q_0 is the surface kinematic heat flux, and T_0 is the surface temperature. The convective velocity scale, w_*, is defined by

$$w_* = \left(\frac{g}{T_0} Q_0 z_i\right)^{1/3} \tag{3.15}$$

where z_i is the mixed layer height.

The turbulent plume spreads are combined with buoyancy induced plume spreads using

$$\sigma_z = \left(\sigma_{zt}^2 + \sigma_{zp}^2\right)^{1/2}$$
$$\sigma_y = \left(\sigma_{yt}^2 + \sigma_{yp}^2\right)^{1/2} \tag{3.16}$$

3.3. Sensitivity studies

The exhaust gases from a DG are hot (temperature ~700 K without heat recovery), plume rise can play a major role in governing ground-level concentrations. Thus, concentrations are sensitive to heat recovery, which determines the temperature and thus the buoyancy of the plume. Wind speed is also important because it affects plume rise as well as dilution of the plume. Decreased plume rise can also increase the potential for downwash, which increases concentrations. Thus, in the sensitivity studies described next, we vary the wind speed and the heat recovery efficiency to examine the effect of these variables on maximum ground-level concentrations as a function of power output. We take w_* =1 m/s, typical of daytime conditions, to model the contribution of convection to turbulent velocities. The roughness length, z_0, is

taken to be 0.1 m, and z_i=1000 m. The wind speed is assumed to be specified at the height of the building, h_0, housing the generator.

We model the generator building using the dimensions of the 650kW power plant studied in the Palm Springs study (Jing et al., 2008). These are h_0=7 m, and h_s=9.3 m.

The buoyancy parameter, F_b, can be related to output power, P_o, of the DG through

$$F_B = \frac{g(1-\eta_t)(1-\eta_h)P_o}{\pi\rho_e C_p T_s \eta_t} \tag{3.17}$$

where η_t is the thermal efficiency of the power plant, η_h is the efficiency of heat recovery from the exhaust gases, and ρ_e and C_p are the density and specific heat of the exhaust gases. Note that the overall efficiency of a power plant with heat recovery is given by

$$\eta = \eta_t + \eta_h - \eta_t\eta_h \tag{3.18}$$

The momentum flux, F_M, can be conveniently written in terms of the buoyancy flux, F_B,

$$F_M = F_B \frac{v_s T_s}{(T_s - T_a)g} \tag{3.19}$$

Figure 3-1 shows the variation of the maximum normalized ground-level concentration, C/Q, as a function of wind speed for different power plant sizes. The dilution can be converted into concentration (mass/volume) by multiplying with the emission rate, Q, which can be expressed as

$$Q = \frac{e_f P_o}{\eta_t} \tag{3.20}$$

where e_f is the emission factor in units of mass/(Power.Time). In the results presented here, we use a nominal emission factor of 525 g/MWh corresponding to that for NO_x from a natural gas internal combustion engine (Heath and Nazaroff, 2007).

We notice from the left panel of Figure 3-1 that maximum normalized concentration increases with wind speed. The normalized concentration decreases as the power output increases because the buoyancy and hence the plume increases with power output. The right panel of Figure 3-2 indicates that that the 50 MW plant causes the highest nominal concentration, but the spread between the concentrations associated with power plants is not as large as the range of power outputs. For example, at wind speed of 4 m/s, there is little difference between the nominal concentrations although the power output varies by a factor of 50. It is only at a high wind speed of 8 m/s that we see a factor of two differences in the concentrations associated with the 1 MW and 50 MW power plants.

Figure 3-2 indicates that downwash effects can actually increase the concentration of the 1 MW plant to that extent that it is greater than the nominal concentration associated with the 50 MW plant. Below 4 m/s, there is little difference among the concentrations associated with power plants with outputs ranging from 1 to 50 MW. At a wind speed of 8 m/s, the 10 MW plant has the lowest maximum concentration of 25 $\mu g/m^3$, while the 1 MW plant has a concentration of 40 $\mu g/m^3$.

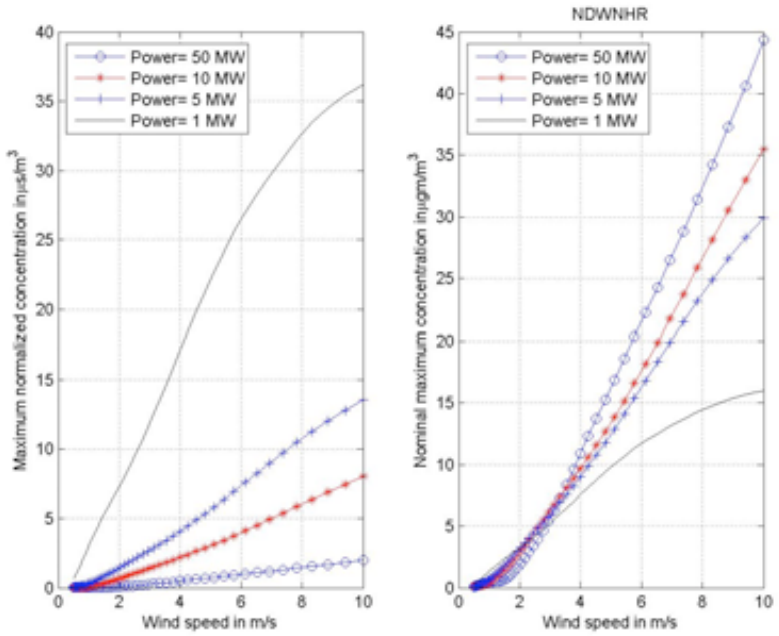

Figure 3-1. Variation of normalized and nominal concentrations as a function of wind speed. Building downwash is not considered and heat recovery is zero.

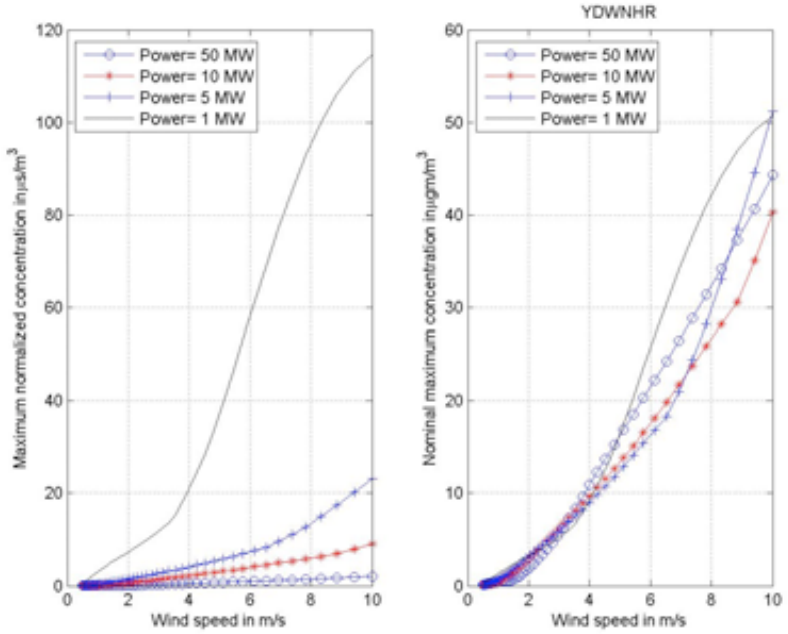

Figure 3-2. Variation of normalized and nominal concentrations as a function of wind speed. Building downwash is considered but heat recovery is zero.

Heat recovery of 50% increases the concentrations even further, as seen in Figure 3-3. The maximum concentration at 6 m/s goes up to 60 $\mu g/m^3$. At 8 m/s, the 5 MW power plant has the highest concentration of 80 $\mu g/m^3$.

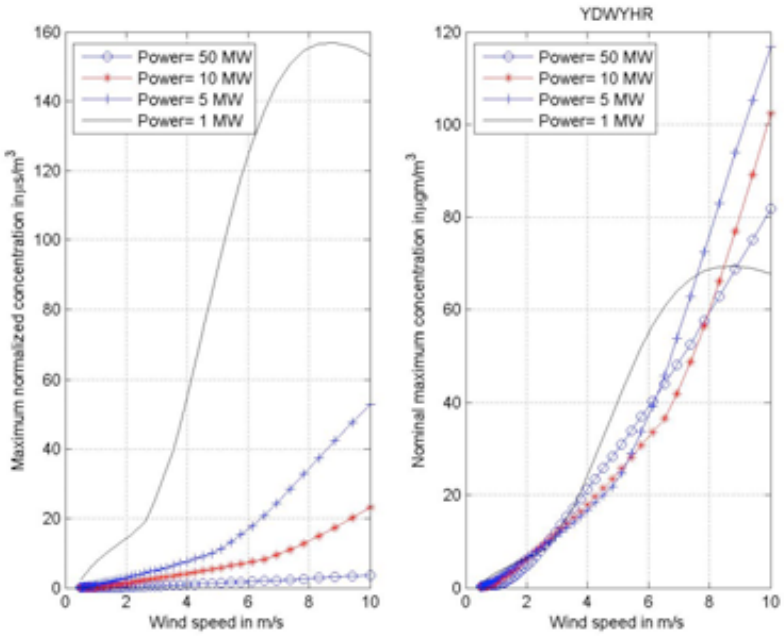

Figure 3-3. Variation of normalized and nominal concentrations as a function of wind speed. Building downwash is considered and heat recovery is 50%.

The effects of increasing the overall efficiency - Equation (19) - of a 12 MW DG on normalized concentrations is shown in Figure 3-4. The concentration increases with wind speed as we saw before. The concentration increases by almost an order of magnitude as the overall efficiency increases from 33% to 95% through heat recovery from the exhaust gases.

3.4. Conclusions

Small power plants located in urban areas emit their hot exhaust gases through relatively short stacks mounted on buildings that rarely exceed 10 m. The ground-level concentrations associated with these emissions are governed by plume rise of the buoyant exhaust, and the effects of the building wake on the emissions. We have accounted for these effects in a dispersion model. Sensitivity studies conducted with the model indicate that ground-level concentrations increase with wind speed because plume rise decreases and downwash effects increase with wind speed. We also see that heat recovery from exhaust gases has the potential of magnifying these effects by decreasing plume buoyancy.

These preliminary studies indicate that ground-level concentrations do not necessarily increase with power plant capacity. The higher plume rise from a larger plant can counteract its larger emissions to the extent the ground-level impact of 1 MW power plant can exceed that of a 50 MW plant for wind speeds less than 6 m/s. These results suggest that modeling the air quality of DGs requires careful consideration of a number of interacting processes, described in this section. In the next section, we apply AERMOD, a state-of-the-art model, which includes the relevant processes to estimate the impact of DG emissions.

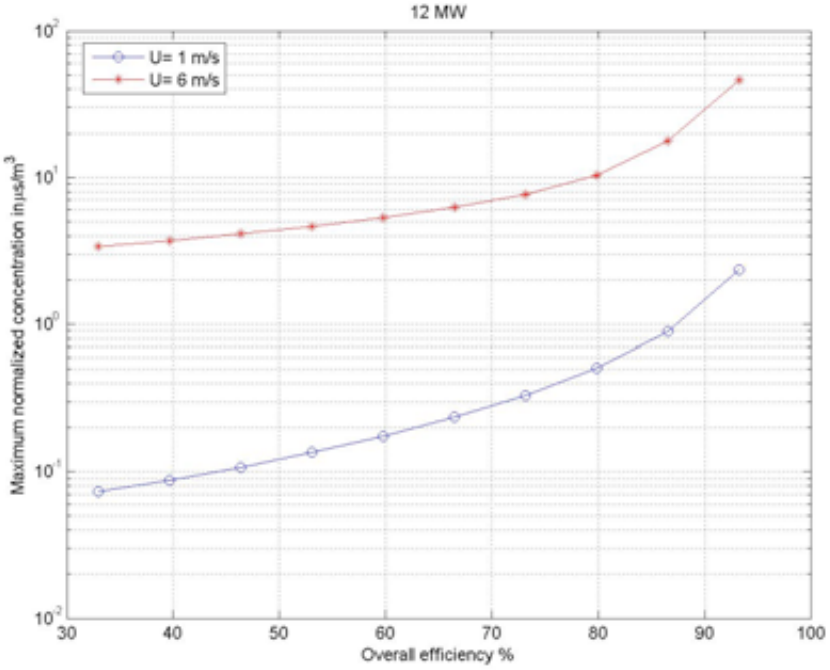

Figure 3-4. Variation of normalized concentration with overall efficiency of power plant as a function of wind speed. Building downwash is considered.

4.0 AERMOD application to the South Coast Air Basin

This section describes the application of AERMOD to estimate the air quality impact of DG penetration in the South Coast Air Basin. The first task was to generate meteorological inputs required to run AERMOD.

We have developed meteorological inputs for AERMOD for 2007 using land use data, surface meteorology from the National Weather Service (NWS), and upper air data. Details of the construction of the data set are described in the appendix. During the last year, the South Coast Air Quality Management District (AQMD) released a new set of AERMOD ready files for the period 2005-2007 (AQMD, 2009a). These inputs are based on data from 26 surface sites maintained by the AQMD, shown in Figure 4-1(purple circles for later on analysis).

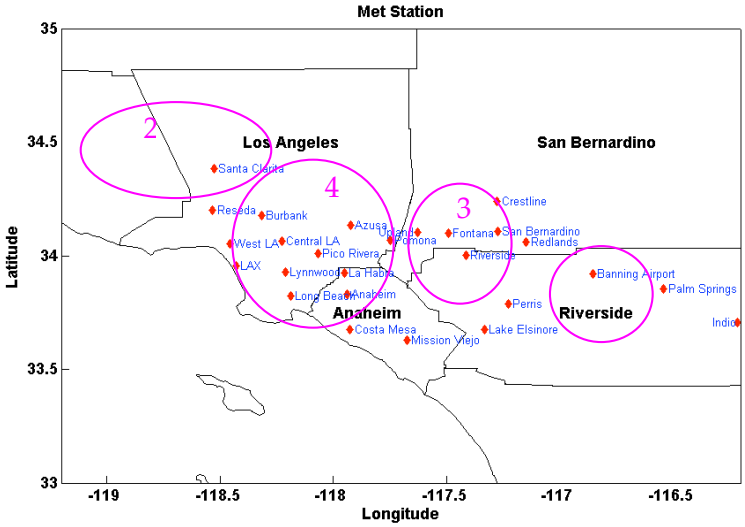

Figure 4-1. Positions of Meteorological stations used to construct the AQMD database

The AQMD meteorological AERMOD inputs were constructed solar flux data available at the AQMD sites, but not at the NWS stations; the solar flux data are used to calculate surface heat fluxes. The data set was quality controlled by the AQMD before release to the public for regulatory applications. The data has also been partially evaluated against observations collected in Riverside. Thus, the AQMD data set improves upon that constructed earlier using NWS Data. In the simulations described next, we have used this improved data set.

Sensitivity studies showed little difference between the AERMOD results based on 2006 meteorological data set and those based on 2007 data set. So we decided to use the most recent 2007 data set in the simulations described in section 4.

As described in section 2.4, we assume DG units in the LU1 and LU2 areas have negligible emissions. Since the DG unit in the LU6 area is the same size as that in the LU4 area, we represent them as units corresponding to the LU4 area. We refer to the DG units in the LU5 area

as small DG units (625 KW), those in the LU3 area as medium DG units (2.5 MW), and those in the LU4 area as large DG units (12.5 MW). The stack parameters for DG units in different areas are listed in Table 4-1, which are based on a literature review of current DG units.

Table 4-1. Stack parameters for DG units (heat recovery is taken to be 50%)

Parameters	Small DG units	Medium DG units	Large DG units
Stack height	9.3 m	10.3 m	11.3 m
Stack diameter	1.5 m	1.8 m	2.6 m
Exit velocity (W | W/O Heat Recov.)	2.99 | 3.29 m/s	8.32 | 9.15 m/s	19.95 | 21.93 m/s
Exit temperature (W | W/O Heat Recov.)	177 | 500 ºC	177 | 500 ºC	177 | 500 ºC

Before AERMOD was applied to examine the impact of DG penetration we first evaluated the performance of AERMOD using data collected in Palm Springs during a field study conducted in 2008.

4.1. Evaluate AERMOD using Palm Springs field observations

The USEPA recommends the use of the American Meteorological Society (AMS)/U.S. Environmental Protection Agency (EPA) Regulatory Model (AERMOD) (Cimorelli et al. 2005) for estimating the impact of emissions at source-receptor distances of less than a few kilometers. AERMOD includes state-of-the art formulations for dispersion, and has undergone extensive evaluation with 17 data bases (Perry et al. 2005). Of these 17 databases, only one included an urban case. Furthermore, none of the field studies included a source similar to that considered in this study: a relatively short stack located in an urban area. This motivated a field study in the vicinity of a small DG unit located in urban Palm Springs to collect the data to evaluate AERMOD. This section describes the evaluation of AERMOD with tracer data collected in the field study.

4.1.1. Tracer Study

The tracer experiment was conducted from July 15th, 2008 to July 21st, 2008 at the Sunrise Park in Palm Springs. During the experiment, Sulfur hexafluoride (SF_6) was released after mixing with hot exhaust gases from a DG stack, which is 2.3 m above the roof top of a 7 m high building surrounded by one storey residences. The DG is driven by a 650KW gas fired IC engine with heat recovery. The exit velocity of the exhaust air is 11 ms^{-1}. The emission rate of SF_6 was 0.9 g/s.

SF_6 concentrations were measured continuously in arcs at distances ranging from 60 m to 2000 m from the source during the release time. The governing meteorological variables were measured with instrumentation consisting of two 3-D Sonic Anemometers (CSAT3), two Krypton Hygrometers (KH20), one Net Radiometer (CNR1), one Temperature and RH Probe (HMP45C), two Temperature Probes (Campbell Sci. Model 107), one Infrared Temperature Sensor (Apogee Instruments IRR-P), and two Data Loggers (Campbell Sci. CR5000). There were two groups of instruments: one on a tower (called the "Lower" station at 4 m above ground level) and another on a tripod (referred to as the "Upper" station, which is approximately 10.5

m above the ground level). Each group was connected to a CR5000 Data Logger (For full description of the field studies, see Jing et al., 2009).

Figure 4-2 shows the variation of meteorological parameters as a function of time of a day over the experiment. The wind speeds were lower than 1 m/s during most of the nighttime hours. The wind speeds started to increase around 8:00 hours and reached a maximum of about 2 m/s around 17:00 hours. The maximum wind speed never exceeded 3.5 m/s. The dominant wind directions were easterly during most of the day. The figure also shows that the lateral turbulent velocities (σ_v as shown in Figure 4-2) were above 0.5 m/s during most of the day; the large lateral turbulent intensities (bottom left panel) indicate the importance of plume meandering.

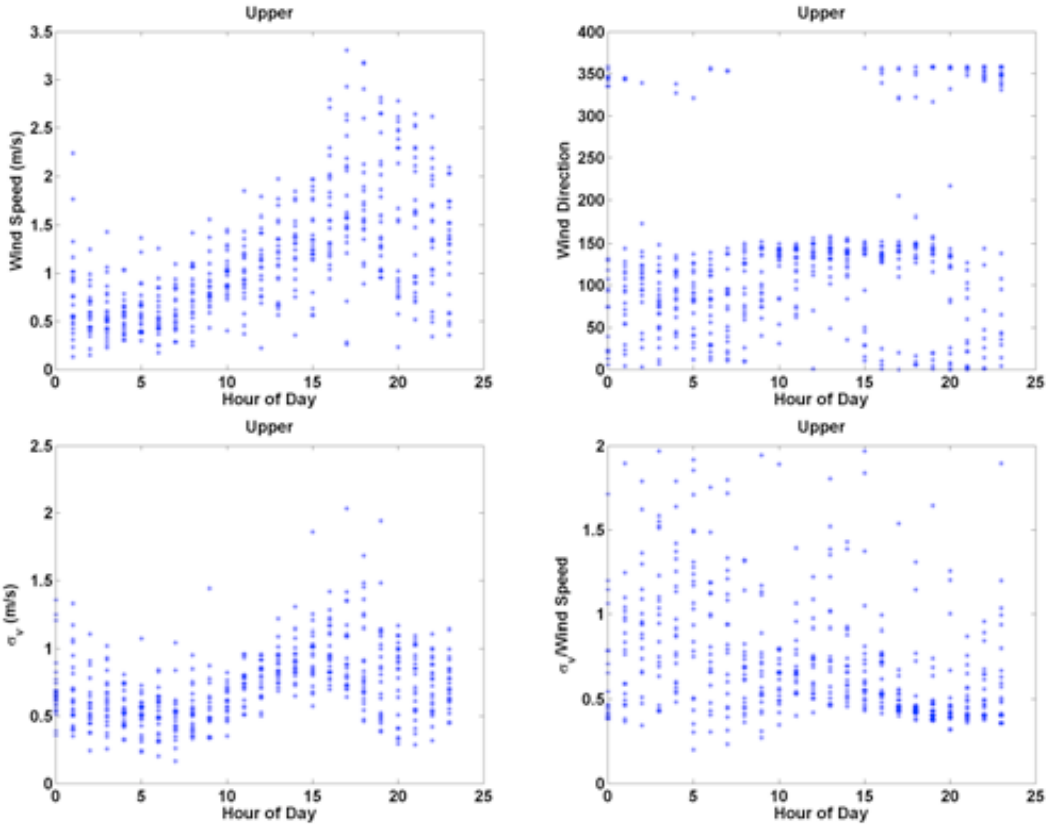

Figure 4-2. Variation of dispersion parameters during experiment by "Upper" station

Figure 4-3 shows examples of observed daytime and nighttime concentrations at each site. The upper two panels show daytime concentrations. During the period 12:00 to 13:00 (denoted as 13:00 7/17/2008 in Figure 4-3), the wind direction was 158 degrees, and the maximum ground concentrations were found at downwind sites located in the northwest and at about a hundred meters form the source; also, as expected, the daytime mixing in the boundary layer resulted in a rapid decrease in concentration with downwind distance.

However, the nighttime concentrations showed a very different pattern. The concentrations at downwind sites beyond 500 m were high relative to those found during daytime; high concentrations were also found at almost every site in the vicinity of the source, not only those located downwind. This suggests that the DG plume was trapped in a relatively shallow boundary layer during the night, and was spread in all directions by the meandering wind.

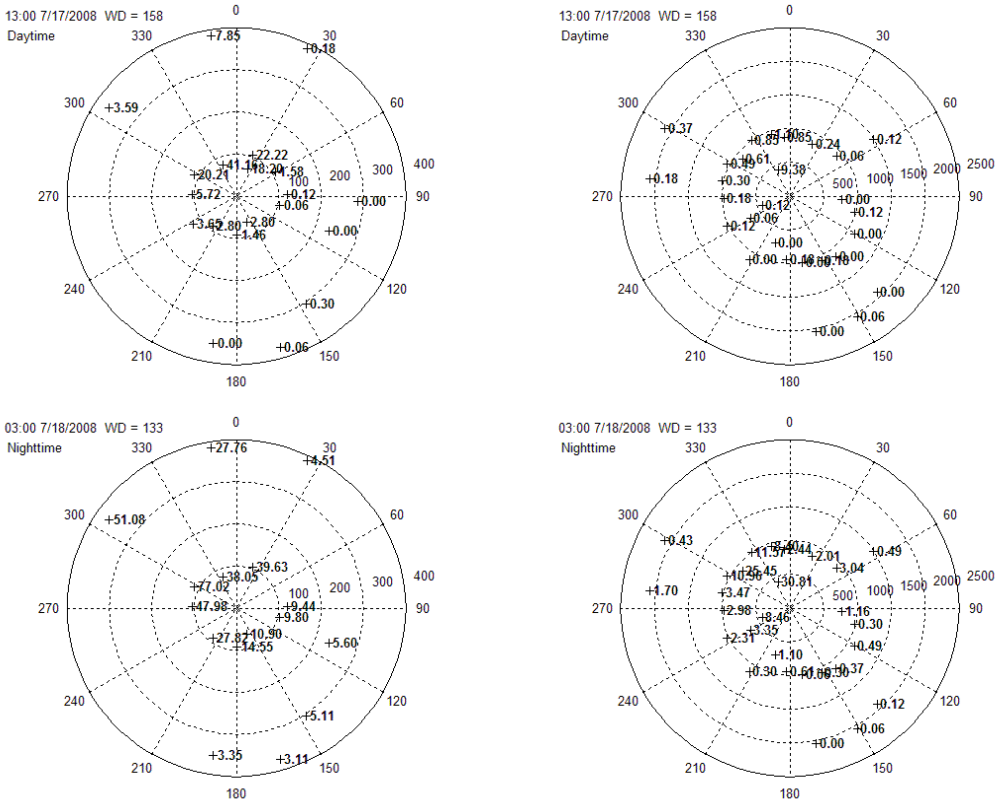

Figure 4-3. Observed concentrations (µg/m^3, boldface numbers) at 17th, and 18th July, 2008 (The center denotes the source; the boldface numbers stand at sampling sites; the numbers along different circles are the radius (in meters); the numbers along the outer circle are the degrees from the North.)

4.1.2. Model Performance results

Because of inevitable uncertainties in model inputs, dispersion models perform poorly when concentration estimates are compared to observations paired in space and time. This problem can be ameliorated to some extent by evaluating the ability of the model in describing the distribution of observed concentrations. This assumes that the distribution of model inputs is similar to the correct observed values (Venkatram et al., 2001). A comparison of the distributions of concentrations is adequate for regulatory purposes where the emphasis is on peak concentrations. In practice, the comparison is performed through quintile-quintile (Q-Q) plots in which ranked model estimates are plotted against ranked observations. Good correlation between the two sets indicates that the model is capable of simulating reality even if it cannot predict the precise time and location of the observed concentrations.

Figure 4-4 shows the difference in model performance between day and night using Q-Q plots. We see that AERMOD yields concentration estimates that are within a factor of two of the observed values over most of the concentration range during the daytime and during the nights of 20th and 21st. However, AERMOD underestimates concentrations substantially during the nights of 18th and 19th. On the 19th and 21st AERMOD tends to underestimate the middle concentration ranges, while the performance is poor at both the low and high concentration ranges.

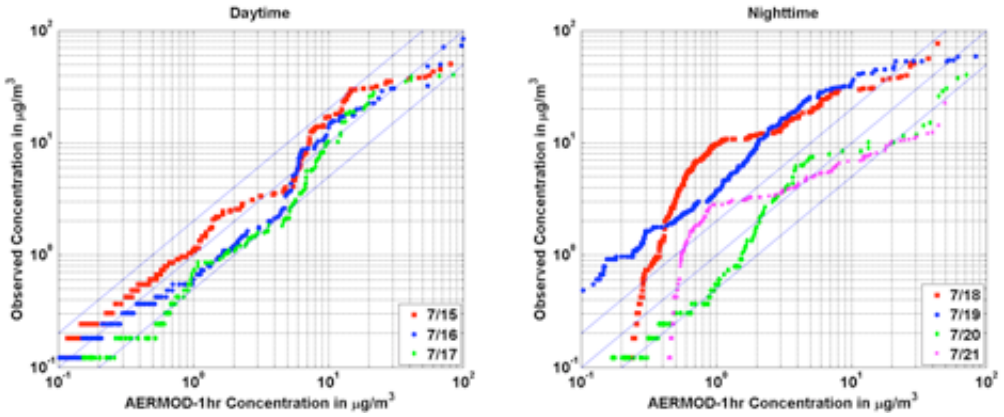

Figure 4-4. Comparison of observed and estimated concentration distributions using a Q-Q plot.

To minimize the effects of smoothing of the turbulence statistics implicit in one-hour averages, we used 5-minute averaged meteorological data instead of one hour averaged data. The 12 five-minute averaged AERMOD estimates were combined to obtain one-hour estimates. This procedure did not result in a noticeable improvement in model performance.

Figure 4-5 indicates that AERMOD provides an adequate description of the variation with distance of the maximum ground-level observations of SF_6 concentrations, which generally occur within hundred meters form the source. As expected, the daytime mixing in the boundary layer results in a rapid decrease in both observed and estimated concentrations with radial distance from the source.

The maximum ground-level estimates from AERMOD are generally lower than the concentrations observed at night. These maximums occur at sites located within one hundred meters from the source. However, the concentrations do not fall off rapidly as in the daytime because the mixed layer is relatively shallow. We see that modeled and observed concentrations are 1/10th of the maximum values even at 1 km from the source.

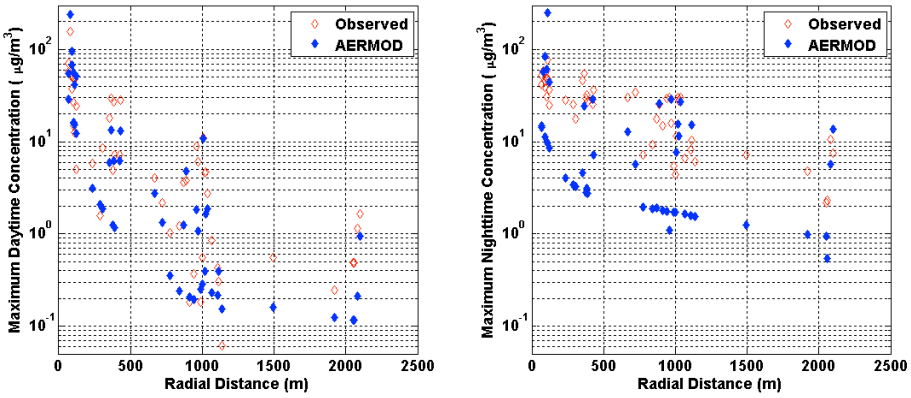

Figure 4-5. Maximum nominal concentration as a function of radial distance

In view of the effects of wind speed on maximum concentrations seen earlier, we plotted the maximum observed and estimated concentrations as a function of wind speed. Figure 4-6 shows that although both modeled and observed maximum concentrations increase with wind speed, modeled values have a stronger correlation with wind speed than the observed maximum concentrations have, especially at night. However, one has to be cautious about drawing any general conclusions from these results because the wind speeds are relatively low: (less than 2 m/s) when downwash effects are not important.

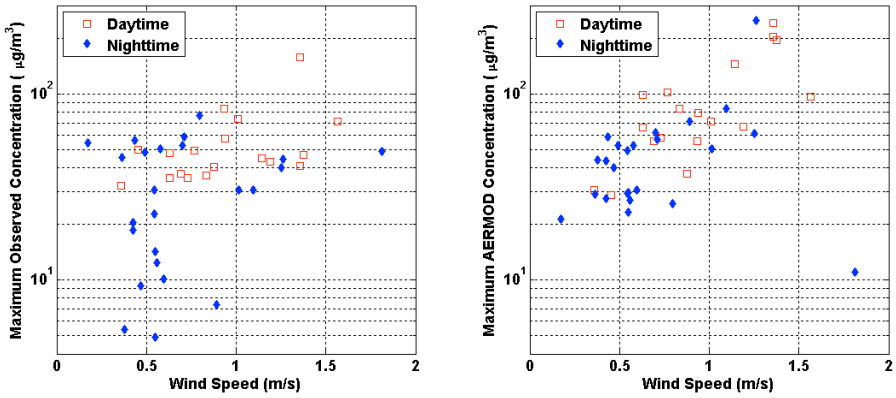

Figure 4-6. Maximum nominal concentration as a function of wind speed

4.1.3. Summary

AERMOD captures the peak ground-level concentrations and performs well in reproducing the concentration distributions for daytime convective conditions. However, the uncertainties with characterizing the nighttime stable boundary layer prevent AERMOD from making reliable predictions. AERMOD underestimates the nighttime concentrations on two of the four nighttime experiments. It should be noted that nighttime concentrations were generally lower than the daytime concentrations. So AERMOD performed adequately when the concentrations were relatively high. The low wind speeds during the field study do not allow evaluation of

AERMOD for the high wind conditions that result in the high concentrations discussed in the previous section.

4.2. Sensitivity studies

Section 3 provides a preliminary understanding of the effects of meteorology and downwash on ground-level concentrations. Here we reexamine the results using AERMOD, which is a more complete model. The thermal efficiency of the power plant used in this section is 0.33, and the emission factor here is 560 g/MWh corresponding to that for NO_x from a natural gas turbine (Heath and Nazaroff, 2007). The building used in the sensitivity studies is a 13 m × 25 m × 8 m (L × W × H) one-story residences, with the stack standing in the center of it (The stack height in Table 4-1 accounts for building height). We ran AERMOD with and without this building to examine the effects of building downwash of ground-level concentrations. The meteorological data corresponded to SQAQMD Anaheim station. We also used AERMOD to estimate the effects of heat recovery. The maximum concentration corresponding to each hour of 2007 is used as measure of ground-level impact.

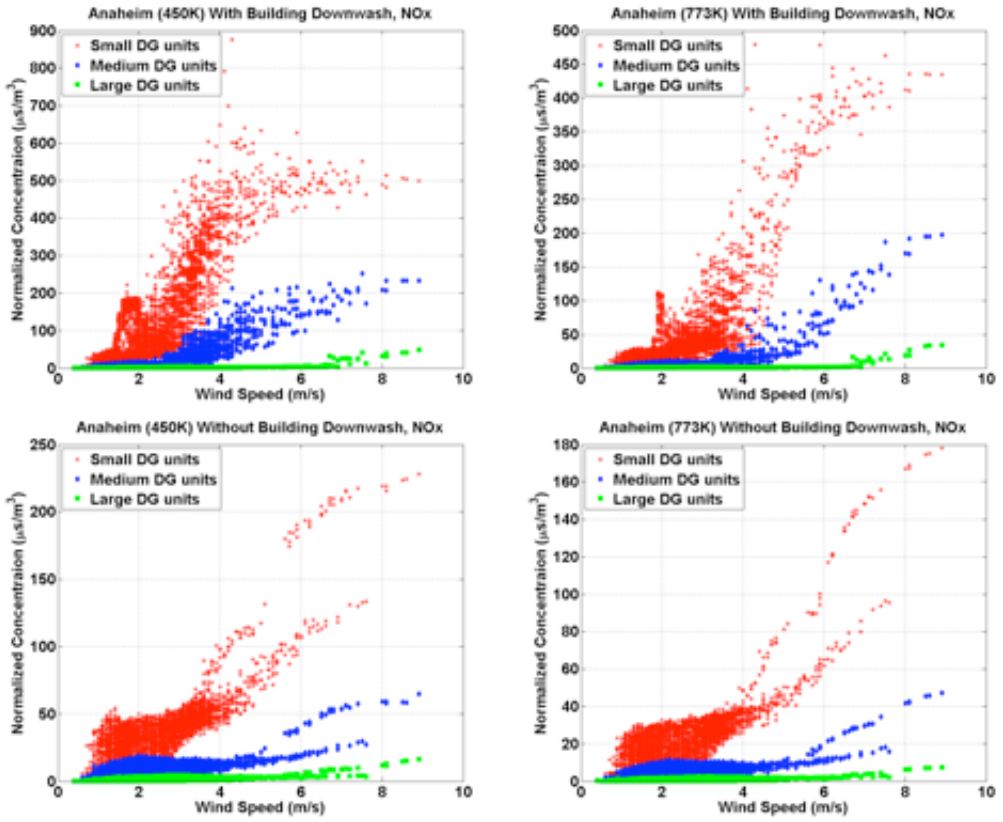

Figure 4-7. Normalized concentrations (Concentration/Emission rate) as a function of wind speed.

Figure 4-7 shows that the normalized maximum concentration, which is concentration divided by emission rate, decreases as the size of the unit increases. This is consistent with results

shown in Section 3. The normalized concentration is only a function of dispersion; the concentration decreases as plume rise increases with plant size.

However, the nominal concentration, obtained by multiplying the normalized concentration by the emission rate (NO_x was treated as NO_2 when converting to ppb), does not exhibit this monotonic behavior with plant size. The nominal maximum from the 12. 5 MW unit (medium) can exceed that from the 2.5 MW unit at wind speeds over 5 m/s as seen in Figure 4-8.

Both normalized and nominal concentrations increase with the wind speed because of the decrease of plume rise with wind speed. With heat recovery, the concentration starts to increase when the wind speed is greater than 2m/s, while without heat recovery the concentration starts to increase when the wind speed is greater than 4m/s.

Building downwash increases the nominal concentration especially when the wind speed is larger than 4 m/s. Heat recovery (referred to as 450K) increases the concentration even further because of its effect on reducing plume rise.

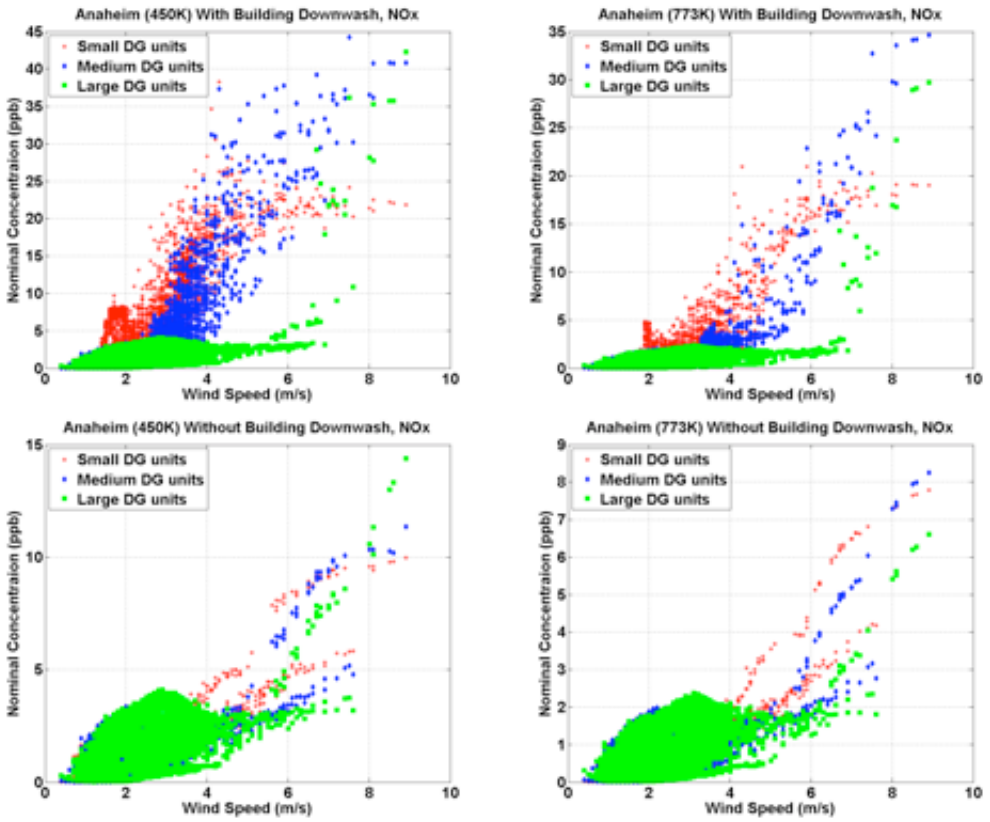

Figure 4-8. Nominal concentrations as a function of wind speed.

Table 4-2 shows detailed statistics of nominal concentrations for all 26 meteorological sites and all three types of DG units. The concentration statistics are based on maximum hourly averages over 8760 hours of the entire 2007 year. 50% of the maximum hourly concentrations are less than or equal to the median value, while 95% of the maximum hourly concentrations are less

than or equal to the 95th percentile Table 4-2 also gives the reference height of the winds and statistics of wind speeds for different meteorological stations. The reference height is 9.1 m at all the stations, except at Burbank, which is 12.2 m, Central LA is 21.3 m, Long Beach is 12.2 m and Reseda is 12.2 m.

Table 4-2. Statistics for all meteorological sites and DG unit sizes. With heat recovery and building downwash.

Station	Name	Wind Rf. Height (m)	Median				The 95th percentile				Maximum			
			Concentration (ppb)			Wind Speed (m/s)	Concentration (ppb)			Wind Speed (m/s)	Concentration (ppb)			Wind Speed (m/s)
			Small DG	Medium DG	Large DG		Small DG	Medium DG	Large DG		Small DG	Medium DG	Large DG	
anah	Anaheim	9.1	2	0.3	0.1	1.6	15	10	3	3.7	38	44	42	8.9
azus	Azusa	9.1	2	0.4	0.2	1.8	12	7	3	3.6	39	58	46	8.6
bnap	Banning Airport	9.1	12	8	0.7	4.4	21	32	20	7.9	35	44	72	15.0
burk	Burbank	12.2	1	0.3	0.2	1.7	14	6	3	3.4	39	61	44	8.0
cela	Central LA	21.3	0.4	0.1	0.1	1.8	9	5	3	4.2	31	51	52	9.7
cres	Crestline	9.1	1	0.4	0.7	1.4	10	5	3	3.1	32	36	5	6.2
csta	Costa Mesa	9.1	0.5	0.1	0.5	1.0	7	3	3	2.9	28	40	28	7.4
elsi	Lake Elsinore	9.1	1.0	0.1	0.1	1.3	11	6	3	3.5	38	57	64	13.8
font	Fontana	9.1	3	0.7	0.3	1.9	22	38	17	6.8	39	62	90	15.0
indi	Indio	9.1	4	1	0.5	2.0	22	24	3	4.8	39	56	38	7.9
lahb	La Habra	9.1	0.5	0.2	0.7	0.7	6	3	3	2.8	30	37	21	7.8
laxh	LAX	9.1	2	0.3	0.2	1.9	19	18	3	4.7	38	56	47	11.3
lgbh	Long Beach	12.2	0.9	0.1	0.1	1.6	11	5	3	3.6	36	33	4	7.4
lynn	Lynnwood	9.1	0.6	0.2	0.7	0.8	7	4	3	3.0	37	45	30	7.0
msvj	Mission Viejo	9.1	1	0.0	0.1	1.4	11	4	3	3.0	38	51	46	8.5
peri	Perris	9.1	0.8	0.2	0.4	1.1	20	19	3	4.7	38	62	59	10.0
pico	Pico Rivera	9.1	3	0.4	0.2	1.9	23	21	3	4.1	40	54	4	6.6
plsp	Palm Springs	9.1	1	0.8	0.7	1.3	24	26	3	4.4	41	54	35	7.1
poma	Pomona	9.1	0.3	0.1	0.8	0.6	6	4	3	2.9	26	23	5	4.4
rdld	Redlands	9.1	0.3	0.1	0.7	0.7	4	2	3	2.5	21	29	5	5.8
rese	Reseda	12.2	0.3	0.1	0.4	0.8	22	17	2	4.0	43	64	9	8.7
rivr	Riverside	9.1	2	0.3	0.2	1.5	20	19	3	4.5	41	65	71	11.1
sclr	Santa Clarita	9.1	5	0.8	0.4	2.2	30	42	4	6.6	40	63	61	11.1
snbo	San Bernardino	9.1	0.8	0.4	0.6	1.1	18	16	3	4.2	37	53	46	10.7
upla	Upland	9.1	1.0	0.1	0.2	1.4	7	4	3	3.3	26	32	4	5.5
wsla	West LA	9.1	0.5	0.1	0.4	1.1	13	7	3	3.2	37	42	5	5.7
All	Average	--	1.8	0.6	0.4	1.5	15	13	4	4.1	36	49	36	9.8

The lower panels of Figure 4-9 show the maximum (over all meteorological stations) hourly nominal concentration as a function of the wind speed at the hour when the maximum concentration occurred. As expected, the maximum concentration increases with wind speed for all DG units.

We also see that the larger the DG unit size, the higher the wind speed at which the maximum hourly nominal concentration occurs. When the wind speed is less than 6.5 m/s, the maximum concentrations for large DG units are smaller than those associated with the medium DG units, because of the relationship between plume rise and wind speed. At higher wind speeds, the maximum concentrations for large DG units increase dramatically with wind speed.

The upper panels of Figure 4-9 show the 95th percentile nominal concentration as a function of the 95th percentile wind speed. The concentrations from the small DG unit increase with wind speed when the 95th percentile wind speed is less than 6.5 m/s, but then decrease with wind speed. The concentrations from the medium DG units show a similar trend. The 95th percentile concentrations of large DG units vary little when the wind speed is less than 6.5 m/s, but for wind speeds larger than 6.5 m/s, the concentration starts to increase.

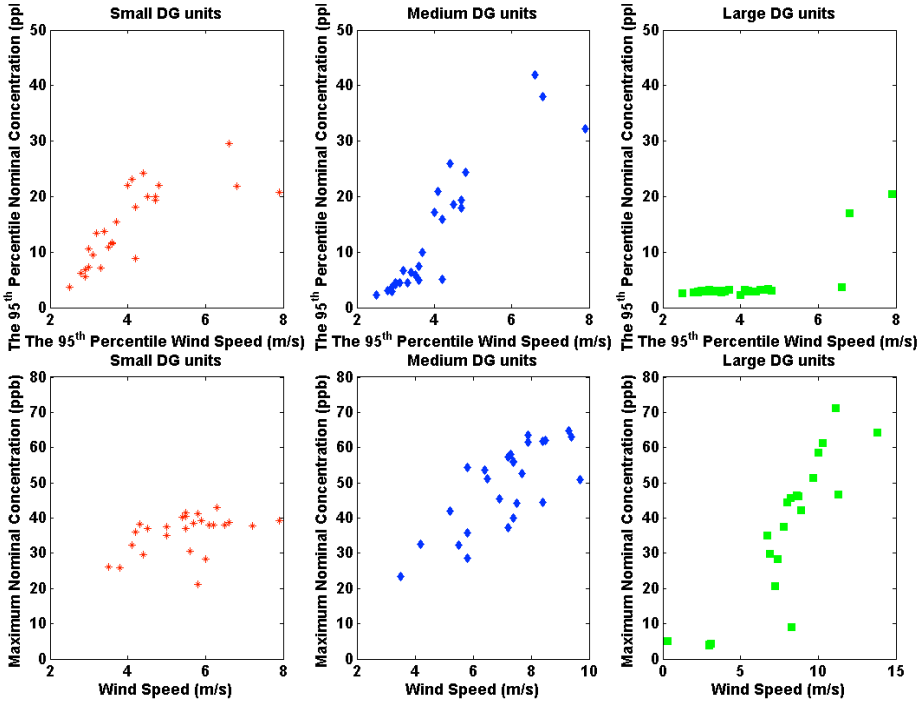

Figure 4-9. Hourly nominal Concentration as a function of wind speed

The maximum concentration is 90 ppb as shown in Table 4-2, which is associated with the large DG unit when the maximum wind speed is 15 m/s at the Fontana station. The maximum values vary little with different types of DG units, except those associated with the Crestline, Long Beach, Pico Rivera, Pomona, Upland, and West LA meteorological stations, where large DG units have smaller maximum values, because the maximum wind speeds at those stations are less than 6.5 m/s, as shown in lower panel of Figure 4-9: when the wind speed is less than 6.5

m/s, the maximum concentration for large DG units is smaller than those for small and medium DG units. Medium DG units have larger maximum concentrations than small DG unit at most meteorological stations except at Long Beach and Pomona, where maximum concentrations of small and medium DG units have a slight difference.

Large DG units have smaller 95th percentile concentrations than medium and small DG units, because most 95th percentile wind speeds are less than 6.5 m/s, as shown in the upper panel of Figure 4-9; when the 95th percentile wind speed is less than 6.5 m/s, large DG units have relatively low 95th percentile concentrations because of high plume rise. The only exception was found at the Redlands meteorological station, where the 95th percentile wind speed is 2.5 m/s, where large DG units have higher 95th percentile concentrations than medium DG units and smaller values than small DG units. The 95th percentile concentrations of small and medium DG units are close to each other and are usually larger than those from the large DG units. The top three 95th percentile concentrations are all associated with medium DG units, 42 ppb at Santa Clarita station, 38 ppb at Fontana station, and 32 ppb at Banning Airport, where the 95th percentile wind speeds are all above 6.5 m/s.

Small DG units have the largest median concentrations except when the median wind speed is less than 1 m/s. As shown in Table 4-2, when median wind is calm, large DG units have highest median concentration, which, however, are less than 0.8 ppb.

Table 4-2 and Figure 4-9 show that median concentrations are less than 1 ppb for all three types of DG units. When the wind speed is low, large DG units have the lowest maximum and 95th percentile nominal concentrations; when the wind speed is high, large and medium DG units have the highest maximum and 95th percentile concentrations

These sensitivity studies suggest that large DG units should be located in low wind areas, such as Pomona, Redlands, Reseda, Lynnwood, and La Habra. Small DG units are best suited for high wind areas such as Banning, Fontana and Santa Clarita. In moderate wind speed areas, a mix of small and large DG units is optimum. Medium (12.5 MW) DG units lead to high concentrations in most locations.

The conclusions of this section are specific to the dimensions of the building and the stack height chosen to represent the DG units. For example, the breakpoint wind speed of 6.5 m/s applies to these particular building and stack dimensions. However, the results on the effects of wind speed on concentrations associated with different sizes of DG units have general applicability.

To see how the concentration varies with distance, and where the maximum concentration occurs, we plotted the maximum concentration (this maximum concentration is taken from those receptors which have the same radius in a polar system) against the radial distance for all three types of DG units under lower wind (Pomona meteorological station at 15:00, Jan. 15, 2007) and high wind (Banning Airport meteorological station at 15:00, Jan. 15, 2007) conditions respectively in Figure 4-10. All three types of DG units show the same trend: the concentration increases with distance, reaches a maximum and then starts to fall off with distance. The maximum concentration occurs at the distance of ten to a hundred meters. When the wind speed is 11.8 m/s, the maximum concentration occurs closer to the source (around 30 meters) than when the wind speed is 1.7 m/s (around 150 meters). This is expected because the higher

wind speed reduces the plume rise and brings the pollutant down to the ground earlier than a lower wind speed. Note again that the maximum concentrations increase with wind speed.

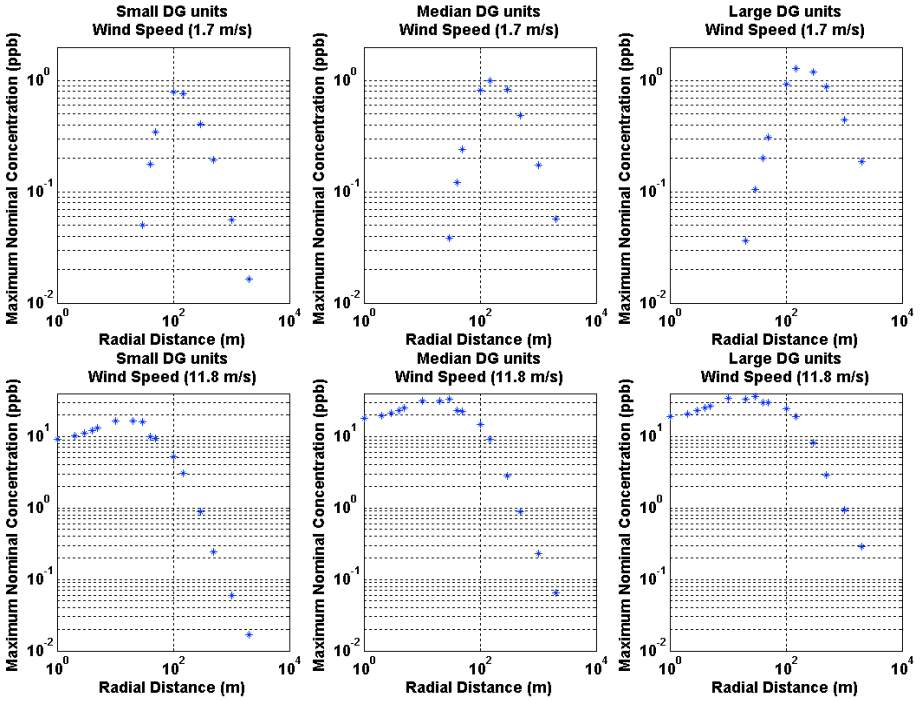

Figure 4-10. Maximum nominal concentration as a function of radial distance

In order to examine the effects of meteorology on the air quality impact of DG penetration in the South Coast Air Basin in California, we conducted two simulations, one using meteorology from the Fontana station, the other based on meteorology from the Pomona station. As indicated by Table 4-2, the meteorology in Fontana station has the potential to give rise to high concentrations because the median wind speed is high, while that at Pomona will give rise to relatively low concentrations because the median wind speed is low.

Figure 4-11 shows the results from the simulations. The left panels, corresponding to the Pomona low wind speed station, show lower median, 95th percentile and maximum concentrations than the right panels corresponding to the Fontana station. Notice that for the maximum concentration, there are only at most three possible values which are listed in the column of maximum in Table 4-2.

We also plotted the difference (Figure 4-12) between the concentrations for each of these simulations and those corresponding to the appropriate meteorology for the DG units. The concentration differences corresponding to the low wind are largely negative as expected, while those corresponding to the high wind Fontana station are largely positive. These results again point to the importance of meteorology in siting DG units. The next section presents results on the spatial distribution of hourly concentration impacts for the two emission scenarios.

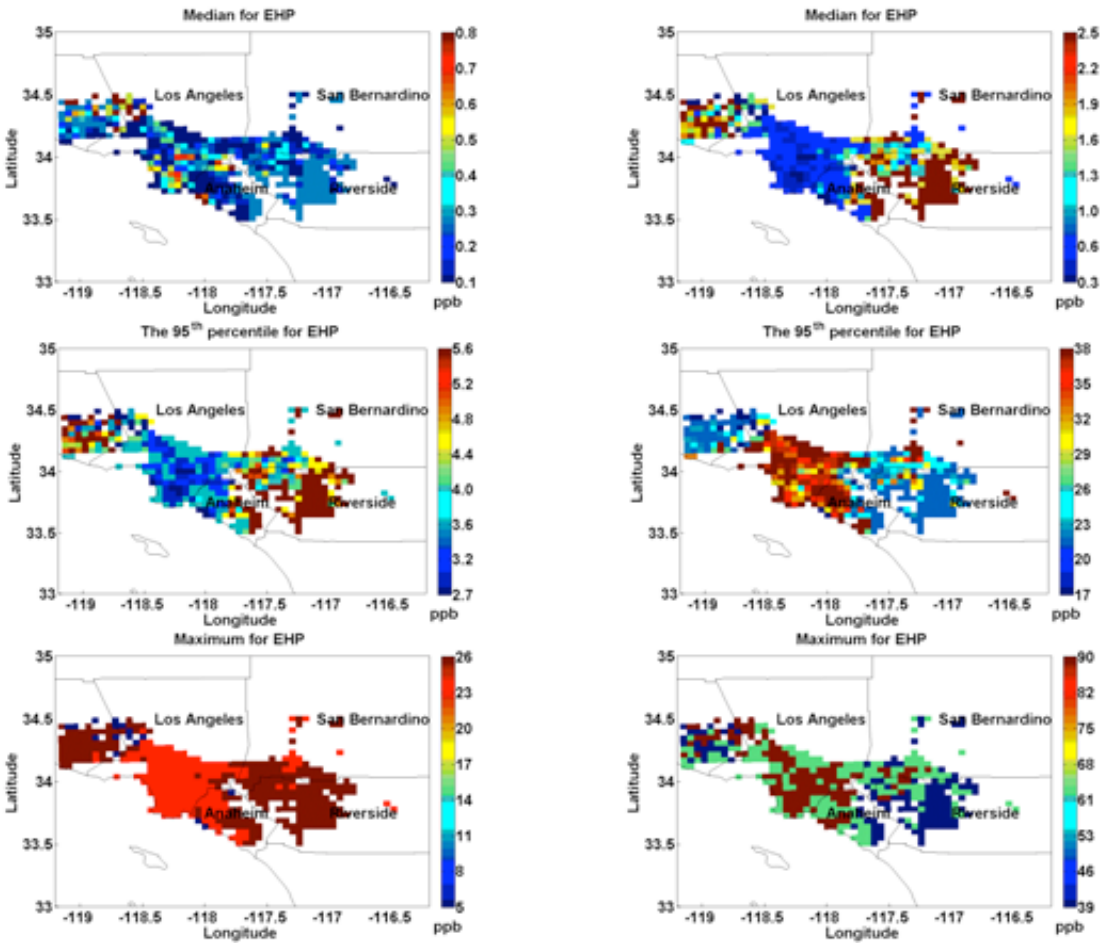

Figure 4-11. Sensitivity studies for the effect of meteorology. (Left panels using data from Pomona meteorological station; right panels using data from Fontana meteorological station)

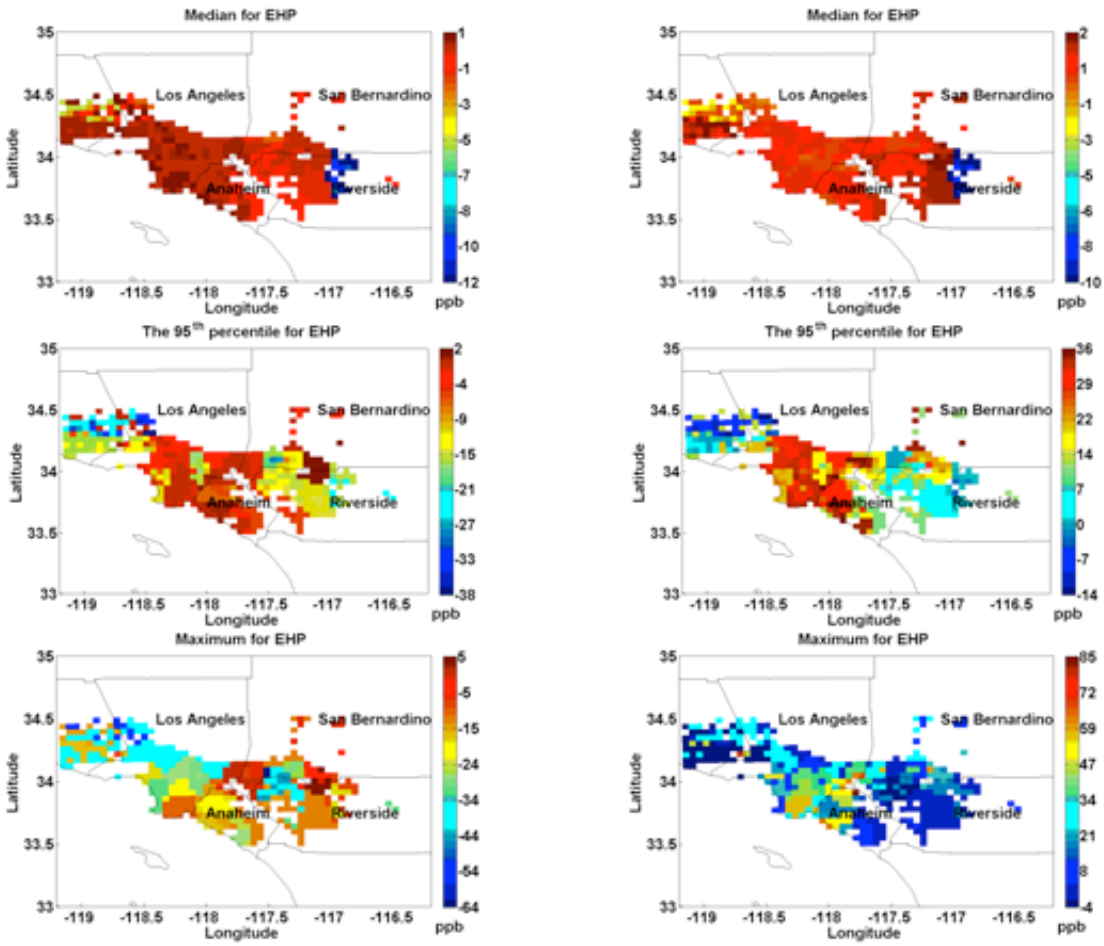

Figure 4-12. Difference between using fixed meteorology station and using the closest meteorological station. (Left panels fixed Pomona station; right panels fixed station)

4.3. Short range impacts of DG units

This section presents the spatial distribution of short range impacts of DG units for the EHP and PW2010 penetration scenarios. The thermal efficiency of the power plant used in this section is taken to be 0.33, the heat recovery efficiency is 0.5. The emission factor here is the same as section 4.1. The locations of the 26 meteorological stations used to derive the meteorology are presented in Figure 4-1.

As described in section 2, we used 5 km by 5 km grids for the South Coast Air Basin in California, to place three types of DG units into those grids. We ignored those grids without DG units. The numbers of final grids containing DG units turn out to be 426 grids for the EHP scenario and 224 grids for the PW2010 scenario. Each grid has different total DG units, different mix of the three types of DG units and different locations for DG units within it. Figure 4-13 and Figure 4-14 show the distributions of DG units for EHP and PW2010 scenarios respectively.

We see that in the EHP scenario, most DG units in area '4' are medium and large size Area '3', area '2' and area '1' have a mix of all three sizes DG units; area '3' and '2' have high

penetrations of small and medium size DG units. Since total DG units needed in the PW2010 scenario are much less than those in the EHP scenario, they are sparsely distributed although they have the same technology mix. Both EHP and PW 2010 scenarios have high penetrations of medium size DG units.

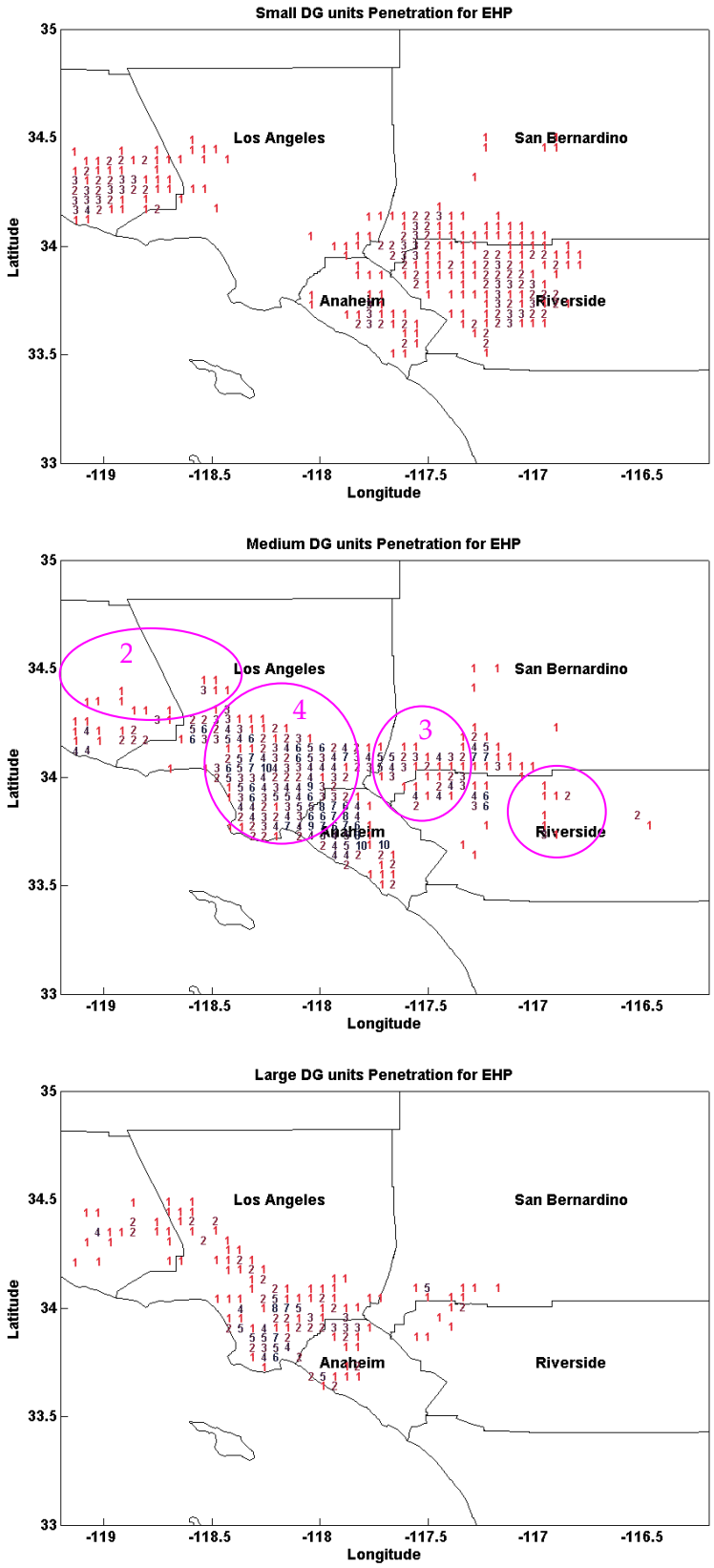

Figure 4-13 Penetration of DG units for the EHP scenario.

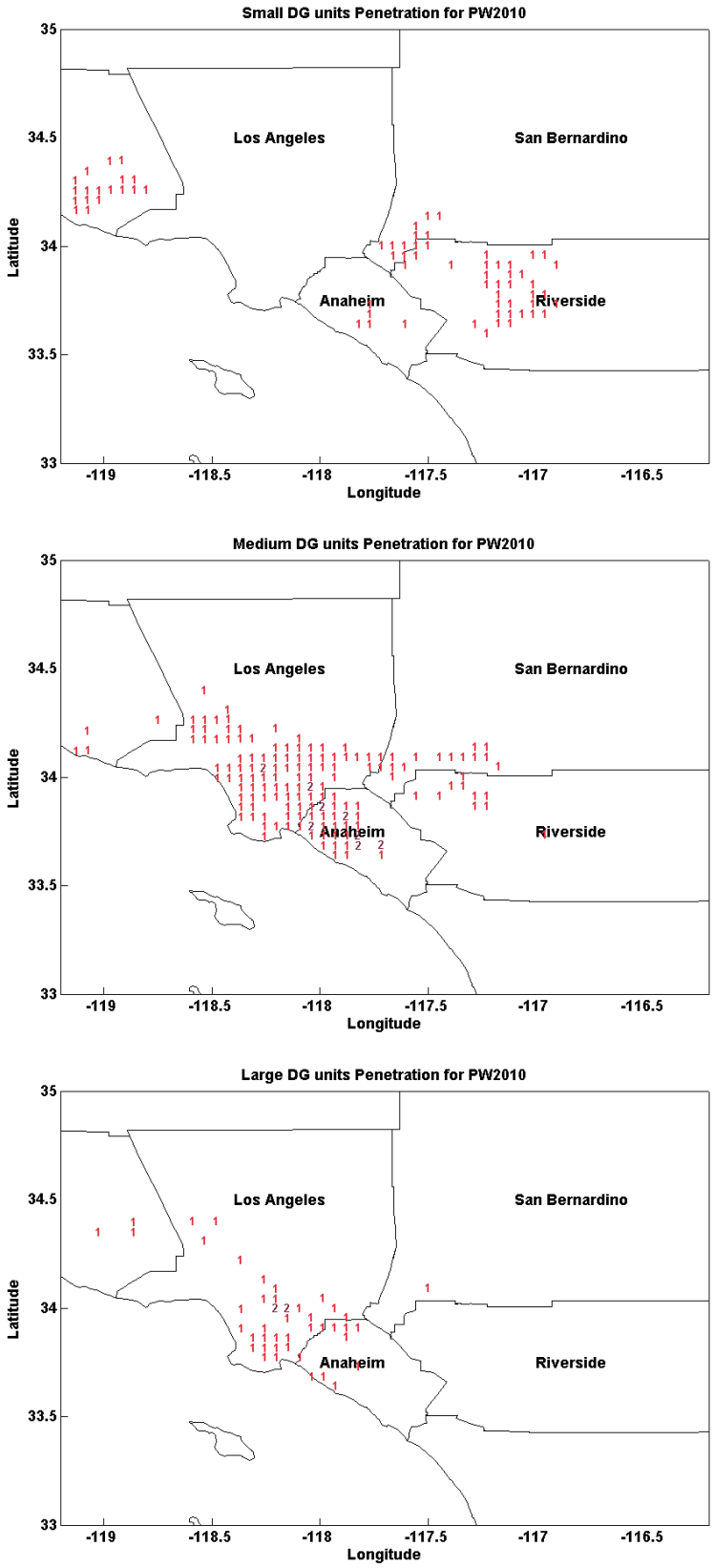

Figure 4-14 Penetration of DG units for the PW2010 scenario.

4.3.1. Hourly averaged concentration

We treated DG units in each grid as independent of each other. This assumption is based on calculations of the minimum, maximum and average distances between DG units in each grid. These values turn out to be 250 m, 5977 m and 2399 m respectively for the EHP scenario, and 269 m 3386 m, and 1727 m respectively for the PW2010 scenario. There are only 3 distances between 250 m and 300 m, and all the other distances are above 300 m. We also calculated the maximum and average distances where the maximum hourly daytime concentration, 10 ppb (10 ppb for large DG units), occurs. These distances turned out to be 300 m and 65 m. During nighttime, the maximum concentrations occur at larger distances from the source but the concentration itself is much lower than that during daytime. Thus, most DG units are unlikely to affect each other's hourly maximum concentrations, and can be considered to be independent. This assumption avoids the large computational effort required to superimpose concentrations associated with the DG units in the grid.

Furthermore, in order to test the influence of one DG on the other, we ran AERMOD for a 5 km×5 km grid with the maximum number of DG units within it (9 of them are medium DG units and 2 of them are large DG units). Meteorological files for Central LA station were used since it is closest to this grid. The exit gas temperature is 423 K. The emission factor for NO_x is 120 g/MWh for medium DG units and 101 g/MWh for large DG units. One hour maximum concentration for the year 2007 is plotted in the following figures in ppb. We used a polar coordinate system with 23 arcs. The closest arc distances are 0, 10, 20, 30, 40, 50, 75, and 100 m away from the source. The furthest arc distance is 3000 m. The receptors are 5 degrees apart on each arc.

The concentration estimates for individual DG units are shown in Figure 4-15. For the medium DG unit, the maximum concentration is 26 ppb, and is 14 ppb for the large unit. The figure shows a rapid drop off of concentration with downwind distance.

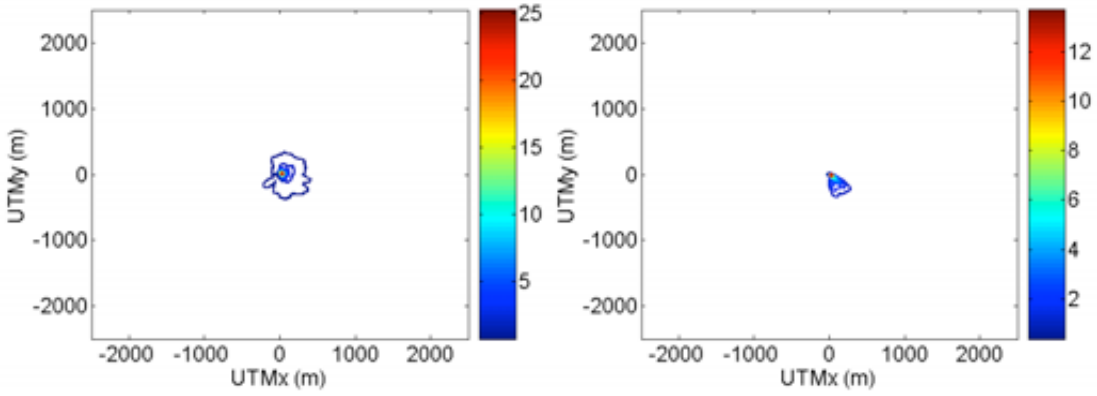

Figure 4-15. One hour maximum NO_x concentration in ppb for medium (left) and large (right) DG units using Polar co-ordinate

Next, we analyzed the mutual influence of DG units using results obtained from the polar co-ordinate system. The origin for each DG unit is placed according to the locations calculated in Chapter 2. In order to add concentrations from different sources, we first interpolated the

concentrations from the polar co-ordinate to the Cartesian coordinate system. The resolution of the Cartesian co-ordinate was taken to be 10 m for the grid to avoid unnecessary reduction of maximum concentrations from the polar coordinate and to compare results in Figure 4-15. Then we accumulated the interpolated concentrations on the Cartesian coordinate.

In Figure 4-16,the maximum concentration is 27 ppb after accumulation of impact due to individual DGs. The difference is only 4% compared to the maximum concentration of individual medium DG units (26 ppb) in the previous figure.

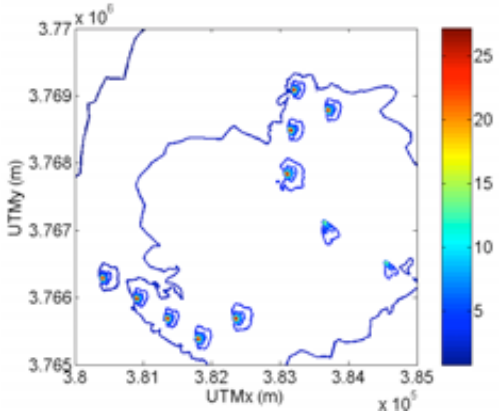

Figure 4-16. Accumulation of one hour maximum NO_x concentration in ppb from polar co-ordinate to Cartesian co-ordinates

These results indicate that the mutual influence between DG units is negligible. Besides, running AERMOD with Cartesian coordinate of 10 m resolution is time-consuming. The total number of grids is 251001 (= 501×501), since the domain is 5 km×5 km. It took 3 days to run just one grid. Moreover, Cartesian coordinates with 10 m resolution may still not capture the maximum concentration. Using polar coordinates can save computing time because the total number of receptors is 1656 (= 23×72), which is reduced about 150 times less than the Cartesian coordinate system. The maximum concentration is more likely to be captured with the polar co-ordinate because receptors are only 5 degrees apart from each other.

After convincing ourselves that DG units within a grid are independent of each other, we collected the maximum hourly averaged concentration of each hour of the entire 2007 year, and assumed the hourly maximum concentration could occur anywhere within the grid. Therefore, we could combine all the maximum hourly averaged concentrations to compute statistics for all grids. For example, if there is a grid with a total of 5 DG units, say 2 small DG units, 2 medium DG units, and 1 large DG units, we have 5 × 8760 data set, consisting of 2×8760 data sets for two small DG units, 2×8760 data sets for two medium DG units, and 1×8760 data set for one large DG units. Then we use the 5 × 8760 data sets to compute statistics for the grid. Figure 4-17 shows the results for both EHP and PW2010 scenarios. As shown before in Table 4-2, the maximum median concentration is 12 ppb related to Banning Airport meteorology, because the highest median wind speed there is 4.4 m/s. The maximum 95th percentile concentration is 42 ppb associated with Santa Clarita meteorology with the high 95th percentile wind speed of 6.6

m/s. The highest maximum concentration is 90 ppb, which is related to the high wind speed of 15 m/s at the Fontana meteorological station.

Figure 4-17 indicates that for the EHP scenario, area '1' has the highest median concentration because DG units in this area are a mix of small and medium sizes (Figure 4-13). The meteorological station associated with it is Banning Airport (Figure 4-1), where the median wind speed is the highest at 4.4 m/s. The median concentration for small and medium DG units associated with Banning Airport row are the highest at 12 ppb and 8 ppb respectively (Table 4-2). The 95^{th} percentile concentrations for these two types of DG units are also high, 21 ppb and 32 ppb respectively, which result from the high 95^{th} percentile wind speed at Banning Airport, 7.9 m/s. Area '2' has the highest 95^{th} percentile concentration while area '3' has the highest maximum concentration where the Fontana station is located. Area '4' experiences the lowest median and 95^{th} percentile concentrations because large DG units in this area are coupled with low wind speeds. In summary, the maximum hourly concentrations occur in area '3', while areas '1' and '2' have relatively high median concentrations.

The hourly averaged concentrations for the EHP and PW2010 scenarios are similar, and they have almost the same magnitudes for median, the 95^{th} percentile and maximum concentrations. This is because these statistics do not depend on the total power increase in each grid. However, the grid averaged concentrations do depend on the total power output in a grid. This is discussed next.

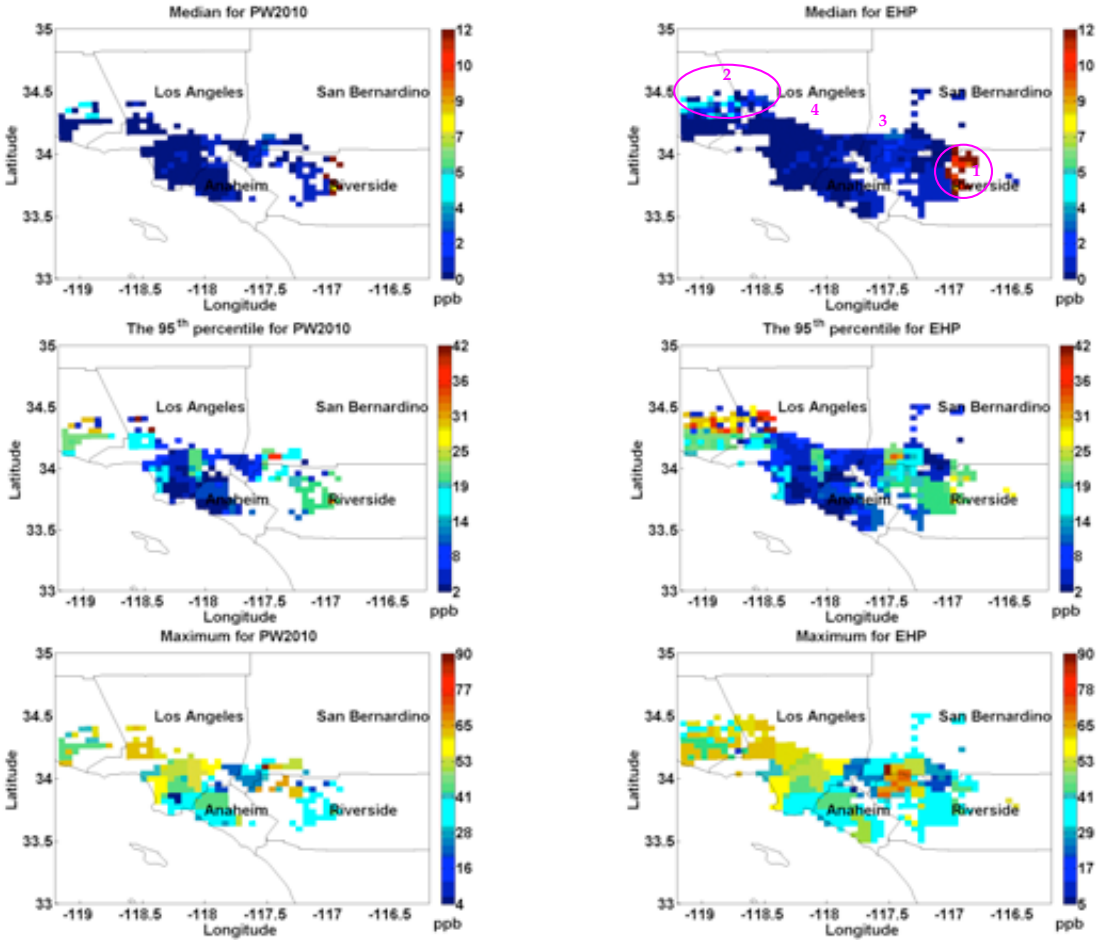

Figure 4-17. Map of Grid median, the 95th percentile and maximum hourly averaged nominal concentrations

4.3.2. Grid-averaged and maximum annually-averaged concentration

To consider grid-averaged and maximum annually averaged concentration, we cannot assume that the annually averaged concentrations from DG units within a grid are independent of each other, and we cannot assume that the grid squares are independent of each other either. There are two ways of computing annually averaged concentrations for all grids over the domain: 1). Run AERMOD for each DG unit over the domain separately to get annually averaged concentrations and then simply add these concentrations; 2). Run AERMOD for all DG units over the domain, and let AERMOD do the adding. The computational effort associated with the second method is prohibitive. The first method is much more efficient because we only need to compute the contributions for three different types of DG units over the domain because the normalized concentrations are the same for each type. When calculating the nominal concentrations, we only need to multiply the normalized concentrations for each DG type by different emission rates and then add the concentrations. The computational efficiency can be increased by using a polar coordinate system to take advantage of the fact that high concentration gradients occur only close to the source.

Considering a 5 km by 5 km grid in the domain, the annually averaged concentrations from the polar coordinate system are processed to get grid-averaged and grid-maximum annually averaged concentrations using the steps:

1. Compute the annually averaged concentrations for a power plant (say 625 kW) in the current grid using a fine scale polar coordinate system. This will give concentrations as a function of (rho, theta).
2. Lay out a 10 m by 10 m Cartesian grid on the current 5 km by 5 km grid with coordinates (x_i, y_i)
3. Locate the power plant at say (X_1, Y_1)
4. For each pair of (X_1,Y_1) and (x_i, y_i), compute (rho_i, $theta_i$)
5. Use bilinear interpolation of concentrations calculated in step 1 to compute concentrations at (x_i, y_i)
6. Use the steps 1-5 to accumulate concentrations associated with other power plants within the current grid located at (X_i, Y_i):

$$AAC\_Ind = \sum_{dgtype=1}^{3} \sum_{dg=1}^{totaldg(dgtype)} AAC_{dgtype} * Q_{dg} \qquad (4.1)$$

   where *AAC_Ind* is the annually averaged nominal concentration everywhere within the current grid in the Cartesian coordinate system without considering DGs outside it, and *AAC* is the annually averaged and normalized concentration of three types of DG units.

7. Compute grid-averaged and grid-maximum annually averaged concentrations (*AAC_GridAvg_Ind* and *AAC_GridAvg_Ind* respectively) for the current grid without considering power plants outside it:

$$AAC\_GridAvg\_Ind = \text{mean}(AAC\_Ind) \qquad (4.2)$$

$$AAC\_GridMax\_Ind = \max(AAC\_Ind) \qquad (4.3)$$

8. Use the steps 1-5 to compute concentrations associated with a power plant (idg) outside the current grid. The difference here is that in step 2 we use an adaptive grid-size Cartesian grid according to the distance between the center of the current grid and the power plant outside it.
9. Compute the grid-averaged annually averaged concentration $(AAC\_GridAvg)_{idg} * Q_{idg}$ due to the power plant in step 8.
10. Use steps 8-9 to accumulate grid-averaged annually averaged concentrations associated with all power plants outside the current grid:

$$AAC\_GridAvg\_Dep = \sum_{idg=1}^{\text{total DG units outside the current grid}} (AAC\_GridAvg)_{idg} * Q_{idg} \qquad (4.4)$$

11. Compute final concentrations by adding the contributions from both step 7 and step 10:

$$AAC\_Grid\_Avg = AAC\_GridAvg\_Ind + AAC\_GridAvg\_Dep \qquad (4.5)$$

$$AAC\_Grid\_Max = AAC\_GridMax\_Ind + AAC\_GridAvg\_Dep \quad (4.6)$$

where AAC_Grid_Avg and AAC_Grid_Max are final grid-averaged and grid-maximum annually averaged concentrations for the current grid.

12. Repeat steps 1-11 to compute the final grid-averaged and grid-maximum annually averaged concentrations for all grids within the domain.

Figure 4-18 shows the annually averaged concentration for a grid of high DG density. The left panel shows the true concentrations which account for all DGs placed in the domain without using the approximation in the step 11, the middle panel shows the concentrations which also account for all DGs but using the approximation in the step 11, and the right panel shows the concentrations which assume the grid squares are independent of each other. As we can see the assumption that the grid squares are independent of each other fails, which will underestimate the annually averaged concentration substantially. However, our approximate shows agreement with the magnitudes of the true concentrations, therefore we can use it to calculate the grid-averaged and grid-maximum concentrations.

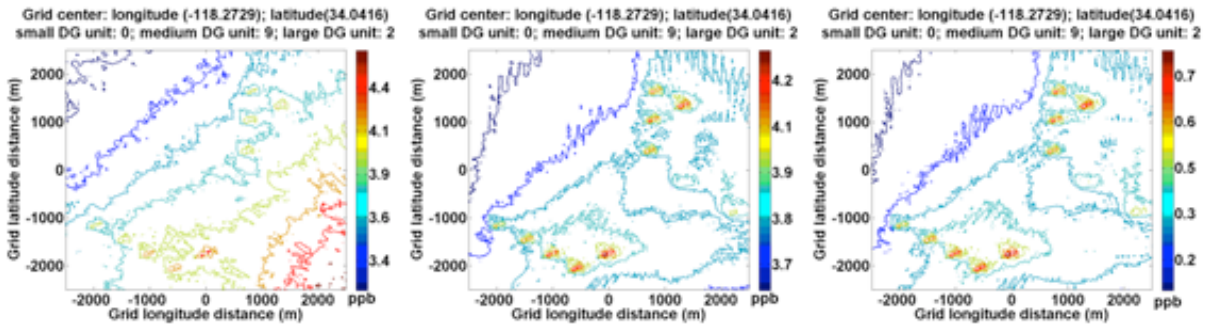

Figure 4-18. Annually averaged concentration for selected grids with high DG units penetration

Figure 4-19 shows the grid-averaged and maximum annual concentrations for the EHP and PW2010 scenarios. The right panels corresponding to the EHP scenario show that the grid maxima are similar to the median hourly averaged concentrations shown in the upper-right panel of Figure 4-17. But their magnitudes are less than the median hourly averaged concentrations. The high values of annual concentrations occur at almost the same locations as the high median hourly averaged concentrations: area '1' and area '2' circled in Figure 4-17 and Figure 4-19. However annually averaged concentrations account for impacts from all distributed DG units, we also see high grid maxima in area '4' where there is a high penetration of DG units.

The grid averaged annually averaged concentrations for EHP scenario are smaller than the annually averaged maxima because they are obtained by averaging the annual concentrations over the 5 km grid square. Area '5' has the maximum grid-averaged concentrations because this area has high DG unit penetration for medium and large DG units.

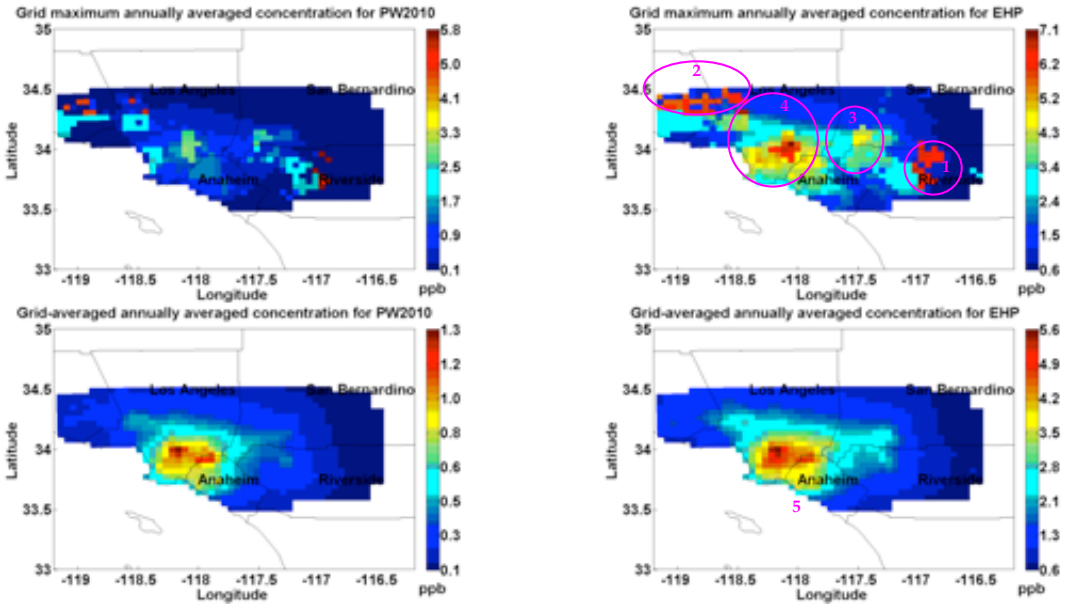

Figure 4-19. Grid maximum and grid-averaged annually averaged nominal concentrations for EHP and PW2010 scenarios

The annually averaged grid maximum concentrations for the PW2010 scenario show a similar pattern to the EHP results, not only in terms of magnitude but also in terms of location. Although area '5' has the highest grid-averaged annually averaged concentration, its magnitude is about four times less than that for EHP scenario because the PW2010 scenario has a lower power increase, that is, a lower emission increase than EHP scenario.

These results indicate that the grid maximum annually averaged concentrations are governed by meteorology and the DG technology mix. On the other hand, the grid averaged annually averaged concentration is dominated by the total emissions or total power within an area. Note that the grid averaged annual concentration is a measure of the exposure to pollutants within the grid square.

4.4. Concentrations of primary criteria pollutants

In this section we present the results on the impact of the two DG penetration scenarios on the concentrations of the primary criteria pollutants: Carbon monoxide (CO), Nitrogen dioxide (NO_2), Sulfur dioxide (SO_2), Particulate matter (PM). We assume that all the emitted NO_x is converted to NO_2, which results in the maximum possible concentration. AERMOD does have two options, the OLM (Ozone limiting method) and the PVMRM (Plume volume molar ratio Method)) to estimate the fraction of NO_x converted to NO_2. But these methods require background ozone concentrations, which were not available to us.

Table 4-3 lists the description of the two DG penetration scenarios reported in Samuelsen et al. (2005). Table 4-4 lists the absolute increase of primary criteria pollutant emissions showing that the PW2010 scenario has a smaller absolute increase of emissions than the EHP scenario.

Table 4-5 lists the emission factors appearing used by UCI (Samuelsen, 2005) to construct the emission inventories used in this study. For comparison, it also includes emission factors reported in the literature. Table 4-6 lists the equivalent emission factors used in this study. These were obtained by distributing the absolute increase of pollutant emissions among the three types of DG units used in this study. These factors are within the range of values shown in Table 4-5.

Table 4-3. Summary of the key features of the spanning scenarios

Scenarios	Description	Increased power demand	Spatial distribution	Technology mix %
PW2010	Population weighted 2010	20%	Population-weighted	39 (Advanced gas turbine) 52 (Conventional gas turbine) 9 (Fuel cell)
EHP	Extra high penetration	20% of total power met by DG	Population-weighted	39 (Advanced gas turbine) 52 (Conventional gas turbine) 9 (Fuel cell)

Table 4-4. Basin-wide absolute increase of primary criteria pollutant emissions per each scenario (tons/day)

Scenarios	CO	NO_x	SO_x	PM
PW2010	8.19	2.54	0.10	0.61
EHP	44.35	13.76	0.54	3.01

Table 4-5. Emission factors from literature:

DG Type	η_t	Emission Factor (g/MWh)				Source
		CO	NO_x	SO_x	PM	
Diesel Internal combustion engine (ICE)	0.44	-	7700	-	1400	Heath et al. 2007
Natural gas-ICE	0.35	-	1500	-	220	Heath et al. 2007
Natural gas turbine	0.28	-	560	-	41	Heath et al. 2007
Microturbine	0.25	-	320	-	38	Heath et al. 2007
Low-T fuel cell	0.36	-	32	-	28	Heath et al. 2007
Micro-turbine generators	0.27	45	32	5	38	Samuelsen et al. 2005
Gas turbine (<3MW)	0.24	142	210	5	42	Samuelsen et al. 2005
Gas turbine (>3Wm)	0.36	91	57	3	28	Samuelsen et al. 2005
Natural gas-ICE	0.32	803	201	4	32	Samuelsen et al. 2005
Low temperature fuel cell	0.36	45	32	3	28	Samuelsen et al. 2005
High temperature fuel cell	0.48	45	32	3	21	Samuelsen et al. 2005
Stirling engine	0.27	45	32	5	38	Samuelsen et al. 2005
Hybrid fuel cell gas turbine systems	0.70	45	32	2	15	Samuelsen et al. 2005
Micro-turbine	0.27	1293	635	9	41	Allison et al. 2002
Advanced turbine system	0.36	1179	494	9	32	Allison et al. 2002

Conventional turbine	0.28	685	562	14	41	Allison et al. 2002
Gas powered ICE	0.35	3629	1452	5	218	Allison et al. 2002
Diesel ICE	0.44	13608	7711	136	1361	Allison et al. 2002
PEM fuel cell	0.36	0	9	5	0	Allison et al. 2002
Solid oxide fuel cell	0.40	0	0	0	0	Allison et al. 2002

Table 4-6. Emission factors in this study:

DG Type	η_t	Emission Factor (g/MWh)			
		CO	NO_x	SO_x	PM
Advanced gas turbine	0.33	523	120	4	25
Conventional gas turbine	0.33	225	101	4	23

Sections 4.4.1 and section 4.4.2 present results on the contributions of the DG emission increases to the hourly averaged and annually averaged concentrations. Section 4.4.3 presents results on how these increases might affect air quality in the South Coast Air Basin.

4.4.1. Maximum hourly averaged Concentrations

Figure 4-20 shows the maximum hourly concentration of all four primary criteria pollutants for the EHP scenario (left panels) as well as the relevant statistics (right panels). Figure 4-21 shows the maximum hourly concentration of all four primary criteria pollutants for the PW2010 scenario (left panels) as well as their statistics (right panels).

The maximum hourly averaged concentrations of CO for both scenarios are 117 ppb from medium DG units (because a medium DG unit has a higher emission factor for CO, 523 g/MWh), located near the Riverside meteorological station with a high maximum wind speed of 11.1 m/s (Table 4-2). However the maximum hourly averaged concentrations of NO_2, SO_2 and PM, 19 ppb, 0.5 ppb and 8 $\mu g/m^3$ respectively for both scenarios, are associated with large DG units located close to the Fontana meteorological station with the highest maximum wind speeds of 15 m/s (Table 4-2). As discussed in section 4.3.1, the maximum hourly averaged concentrations are affected most by the meteorology and the technology mix. The total increase in power demand or total absolute increase of emissions has little effect on the maximum hourly averaged concentrations. Since both scenarios use the same meteorological data set from the 26 meteorological stations, and both of them have the same technology mix as shown in Table 4-3, the similar results for both scenarios are not surprising.

We should point out that small DG units and medium DG units are driven by advanced gas turbines, but large DG units are driven by conventional gas turbines. Table 4-6 shows that both the emission factors for SO_2 and PM are similar for the two types of turbine which result in similar concentration patterns for SO_2 and PM shown in the maximum panels of Figure 4-17. The situation is different for CO and NO_2 for which advanced gas turbines have larger emission factors than conventional gas turbines. Thus, the area of maximum hourly concentrations for CO and NO_2, denoted by the dark red areas of Figure 4-20 and Figure 4-21, occur where medium DG units have the highest penetration.

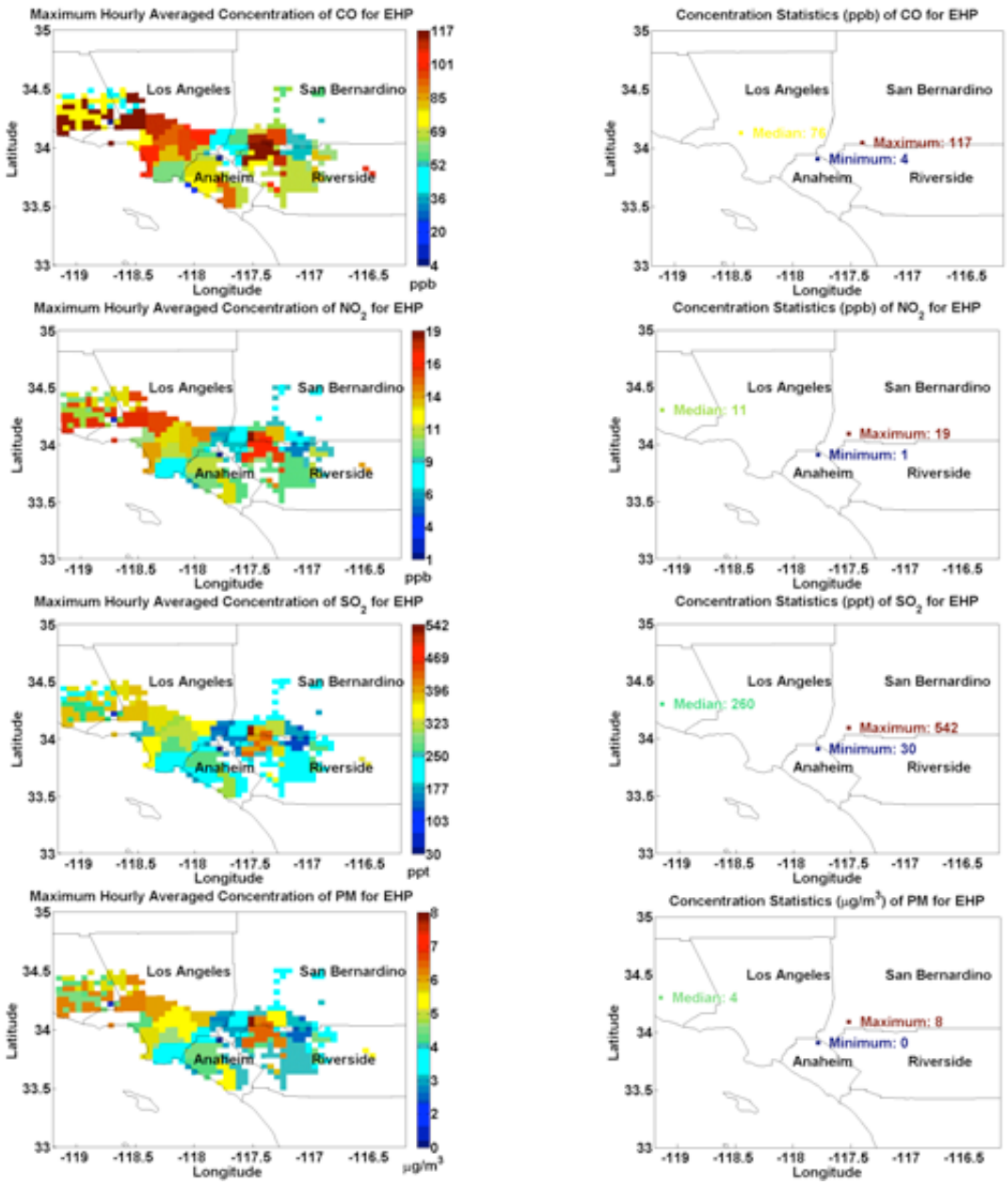

Figure 4-20. Maximum hourly averaged concentration of criteria pollutants for EHP scenario.

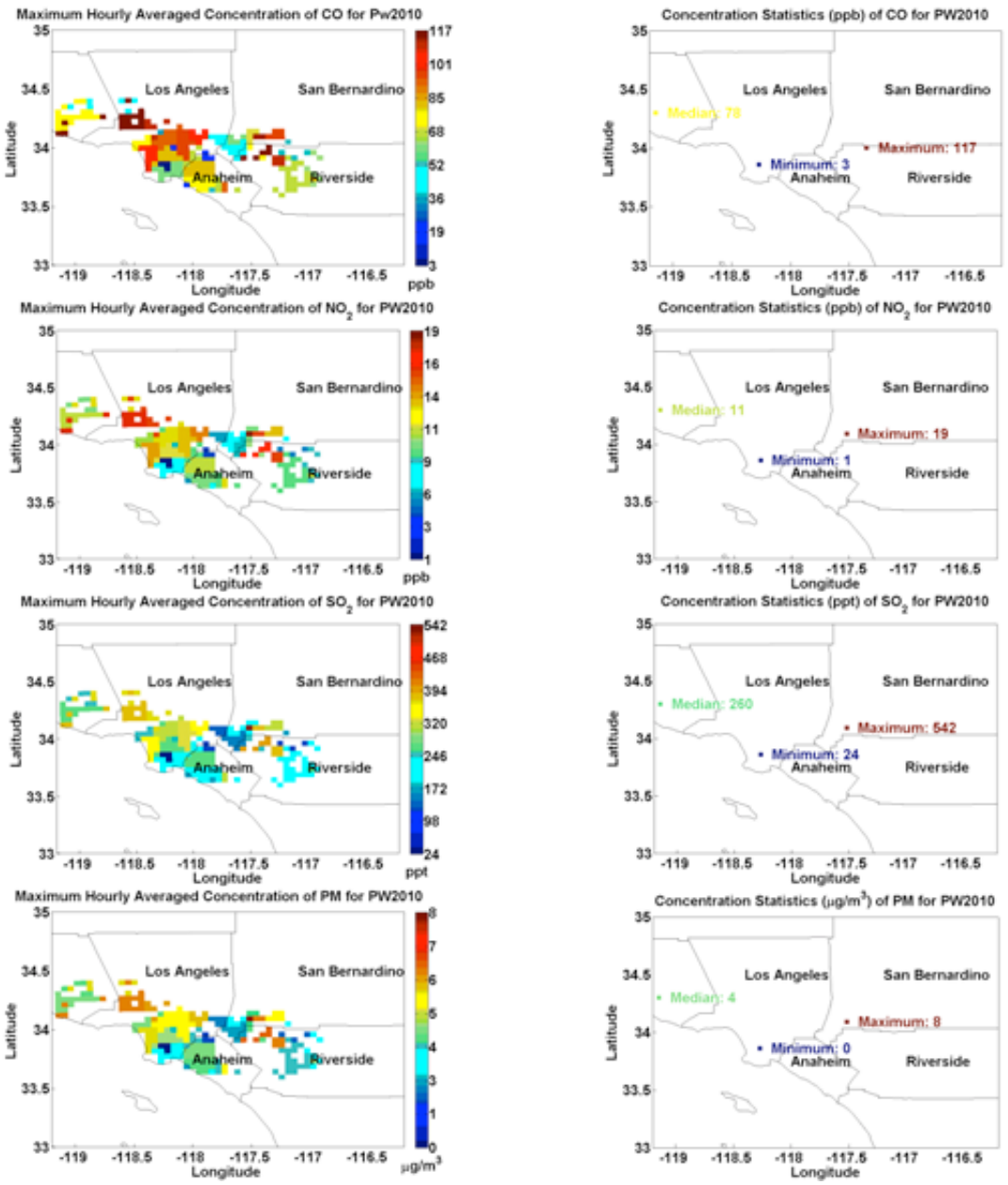

Figure 4-21. Maximum hourly averaged concentration of criteria pollutants for PW2010 Scenario

Table 4-7 lists the highest, median and lowest increases of maximum hourly averaged concentrations due to DG unit penetration, and where they occur. The table also lists current National Ambient Air Quality Standards and California Ambient Air Quality Standards of 1-hour averages for the criteria pollutants, as well as the monitored levels of the South Coast Air Basin of 2007. Based on 2007 levels, if we add the concentrations caused by DG penetration to current levels, CO and SO_2 concentrations will not violate either California or National standards. However, the range of 2007 levels of NO_2 (0.06 – 0.12 ppm) is close to California

standards (0.18 ppm), and covers National standards (0.08 – 0.1 ppm). Thus, DG penetration has the potential of increasing the probability of the air quality levels being violated.

Table 4-7. Statistics of maximum hourly averaged concentrations and the locations of the criteria pollutants for PW2010 and EHP scenarios and EPA standard and current level of the criteria pollutants

Pollutants	Scenario	Maximum		Median		Minimum		Standard		2007 South Coast Level[##]	
		Conc.	Nearest Met. Station	Conc.	Nearest Met. Station	Conc.	Nearest Met. Station	CAAQS[*]	NAAQS[#] (Primary)	Range	Maximum Monitoring Station
CO	PW2010	117 (ppb)	Riverside	78 (ppb)	Reseda	3 (ppb)	Long Beach	20 (ppm) 23 (mg/m^3)	35 (ppm) 40 (mg/m^3)	2-8 (ppm)	Lynnwood
	EHP			76 (ppb)	West LA	4 (ppb)	Pomona				
NO_2	PW2010	19 (ppb)	Fontana	11 (ppb)	Reseda	0.8 (ppb)	Long Beach	0.18 (ppm) 339 ($\mu g/m^3$)	100 (ppb)	0.06-0.12 (ppm)	Azusa
	EHP					1 (ppb)	Pomona				
SO_2	PW2010	542 (ppt)		260 (ppt)		24 (ppt)	Long Beach	0.25 (ppm) 655 ($\mu g/m^3$)	-	0.01-0.11 (ppm)	Long Beach
	EHP					30 (ppt)	Pomona				
PM	PW2010	8 ($\mu g/m^3$)		4 ($\mu g/m^3$)		0.4 ($\mu g/m^3$)	Long Beach	-	-	-	-
	EHP					0.5 ($\mu g/m^3$)	Pomona				

CAAQS[*]: California Ambient Air Quality Standards (CARB, 2010)

NAAQS[#]: National Ambient Air Quality Standards (EPA, 2010)

[##]: AQMD 2007 Air Quality Tables (AQMD, 2009b)

Samuelsen (2005) reported different maximum hourly averaged concentrations for these two scenarios, because their maximum hourly averages are grid averages, which do depend on total power increases within a grid. The maximum concentrations reported here correspond to individual DG units, whose short impacts are not likely to overlap.

Table 4-8 compares the EHP hourly maximum concentrations from this study with those from Samuelsen (2005). As expected, the NO_2 concentrations from this study are higher than the grid averaged values reported in Samuelsen. But the maximum concentrations of PM are much lower than in Samuelsen because this study does not consider secondary PM formed in chemical reactions.

Table 4-8 Comparison of highest maximum hourly averaged concentration with Samuelsen's Results

Studies	PM (μg/m^3)		NO_2 (ppb)	
	PW2010	EHP	PW2010	EHP
Current Studies	8		19	
Samuelsen's Studies(Samuelsen et al. 2005)	18	20	3	9

4.4.2. Grid averaged and grid maximum annually averaged concentrations

Before presenting the grid averaged and grid maximum annual concentrations, we provide relevant information on the spatial distribution of power and emission increases for the two DG penetration scenarios. .

The left panels of Figure 4-22 show the distribution of power increases in each of the 5 by 5 km grids for both scenarios, and the right panels show relevant statistics. Area '5' has the largest total power increase corresponding to the high DG unit penetration (see Figure 4-13 and Figure 4-14). The grid located near the Lynnwood meteorological station has the maximum absolute power increases of 105 MW and 28 MW for the EHP and the PW2010 scenarios respectively. Table 4-9 lists the maximum, median and minimum power increases for both scenarios and their locations.

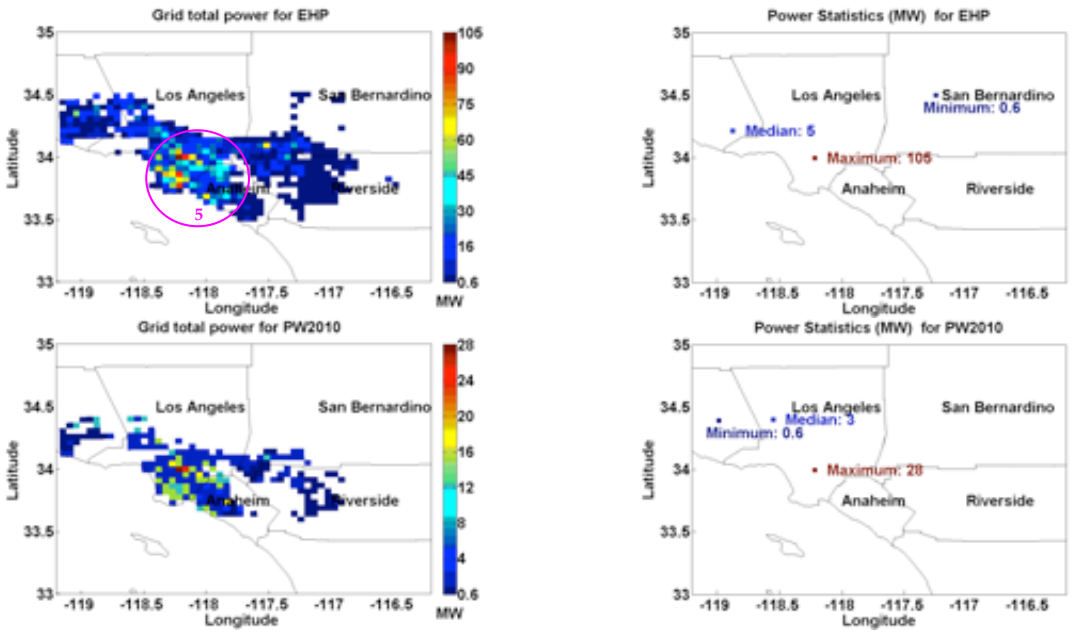

Figure 4-22. Grid total Power for PW2010 and EHP scenarios

Table 4-9. The statistics of power increase and the locations for PW2010 and EHP scenarios

Scenario	Maximum		Median		Minimum	
	Power (MW)	Nearest Met. Station	Power (MW)	Nearest Met. Station	Power (MW)	Nearest Met. Station
PW2010	28	Lynnwood	3	Santa Clarita	0.6	Santa Clarita
EHP	105	Lynnwood	5	Reseda	0.6	Crestline

The left panels of Figure 4-23 and Figure 4-24 show that area '5' also has the largest total emissions for both scenarios. The right panels of Figure 4-23 and Figure 4-24 show the emission statistics for the four pollutants in the two scenarios. The maximum increases of CO, NO_x SO_x and PM for the EHP scenario are 603 kg/day, 257 kg/day, 10 kg/day and 58 kg/day respectively, and those for PW2010 are 166 kg/day, 68 kg/day, 3 kg/day and 15 kg/day respectively. Table 4-10 lists the details of the maximum, median and minimum increases of pollutants, including their locations.

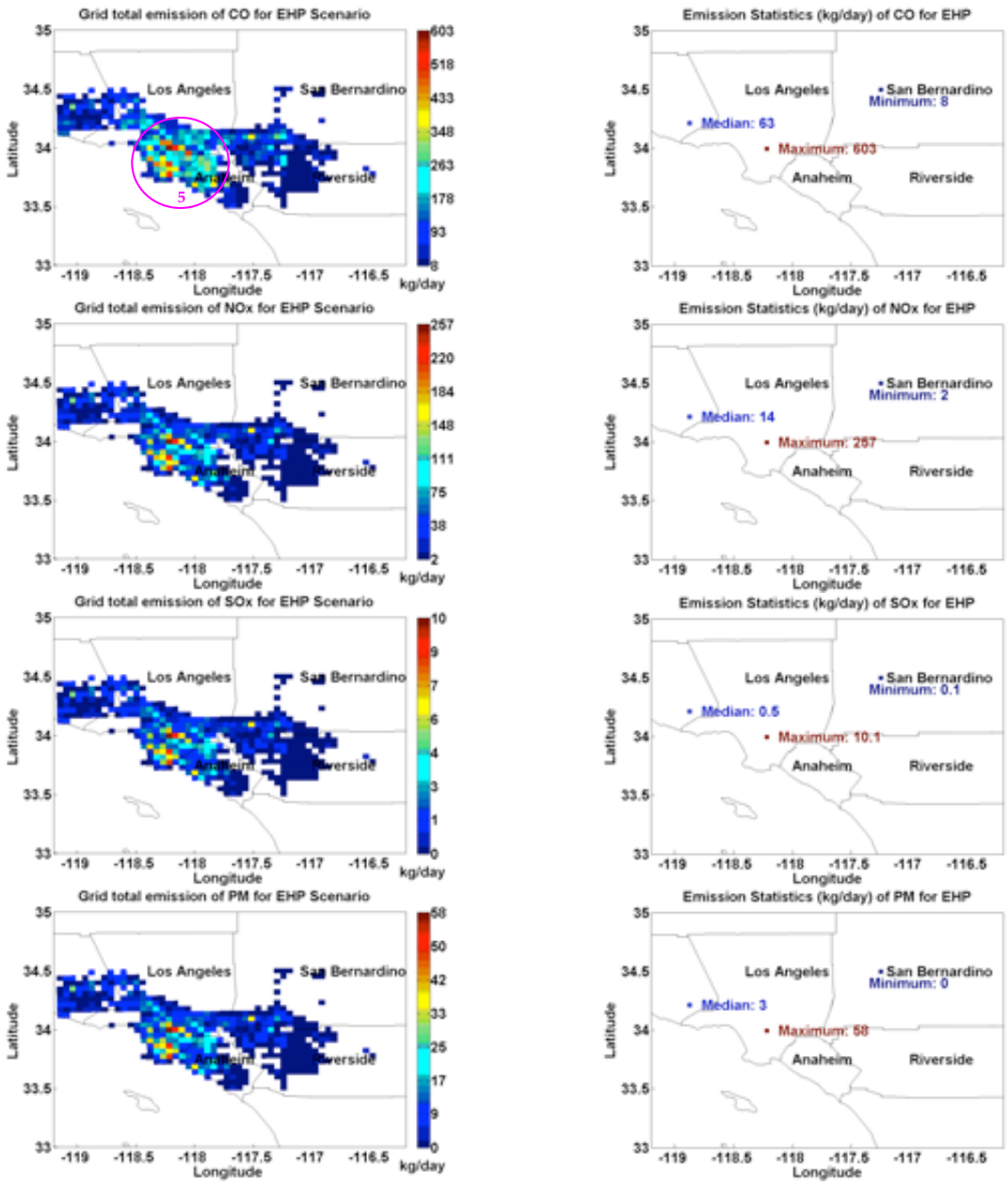

Figure 4-23. Grid total emissions for EHP scenario

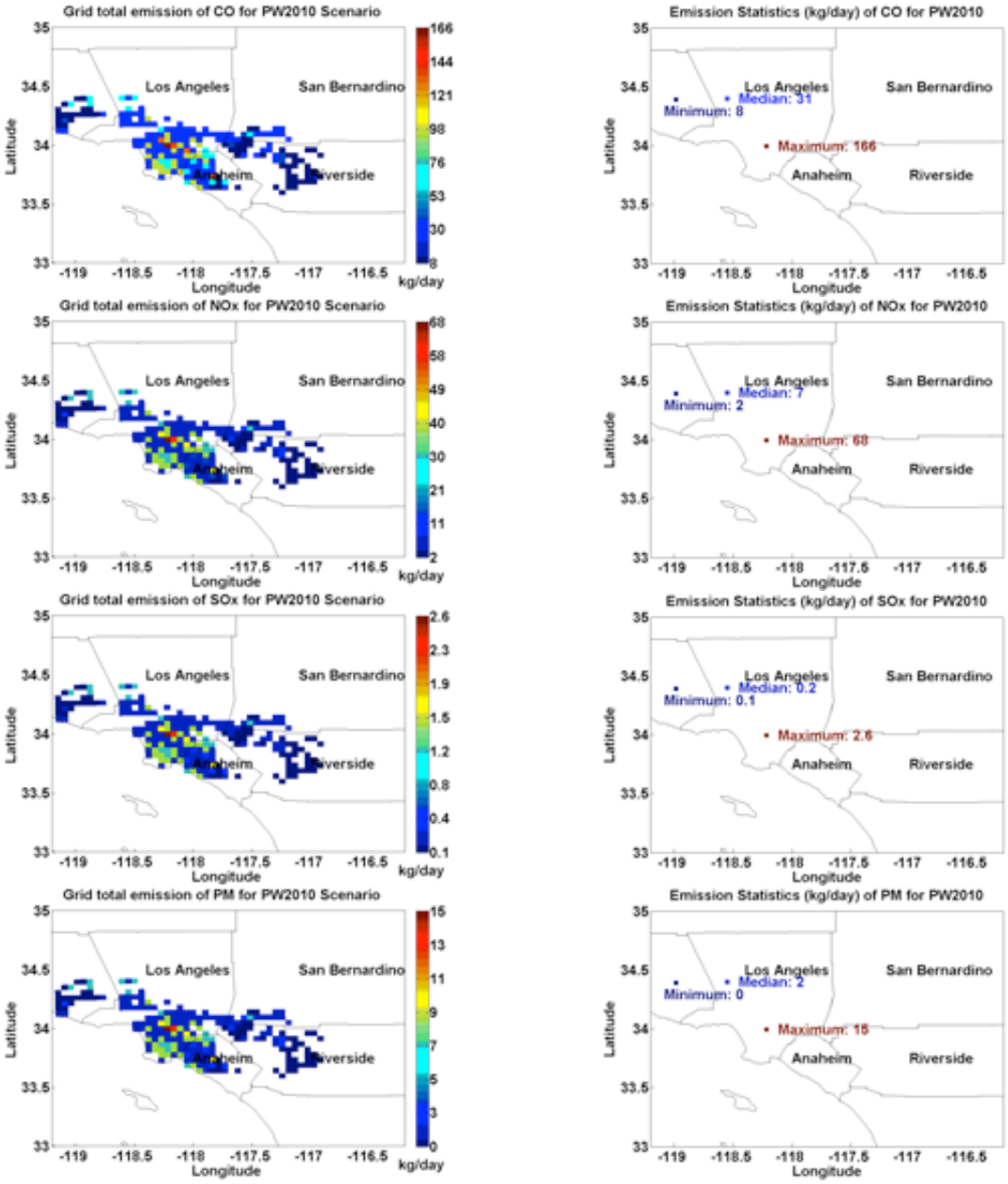

Figure 4-24. Grid total emissions for PW2010 scenario

Table 4-10. The statistics of emission increase and the locations for PW2010 and EHP scenarios

Pollutants	Scenario	Maximum		Median		Minimum	
		Emission (kg/day)	Nearest Met. Station	Emission (kg/day)	Nearest Met. Station	Emission (kg/day)	Nearest Met. Station
CO	PW2010	166	Lynnwood	31	Santa Clarita	8	Santa Clarita
	EHP	603		63	Reseda		Crestline
NO_2	PW2010	68		7	Santa Clarita	2	Santa Clarita
	EHP	257		14	Reseda		Crestline
SO_2	PW2010	3		0.2	Santa Clarita	0.1	Santa Clarita
	EHP	10		0.5	Reseda		Crestline
PM	PW2010	15		2	Santa Clarita	0	Santa Clarita
	EHP	58		3	Rededa		Crestline

Figure 4-25 shows the grid averaged annually averaged concentrations of the four primary criteria pollutants for the EHP scenario. The left panels of Figure 4-25 indicate that the high grid-averaged concentrations occur in area '5', which are similar to those of the lower right panel of Figure 4-19: The grid averaged concentration is affected most by the total emissions in surrounding grids. The right panels of Figure 4-34 show the concentration statistics for the EHP scenario. The highest grid averaged annually averages are located exactly the same place, near the Lynnwood meteorological station, where the highest power is demanded. The lowest grid averaged annually averages are also located the same place, the southeast corner of the modeling domain where these is no DG penetrations nearby.

Figure 4-26 shows the grid maximum annually averaged concentrations of all four primary criteria pollutants for EHP scenario. As discussed in section 4.3.2, the grid maximum concentration is affected most by the technology mix and the meteorology. High grid maximum concentrations always associate with high wind speeds and those DG types which have poor dispersion. Therefore areas '1' and '2' have the red on the map in the left panels of Figure 4-26, and the results are similar to the upper right panel of Figure 4-19. The right panels of Figure 4-26 show the statistics of the grid maximums, now we see that the largest grid maximum annually averaged concentrations for all pollutants occur near the Banning Airport meteorological station where the wind speed is the largest in terms of median, the 95th percentile, and maximum (Table 4-2).

Figure 4-27 shows the grid averaged annual concentrations of the four primary criteria pollutants for the PW2010 scenario. For this scenario, the highest grid averages of all four pollutants occur near the Lynnwood meteorological station, as seen in the right panels of Figure 4-27.

Figure 4-28 presents the grid maximum annual averages for the four pollutants for PW2010 scenario. The grid maximum concentration results are quantitatively similar to the results presented in Figure 4-26 for EHP scenario, because the grid maximum concentrations are related to the technology mix and the meteorology. The largest grid maximums are located again near the Banning Airport meteorological station.

Table 4-11 lists the maximum, median and minimum of the grid maximum annually averaged concentrations of the four criteria pollutants for both scenarios together with their locations. The tables also list the National and California Ambient Air Quality Standards of annually averaged concentrations for all pollutants, as well as the levels in the South Coast Air Basin during 2007. The NO_2 levels in 2007 (0.01-0.032 ppm) include the state standard (0.030 ppm) and are close to the national standard (0.053 ppm). This suggests that DG penetration can increase the likelihood of air quality violations because the grid maximum annual averages are 1.6 ppb and 1.9 ppb for PW2010 and EHP respectively. The PM_{10} levels in 2007 (23-58 $\mu g/m^3$) are above the California standard (20 $\mu g/m^3$). Although the grid maximum increases of PM due to DG penetration are around 0.7 $\mu g/m^3$, DG deployment can make the situation worse. The range of 2007 $PM_{2.5}$ levels (8.7-21 $\mu g/m^3$) covers both national (15 $\mu g/m^3$) and state (12 $\mu g/m^3$) standards. Thus, the grid maximum increase of 0.7 $\mu g/m^3$, is still significant.

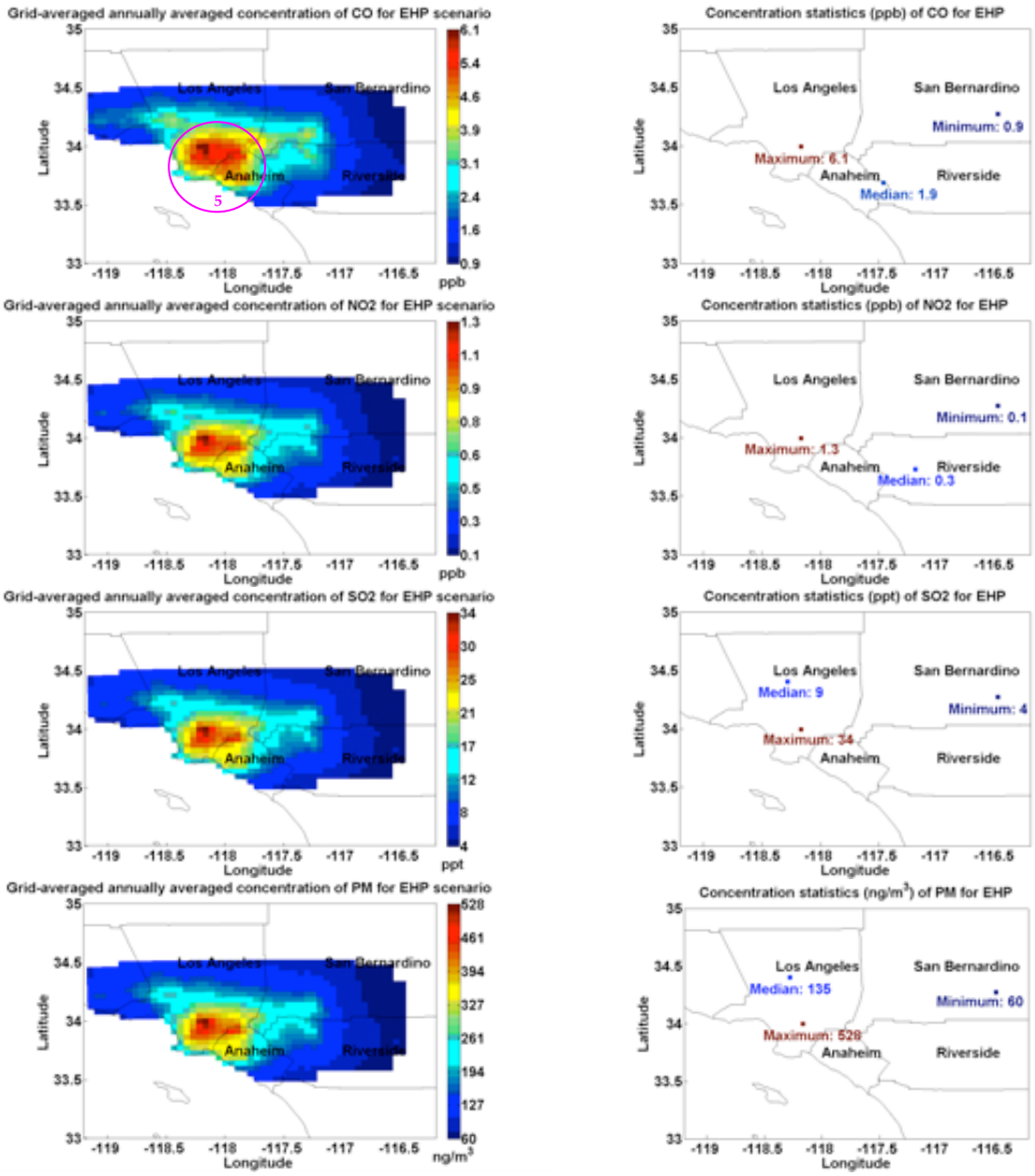

Figure 4-25. Grid averaged annually averaged concentration of all criteria pollutants for EHP scenario.

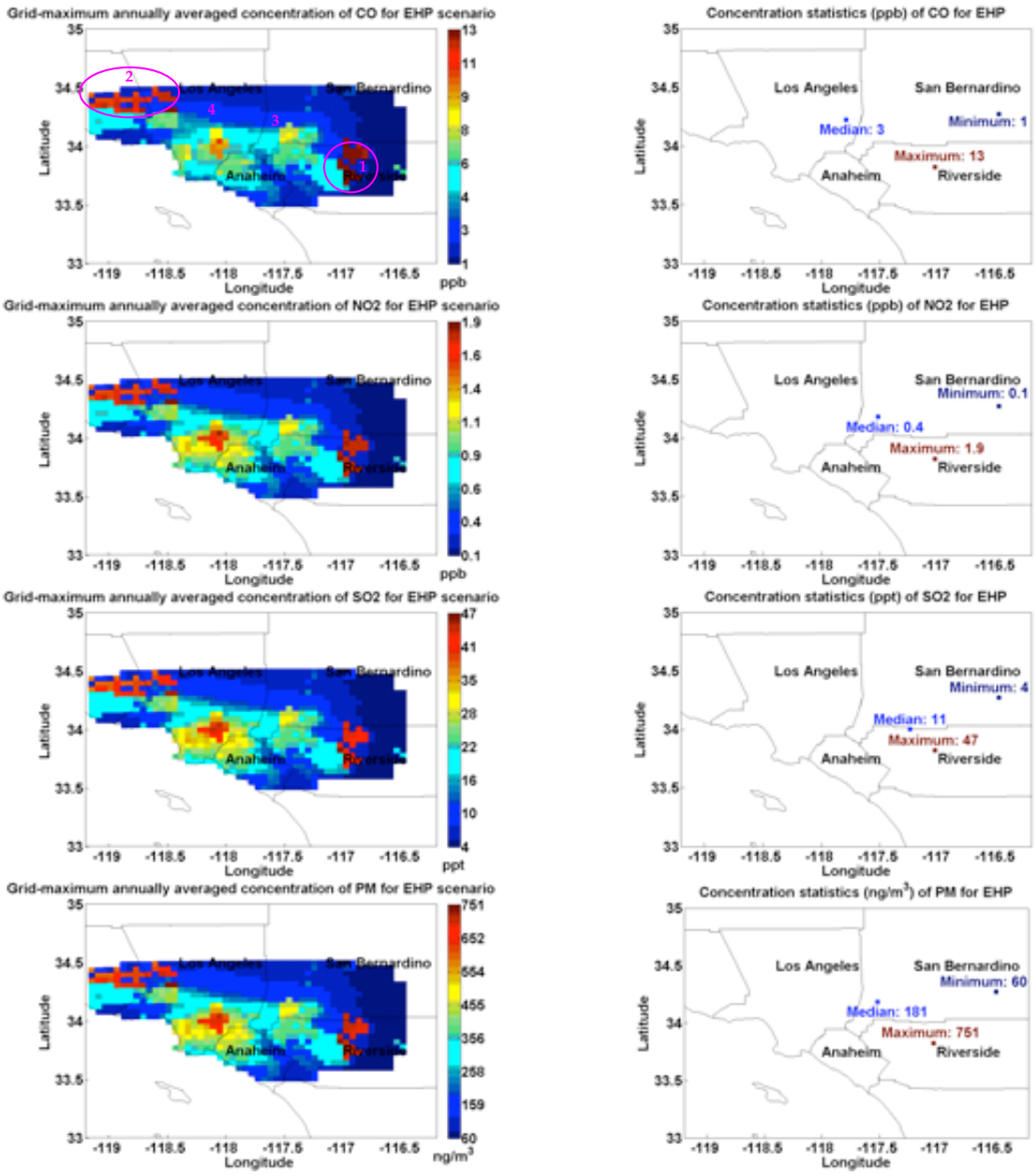

Figure 4-26. Grid maximum annually averaged concentration of all criteria pollutants for EHP scenario.

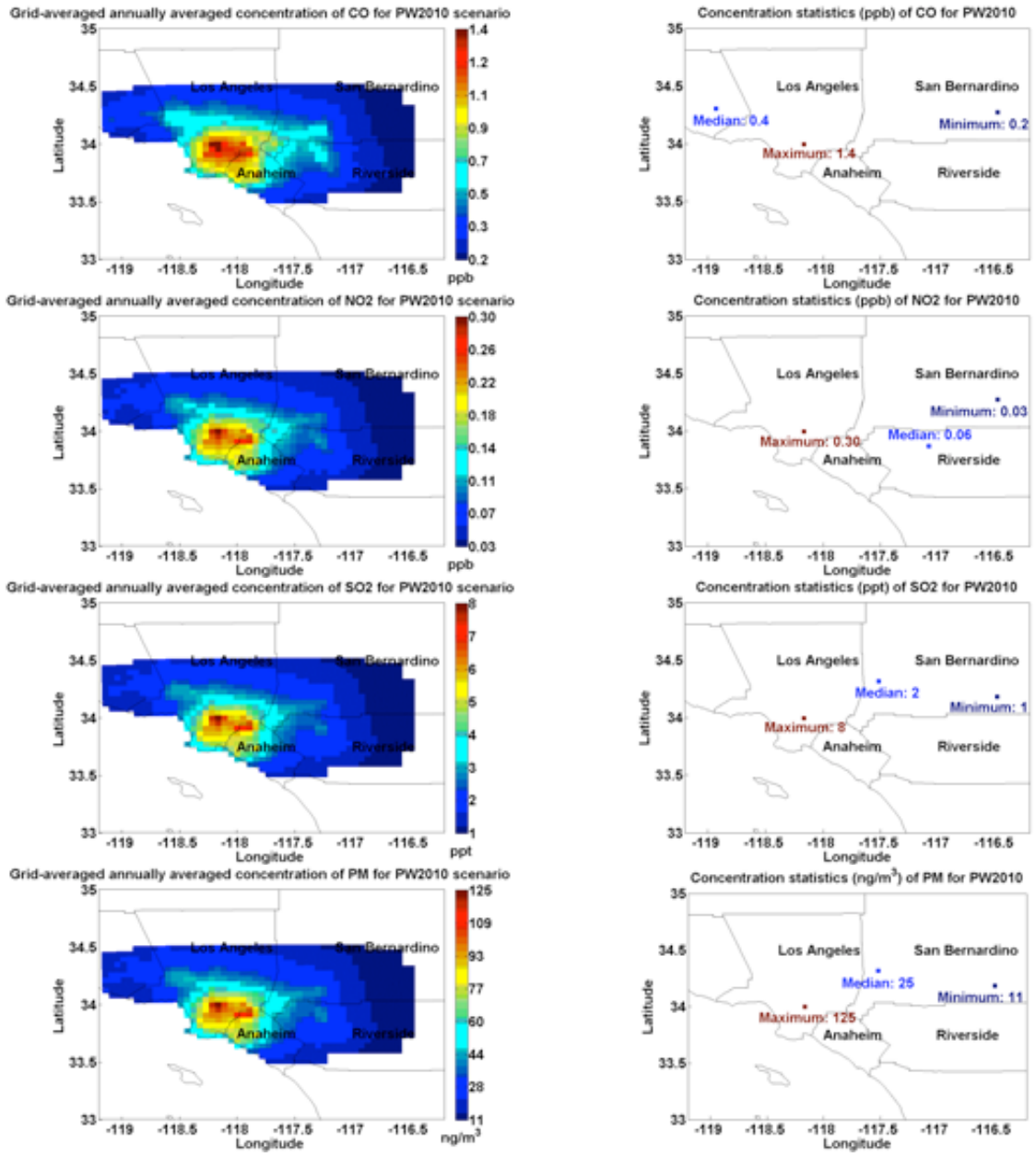

Figure 4-27. Grid averaged annually averaged concentration of all criteria pollutants for PW2010 scenario.

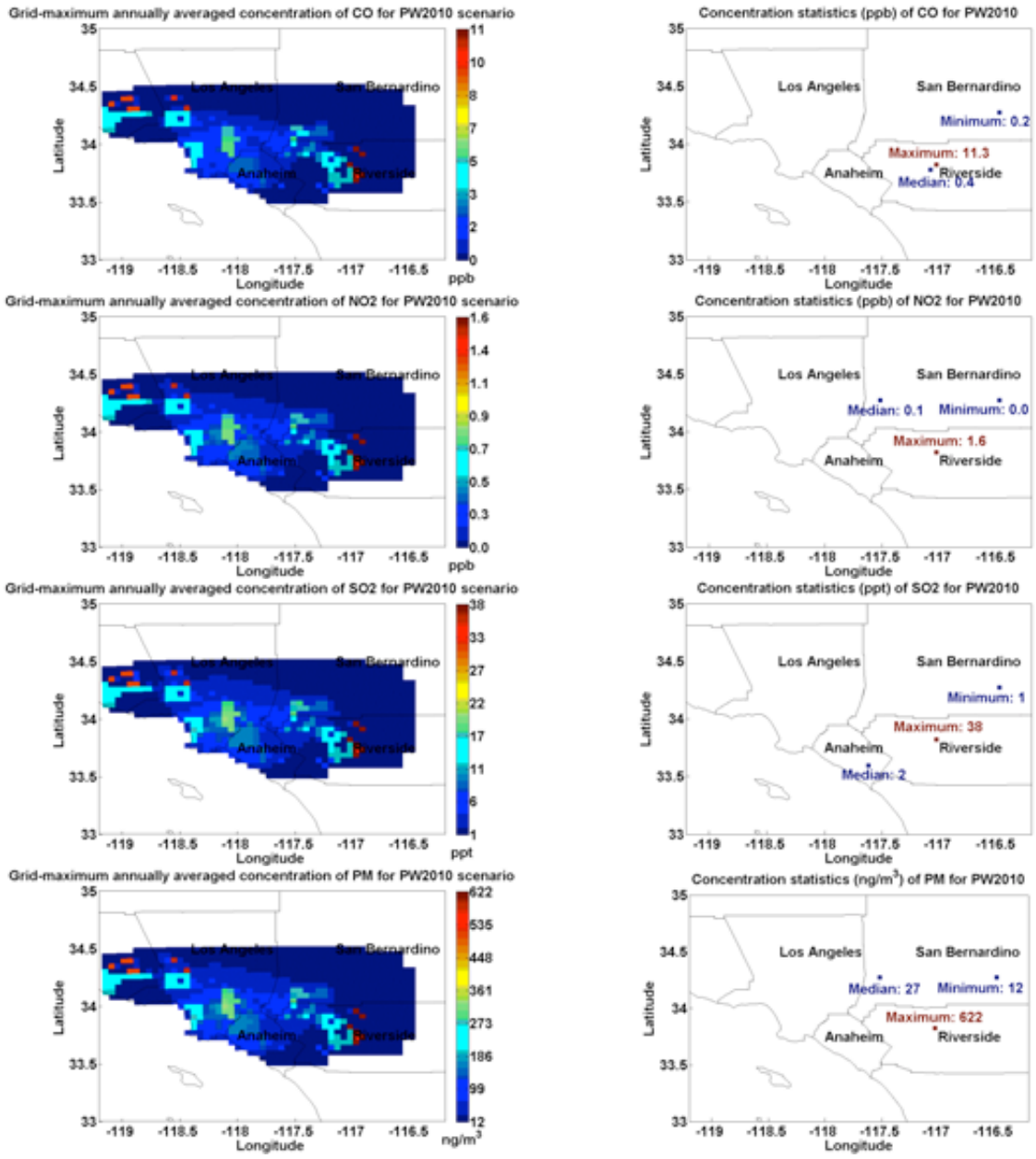

Figure 4-28. Grid maximum annually averaged concentration of all criteria pollutants for PW2010 scenario.

Table 4-11. Statistics of grid maximum annually averaged concentrations and the locations of the criteria pollutants for PW2010 and EHP scenarios and EPA standard and current level of the criteria pollutants

Pollutant	Scenario	Maximum		Median		Minimum		Standard		2007 South Coast Level [##]	
		Conc.	Nearest Met. Station	Conc.	Nearest Met. Station	Conc.	Nearest Met. Station	CAAQS[*]	NAAQS[#]	Range	Maximum Monitoring Station
CO	PW2010	11 (ppb)	Banning Airport	0.4 (ppb)	Perris	0.2 (ppb)	Palm Springs	-	-	-	-
	EHP	13 (ppb)		3 (ppb)	Pomona	1 (ppb)					
NO_2	PW2010	1.6 (ppb)		0.1 (ppb)	Fontana	0.0 (ppb)		0.030 (ppm) 57 ($\mu g/m^3$)	0.053 (ppm) 100 ($\mu g/m^3$)	0.010-0.032 (ppm)	Pomona
	EHP	1.9 (ppb)		0.4 (ppb)		0.1 (ppb)					
SO_2	PW2010	38 (ppt)		2 (ppt)	Mission Viejo	1 (ppt)		-	0.030 (ppm) 80 ($\mu g/m^3$)	0.0009-0.0028 (ppm)	Long Beach
	EHP	47 (ppt)		11 (ppt)	San Bernardino	4 (ppt)					
PM	PW2010	622 (ng/m^3)		27 (ng/m^3)	Fontana	12 (ng/m^3)		PM_{10} 20 ($\mu g/m^3$)	-	PM_{10} 23.0-68.5 ($\mu g/m^3$)	Mira Loma
	EHP	751 (ng/m^3)		181 (ng/m^3)		60 (ng/m^3)					

CAAQS[*]: California Ambient Air Quality Standards (CARB, 2010)

NAAQS[#]: National Ambient Air Quality Standards (EPA, 2010)

[##]: AQMD 2007 Air Quality Tables (AQMD, 2009b)

4.4.3. The resulting concentration of NO_x and PM

We see from Section 4.4.2 that the 2007 levels of NO_2, PM_{10} in the South Coast Air Basin were already close to or exceeded national or state air quality standards. The maximum increases due to DG deployment may not occur where the highest 2007 levels were located. Thus, adding these increases to 2007 levels provides an estimate of the maximum impact. According to the Table 4-7 and Table 4-11, DG deployment has little effect on CO and SO_2. On the other hand, DG deployment is likely to make a significant contribution to the NO_2 levels and to a smaller extent to the PM levels.

There are currently 36 active air quality monitoring stations in South Coast Air Basin according to California Air Resources Board (CARB, 2003). Figure 4-29 shows their positions. Notice that the 26 meteorological stations are located close to the monitoring stations listed in Table 4-12. At these sites, the meteorological station name will be used to represent both of them.

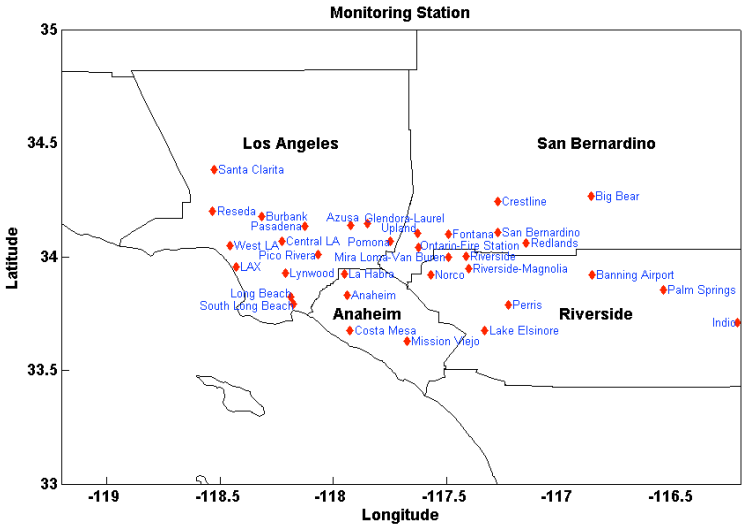

Figure 4-29. The locations of monitoring stations.

Table 4-12. Monitoring Station and 2007 levels of NO_2, PM_{10}

AQMG Area Number*	Meteorological Station Name	Monitoring Station Name##	NO_2* (ppm) Annual Average	PM_{10}*(µg/m^3) Annual Average
1	Central LA	Los Angeles-North Main Street	0.0299	33.3
2	West LA	Los Angeles - VA Hospital	0.0200	--
3	LAX	Los Angeles - LAX	0.0140	27.7
4-1	Long Beach	North Long Beach(Long Beach)	0.0207	30.2
4-2	--	South Long Beach	--	41.7
6	Reseda	Reseda	0.0186	--
7	Burbank	Burbank	0.0289	40.0
8	--	Pasadena	0.0246	--
9-1	Azusa	Azusa	0.0253	35.6
9-2	--	Glendora-Laurel	0.0227	--
10	Pomona	Pomona	0.0318	--
11	Pico Rivera	Pico Rivera #2	0.0249	--
12	Lynwood	Lynwood	0.0291	--
13	--	Santa Clarita-Placerita	0.0196	29.9
16	La Habra	La Habra	0.0219	--
17	Anaheim	Anaheim-Loara School	0.0208	31.0
18	Costa Mesa	Costa Mesa-Mesa Verde Drive	0.0132	--
19	Mission Viejo	Mission Viejo	--	23.0
22	Norco	Norco	--	39.6
23-1	Riverside	Riverside-Rubidoux	0.0181	68.5
23-2	--	Riverside-Magnolia	--	--
23	--	Mira Loma-Van Buren	0.0206	54.6
24	Perris	Perris	--	54.8
25	Lake Elsinore	Lake Elsinore-W Flint Street	0.0174	--
29	Banning Airport	Banning-Airport	0.0147	33.3
30-1	Palm Springs	Palm Springs-Fire Station	--	53.5
30-2	Indio	Indio-Jackson Street	0.0103	30.5
32	Upland	Upland	0.0276	--
33	--	Ontario-Fire Station	--	43.4
34-1	Fontana	Fontana-Arrow Highway	0.0239	54.9
34-2	San Bernardino	San Bernardino	0.0245	51.4
35	Redlands	Redlands	--	39.7
37	Crestline	Lake Gregory (Crestline)	--	27.2
38	Big Bear	Big Bear	--	--

*: AQMD historic data (AQMD, 2009b)

##: CARB, 2003

Table 4-12 also provides the 2007 levels of NO_2, PM_{10} at the available monitoring stations. The annual average of NO_2 at the Pomona station was 0.0318 ppm, which is above the state standard of 0.030 ppm. All available stations indicated that the measured annual averages of PM_{10} violated state standard (20 $\mu g/m^3$), with the highest value of 68.5 $\mu g/m^3$ at Riverside.

Figure 4-30 shows the 2007 annually averaged NO_2 concentration and locations where the concentration exceeded CA standard, and each grid is associated with the nearest monitoring station. In order to estimate the impact of DG deployment, we add the grid averaged annually averaged NO_2 concentration increases to the closest monitored value. We assume that all NO_x is converted into NO_2.

Left panels of Figure 4-31 show that the range of grid-averaged annually averaged NO_2 concentration changes from 10.3 – 31.8 ppb to 10.3 – 32.0 ppb and to 10.4 – 32.7 ppb for the PW2010 scenario and EHP scenario respectively. We also see that DG deployment has the potential of increasing the spatial extent of the region in which NO_2 annual standards are violated. Right panels of Figure 4-31 plot the changes on the map. The new areas affected by DG penetration are located near Central LA station, where the 2007 level, 29.9 ppb, was just below state standard (30 ppb). The EHP scenario results in a larger area violating the standard than PW2010 scenario, because the former has higher DG penetration.

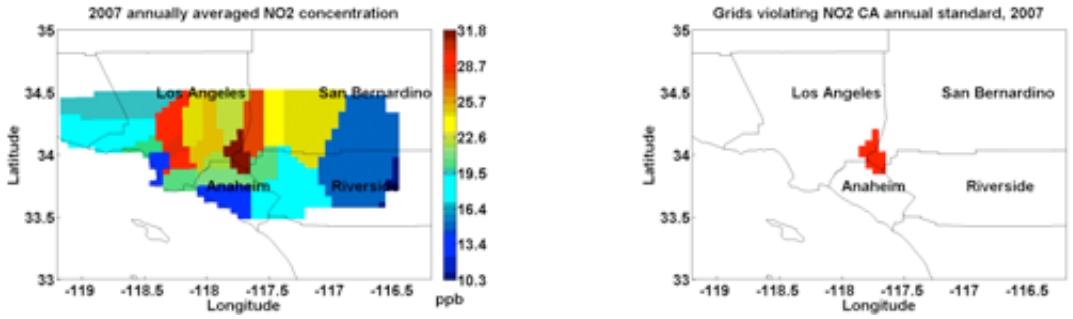

Figure 4-30. 2007 annually averaged NO_2 concentration and locations which violated CA standard.

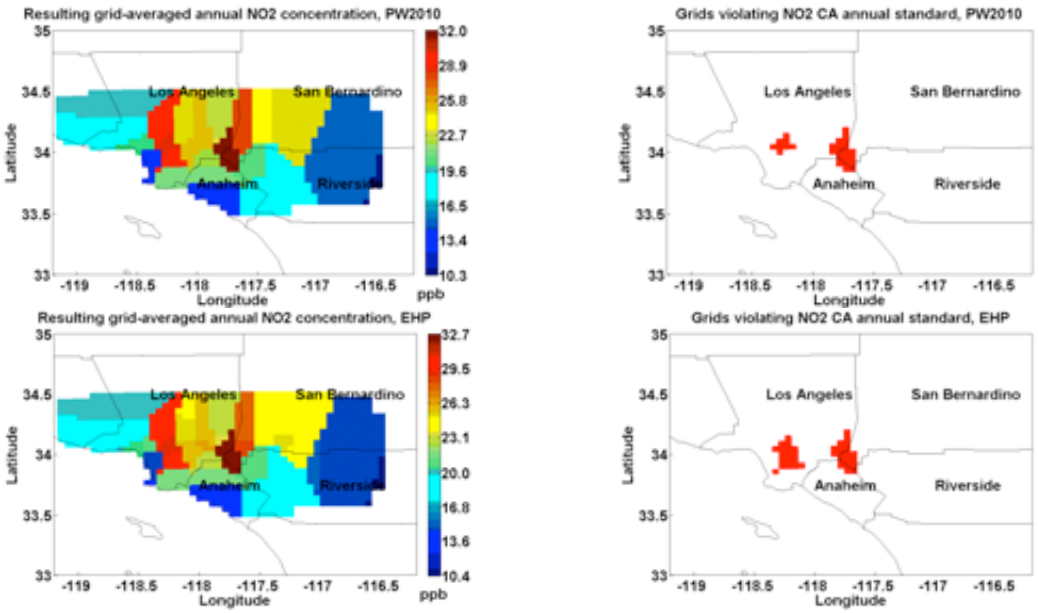

Figure 4-30. Resulting grid-averaged annually averaged NO_2 concentration for EHP and PW2010 scenarios and locations where NO_2 concentration exceeds CA standard.

5.0 The Relative Impacts of Distributed and Centralized Generation of Electricity on Local Air Quality

This section makes a direct comparison between the relative impacts of DG and central generation (CG) explicitly accounting for their differences in stack characteristics and emission rates. The primary result of thissection is a comparison of the relative impacts of CG and DG on air quality in the Southern California Air Basin (SoCAB) when the projected increase in DG is replaced by CG. We estimate the air quality impacts using AERMOD (American Meteorological Society/EPA Regulatory Model, (Cimorelli et al. 2005), which is based on current understanding of dispersion and is recommended by the USEPA for regulatory applications. We first describe our approach to comparing the relative impacts.

5.1. Comparing Relative Impacts

5.1.1. Methods

We use a simple dispersion model to provide preliminary understanding of the relative impacts of CG and DG stations on air quality. We will then refine these calculations using AERMOD (Cimorelli et al., 2005).

Assume that source with an effective stack height of h emits at a rate Q into a boundary layer with a height, z_i, and constant wind speed, U. The maximum ground-level concentration, C_{max}, is given approximately by,

$$C_{max} = \alpha \frac{Q}{h^2 U}, \tag{5.1}$$

where □ is a constant. So the relative impact of a DG station versus a CG station in terms of the maximum concentration is given by the ratio

$$\frac{C_{max}^{DG}}{C_{max}^{CG}} = \frac{Q^{DG}}{Q^{CG}} \cdot \left(\frac{h^{CG}}{h^{DG}} \right)^2. \tag{5.2}$$

So if emission rates are not taken into account, the impact of a DG is substantially higher than that of a CG because the effective stack height of a DG station is generally much smaller than that of a CG station. Note that the effective stack height of emissions from a DG can be several times the physical height because of the buoyancy of hot exhaust gases.

Once the emitted plumes are mixed through the depth of the atmospheric boundary layer, the effective height of emission becomes unimportant, and the concentration as a function of distance, r, from the source is roughly

$$C(r) = \frac{Q}{r \theta z_i U}, \tag{5.3}$$

where θ is the angular spread of the plume. We see immediately from this equation that the relative impact is now proportional only to the ratio of the emission rates of the CG and DG

stations. This implies that once the plume is mixed by atmospheric turbulence, the DG has a much smaller impact than a CG with a higher emission rate.

The long-term average concentration, $C_{av}(r)$ at a distance r from the source is approximately

$$C_{av}(r) = \frac{Q}{2\pi r z_i U} . \tag{5.4}$$

Then, the average concentration that a person is exposed to in moving about in an area that is within a distance R from the source is

$$C_{ex}(R) = \frac{\int_0^R C_{av}(r) 2\pi r dr}{\pi R^2} , \tag{5.5}$$

which for the simple model works out to be

$$C_{ex}(R) = \frac{Q}{z_i U \pi R} . \tag{5.6}$$

Thus, total emission rate plays a major role in determining exposure of a person living a moving around within a radius R from the source.

In terms of the model described here, the inhalation factor, *IF*, defined by Heath et al. (2006) becomes

$$IF = V_b \int_0^R \frac{1}{2\pi r U z_i} \rho(r) 2\pi r dr = \frac{V_b}{U z_i} \int_0^R \rho(r) dr , \tag{5.7}$$

where V_b is the breathing rate, and R is the distance used to define *IF*. If the population density $\rho(r)$ is taken to be uniform, we can write

$$\rho = \frac{P}{\pi R^2} , \tag{5.8}$$

where P is the population within a distance R from the source. With Equation (5.7), the inhalation factor becomes

$$IF = \frac{V_b}{z_i U} \frac{P}{\pi R} . \tag{5.9}$$

This simple model suggests that the *IF* is primarily a function of the meteorology, and the region R used to define the factor. If we take z_i=500 *m*, U= 5 *m/s*, V_b= 12 m^3/day, and R=100 *km*, we obtain,

$$IF \approx 2 \times 10^{-7} P , \tag{5.10}$$

where P is in millions. The magnitude of *IF* is comparable to that presented in Table 1 of Heath et al. (2006), although it does differ in the details. The main point to be made here is that *IF* is

proportional to the population within 100 km for the source, and is a weak function of source characteristics.

In this section we compare the relative impacts of CG and DG using the measures: 1) the maximum hourly ground-level NO_x concentration, which is of regulatory significance, and 2) the annually averaged NO_x concentration as a function of distance from the source, which we see is an estimate of the pollution exposure of a person who travels within the specified distance. Comparing an individual CG to a DG is not meaningful because one does not replace the other. The more relevant comparison is one in which the projected increase in distributed power generation is replaced by central generation. This comparison is performed for the South Coast Air Basin.

The representative central generating stations used in the simulations are described next.

5.1.2. Central Generating Stations

Information on CG stations are taken from the latest EPA eGrid (EPA, 2008a), and are presented in Table 5-1. The total capacities are provided by California energy commission (CEC, 2009). The capacity factors are taken from the eGrid and the stack parameters as well as emission data are taken from the 2002 national emission inventory (NEI) of point stacks for criteria air pollutants (EPA, 2007). We selected CG stations using the following rules: 1) Stations are in the South Coast Air Basin, and are listed in both eGrid and NEI; 2) Total capacity of the CG station is larger than 50 MW; 3) Stations have NOx emissions, and the stacks release them vertically.

Table 5-1. Stack Characteristics for CGs

Generation	Total capacity (MW)	Capacity factor	NO_x emission factor (g/MWh)	h_s (m)	D_s[1] (m)	D_{se}[2] (m)	v_s (m/s)	T_s (k)
Alamitos	1970	0.0779	236	61	4.4	10.8	24.7	401
El Segundo	1020	0.1109	114	61	4.0	7.9	24.2	401
Harbor	597	0.0734	206	53	4.8	6.7	23.0	454
Haynes	1724	0.2380	61	74	7.0	17.3	13.9	386
Huntington Beach 1	507	0.1998	46	62	5.2	7.4	26.2	401
Huntington Beach 2	507	0.1998	69	62	5.2	7.4	26.2	401
Mountainview	1054	0.0153	49	40	3.0	7.5	9.9	392
Placerita	120	0.0165	437	26	3.8	6.6	23.0	412
Redondo Beach	1343	0.0372	583	61	5.1	10.4	15.2	416
Scattergood	803	0.1464	32	99	6.9	12.0	12.7	408

[1] D_s = stack diameter; [1] D_{se} =Equivalent stack diameter.

5.1.3. Impact of a single generator on local air quality

This section examines the air quality impact of a single distributed generator on local air quality. Because wind speed is an important parameter in determining the magnitudes of C_{max} as well as $C_{av}(r)$, we calculated the impacts using two sets of meteorological inputs corresponding to stations with widely differing wind speed distributions. Data corresponding to Pomona and Fontana meteorological stations for 2007 were taken from the AQMD archive

(AQMD, 2009a). These two sets of meteorological data represent low and high wind speed conditions. The maximum, the 95th percentile and the median wind speeds at Pomona meteorological stations are 4.4 m/s, 2.9 m/s and 0.6 m/s respectively, while those at the Fontana meteorological stations are 15 m/s, 6.8 m/s and 1.9 m/s respectively.

A nominal emission factor of NOx of 32 g/MWh, the California emission standard for new generators, is used in the simulations. The receptors for these simulations are placed on arcs ranging from 1 m to 50 km from the source, and receptors on each arc are 3 degrees apart.

The behavior of ground-level concentrations associated with a DG

The ground-level concentration increases with emission rate, and decreases with increases in plume rise. An increase in wind speed has two effects: increases dilution and thus decreases ground-level concentrations, decreases plume rise and thus increases ground-level concentration. Thus, the impact of changes in wind speed, heat recovery and power output on maximum ground-level concentrations is not straightforward. Figure 5-1 illustrates the complex relationships, where the ground-level concentrations are estimated using a nominal emission factor of 32 g/MWh.

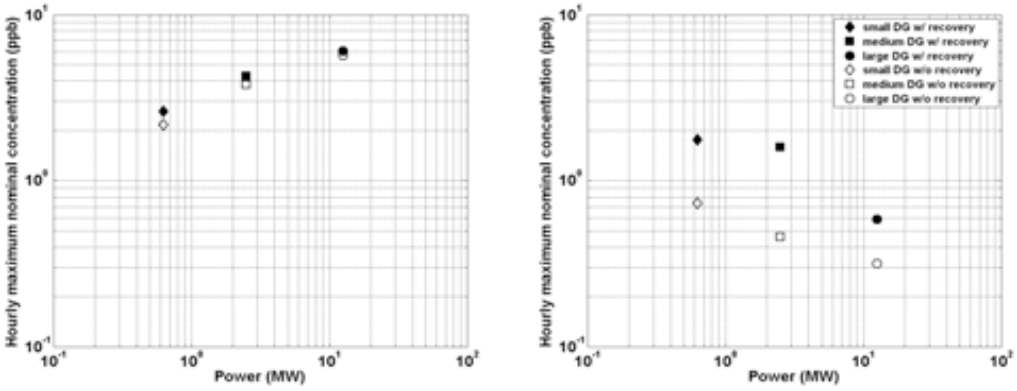

Figure 5-1. Hourly maximum NOx concentration of DGs with and without heart recovery. Left: Fontana meteorological station-High wind speed; Right: Pomona meteorological station-Low wind speed.

The left panel corresponds to the high wind speeds of the Fontana station, while the right panel corresponds to the low wind speeds of the urban Pomona station. We see that the higher wind speeds are associated with concentrations that are higher than those at the lower wind speeds, which indicates the dominance of the effect of wind speed on plume rise.

One expects that as the power increases, the associated increase in emission rate would result in higher maximum concentrations. This is what we see at the high wind speed station, Fontana, where plume rise is kept small. Heat recovery has a small effect on ground-level concentrations because plume rise does not play a role once it is suppressed by the high wind speeds.

When the wind speeds are low, plume rise plays a major role in controlling concentrations. Increased power results in increased plume buoyancy which has a greater impact than increased emissions on ground-level concentrations. Thus, maximum ground-level

concentration decreases with increase in power. Furthermore, heat recovery has a major impact on ground-level concentrations for the small and medium DGs: the maximum concentration decreases by about 50%.

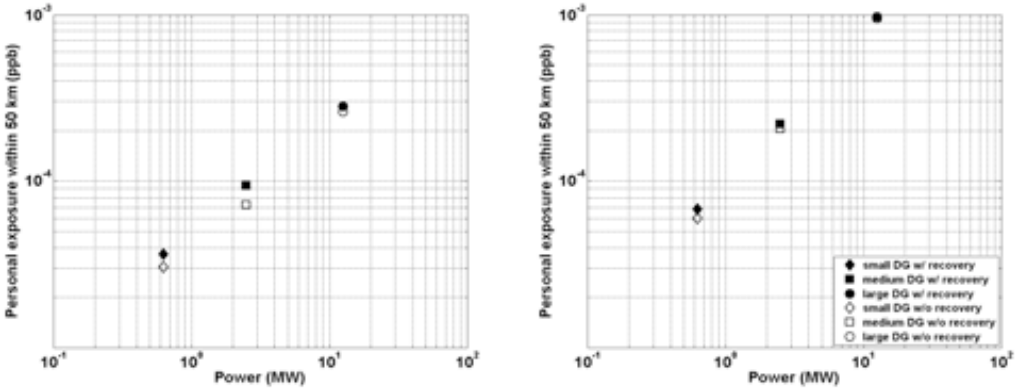

Figure 5-2. Personal exposure to NO_x due to DGs with and without heart recovery. Left: Fontana meteorological station; Right: Pomona meteorological station.

Figure 5-2 shows the personal exposure to NO_x within a radial distance of 50 km from the source. Because plume rise does not play a role here, exposure is determined primarily by dilution and emissions: exposure is lower for higher wind speeds and increases with power output. Heat recovery has a minor impact on exposure.

Comparing impacts of a single DG with that of a single CG

This section compares the air quality impact of DGs with typical CGs in the SoCAB. Figure 4 shows the hourly maximum normalized concentration of different generators as a function of power output. The concentration is normalized by the emission rate, so that it is primarily a function of meteorology and stack exit gas temperature and velocity. The hourly maximum normalized concentration of DGs is at least a factor of ten higher than that of CGs because of the lower final effective stack heights of the DGs, except for the large DG under low wind speed, which has a value comparable to most CGs.

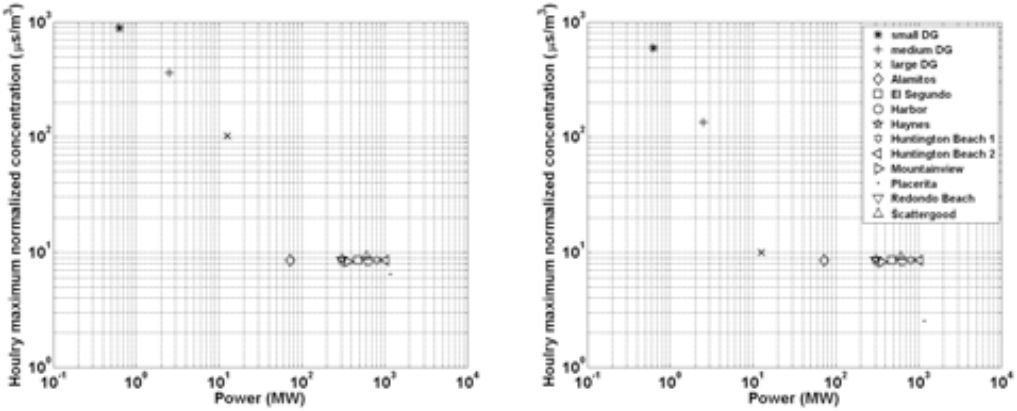

Figure 5-3. Hourly maximum dilution of different generators. Left: Fontana meteorological station; Right: Pomona meteorological station.

For the DGs with short stack heights, the normalized concentration decreases as the increase in power increases plume buoyancy and hence plume rise. Figure 5-3 shows that the maximum normalized concentrations are higher at the Fontana station where the mean wind speed is higher.

The hourly maximum normalized concentrations of CGs vary little with the distribution of wind speeds and the increase of the power because plume rise of the highly buoyant plumes are limited by the maximum mixed layer height. The maximum concentration occurs at a wind speed that is independent of the distribution of wind speeds at the two stations.

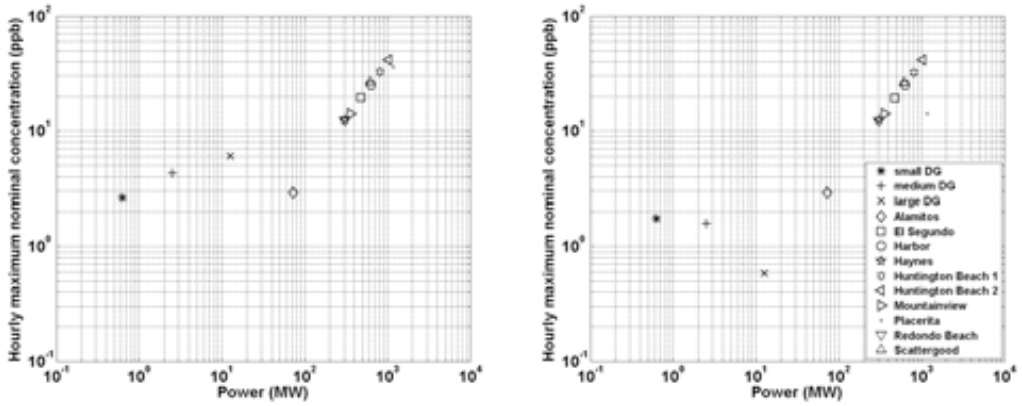

Figure 5-4. Hourly maximum nominal NO_x of different generators. Left: Fontana meteorological station; Right: Pomona meteorological station.

Although the normalized concentrations of most CGs are at least a factor of ten smaller than those of DGs, most CGs produce hourly maximum nominal NO_x concentrations that are at least a factor of two higher than those of DGs because of the much higher emissions from CGs, as is indicated by Figure 5-4. Unlike DGs, the hourly maximum nominal NO_x concentration from CGs is dominated by the emission rate because the normalized concentration, as seen earlier, is insensitive to stack parameters and is controlled by meteorology. We see from Figure 5-4 that the maximum concentration increases with power output.

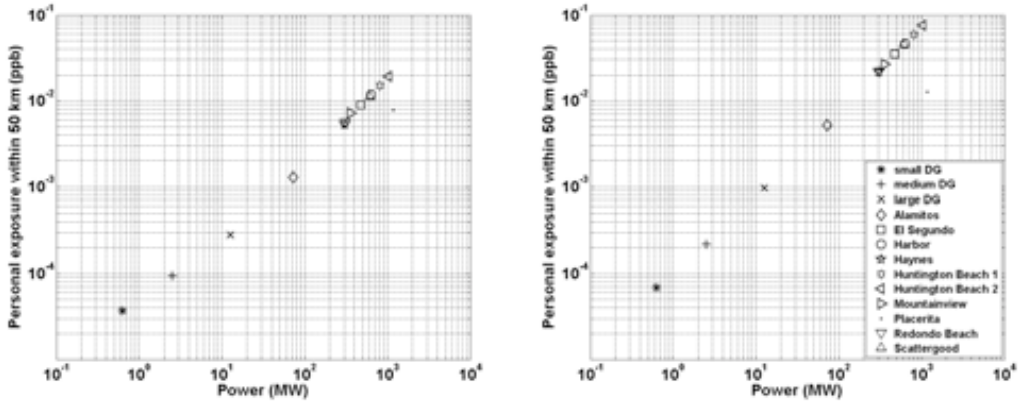

Figure 5-5. Personal exposure to NO_x due to different generators. Left: Fontana meteorological station; Right: Pomona meteorological station.

Figure 5-5 shows the personal exposure to NO_x within a radial distance of 50 km from the source as a function of generator type. Like DGs, the personal exposure due to CGs is insensitive to the effective stack height, and increases with the increase of the power and the decrease of the mean wind speed. Figure 6 indicates the personal exposure due to most CGs is at least a factor of twenty higher than that due to DGs because of much higher emissions from CGs.

5.1.4. Comparing impacts of a DG deployment scenario and existing CGs in SoCAB

This section compares the air quality impact of penetration of DGs relative to the central generating stations that supply most of the power to Southern California. The comparison is performed assuming that the responsible agency has the choice between two options: 1) Expand existing CGs to produce the extra power corresponding to the EHP scenario, 5781 MW, for the DGs (Samuelsen et al., 2005), and 2) Produce the extra power only through DGs. The air quality impact of these two scenarios are compared by assuming that both DGs and CGs meet the California NO_x emission standard for a new generation device, 32 g/MWh, which translates into a NO_x emission rate of 4.44 tons/day. The increase in power at each CG is assumed to be inversely proportional to its current capacity. This assumes that the smaller CGs have more room to expand. Other assumptions about the power distribution make little qualitative difference to the results, described next.

Figure 5-6 shows the locations of the current CGs in SoCAB listed in Table 2. Among these 10 facilities, only the Placerita facility is located in a rural area, while all the other CGs are located in urban areas. These CGs have a total power output of 9644 MW, and emit NO_x at a rate of 42.75 tons/day assuming that they operate all the time.

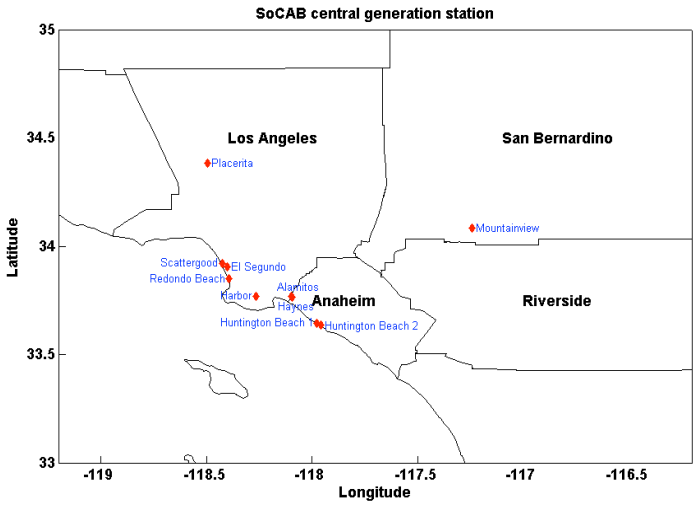

Figure 5-6. Locations of the 10 CGs in SoCAB.

The EHP (Samuelsen et al., 2005) scenario for DGs corresponds to a power of 5781 MW: 39% is produced using advanced gas turbines (small and medium DGs in Table 1), 52% is produced using conventional gas turbine (large DGs in Table 1), and 9% through fuel cells. The total NO_x emission rate from this combination of DGs is 13.76 tons/day. Figure 4-13 shows the locations of the classes of DG penetration for the EHP scenario. The large DGs are located in industrial areas, while the densities of the medium and small DGs correspond to population densities in the LA basin.

The air quality impact of the two scenarios were compared by running AERMOD using meteorological data for 2007 from 26 meteorological stations chosen from the AQMD data base (AQMD, 2009a). Figure 4-1 shows the locations of these meteorological stations. The impact of a specific CG or DG was calculated by using the meteorological data from the nearest station. The modeling domain is divided into 5 km by 5 km grids, and the grid-averaged annual concentration was calculated for each grid cell.

Hourly maximum concentrations

We see from Figure 5-7 that although the averages of hourly maximum concentrations have the same magnitude, 3 ppb for the scenario in which the EHP power demand is met by CGs and 2 ppb for the scenario in which the demand is met by DGs, the former produces a peak hourly maximum concentration of 24.5 ppb which is about four times higher than that of the latter, 6.0 ppb.

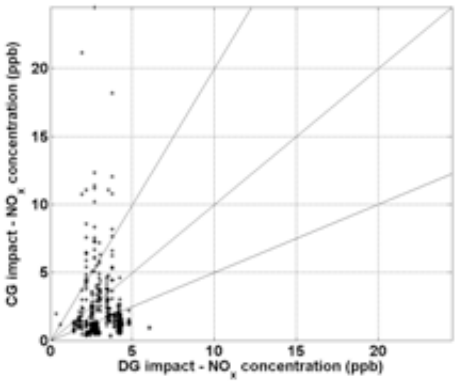

Figure 5-7. Comparison of hourly maximum concentration for the two scenarios.

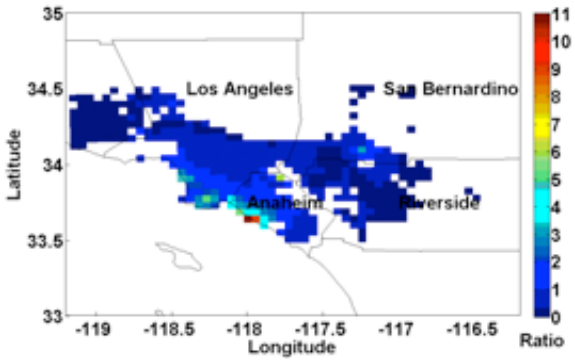

Figure 5-8. The ratio of hourly maximum concentration of the CG scenario to that of the DG scenario in the LA basin.

As expected, grids close to CG stations see larger hourly maximum concentrations when CGs rather than DGs are used to generate power as seen in Figure 5-8. However in the interior of the basin, although the grids are far away from the generators when CGs rather than DGs are adopted, the hourly maximum concentrations are still comparable to each other, because of the much higher emissions from CGs.

Annual concentrations

We see from Figure 5-9 that although the maximum concentrations have the same magnitude, the scenario in which all the EHP power demand is met by CGs results in lower grid averaged annual concentrations for most of the basin than the scenario in which the demand is met by DGs. For about half of the basin, the air quality impact of the CG scenario is a factor of 0.5 smaller than that of the DG scenario. As expected, grids close to CG stations see larger increases when CGs rather than DGs are used to generate power as seen in Figure 5-10.

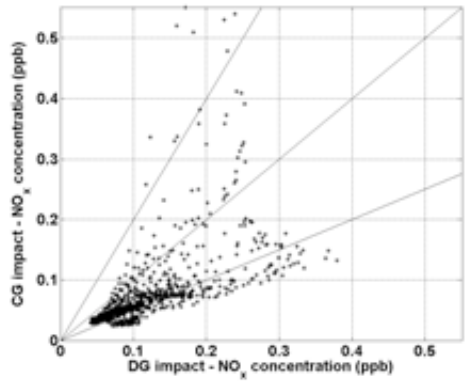

Figure 5-9. Comparison of grid-averaged annually averaged concentration for the two scenarios

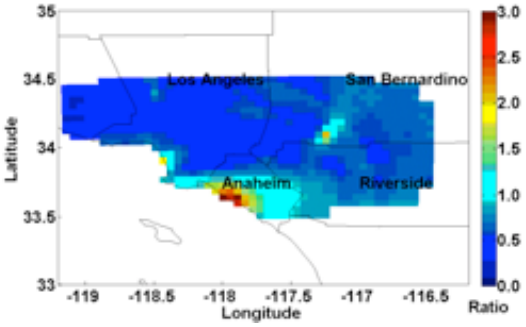

Figure 5-10. The ratio of grid-averaged concentration of the CG scenario to that of the DG scenario.

CGs have lower annually averaged impacts than DGs because they are located at the borders of the basin so that their impacts are evident only when the wind blows from the CGs into the interior of the basin. On the other hand, DGs are densely distributed in the interior of the basin to satisfy local power demands. Thus, their annually averaged impact does not depend on wind direction, and they have an opportunity to act cumulatively for all wind directions. Note that maximum concentrations do not depend of the frequency of wind direction, so that CGs still dominate maximum concentrations.

The marginal impacts of the additional power generation were then estimated by adding the computed annual impacts of these two scenarios to the 2007 NO_2 levels in the SoCAB. This assumes that all the NO_x is converted into NO_2. There are currently 36 active air quality monitoring stations in SoCAB (CARB, 2003). Figure 4-30 shows the 2007 NO_2 annual concentrations for each grid cell, and locations where the concentrations exceeded the California annual NO_2 standard. The annual concentrations are associated with the data of the nearest monitoring stations, which are obtained from the AQMD historic database (AQMD, 2009b). The 2007 annual averages of NO_2 near the Pomona meteorological station was 31.8 ppb, which is above the CA state NO_2 standard of 30 ppb.

Note that the maximum impact of both scenarios is less than 10% of the existing NO_2 levels. Future DG penetration into the SoCAB will add an annual average of 0.1 ppb to the existing

level of 20 ppb in the basin, while expanding existing CGs will add 0.05 ppb to the existing level.

Figure 5-11 plots the resulting impacts of the two scenarios. The resulting NO_2 annual averages near the Central LA meteorological station exceed the CA standard, where the 2007 level was 29.9 ppb, just below the standard. The two scenarios show similar results, except that the DG scenario has a few more grid cells that exceed the standard than the CG scenario.

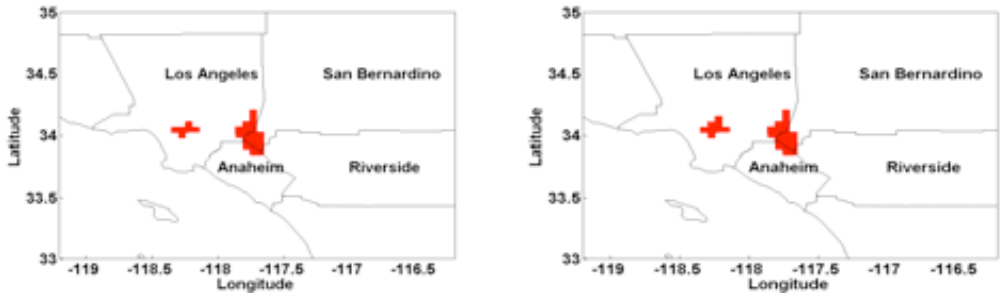

Figure 5-11. Locations where NO_2 concentration exceeds CA standard. Left panel: CG scenario; right panel: DG scenario.

5.2. Conclusions

This section compares the relative impacts of distributed and centralized generation of electricity on local air quality using AERMOD. Air quality impact is measured in terms of maximum ground-level concentration of NO_x and exposure within 50 km, which is defined as the average concentration of NO_x that a person would be exposed to while moving within a distance of 50 km from the source. We examined the air quality impact of generating the increase in power demand in the South Coast Air basin by 2010 by using distributed generators. This impact is compared to that resulting from an expansion of existing CG stations to meet the increased demand. We find that

- Although the hourly maximum NO_x dilution from CGs is at least a factor of ten higher than that of DGs, the hourly maximum NO_x nominal concentration associated with most CGs is at least a factor of two higher than those of DGs because of the much higher emissions from CGs. The maximum impact on hourly concentrations in the basin can be reduced from 24.5 ppb to 6.0 ppb if DGs rather than CGs are used to generate power. This result is important in view of the recently promulgated 1 hour NO_2 standard.
- The grid averaged annual concentrations (long-term exposure from the DG scenario) are generally higher than those from the CG scenario over most of the basin. Over half of the basin, the annually air quality impact of the DG scenario is about a factor of two larger than that of the CG scenario. Future DG penetration into the SoCAB will add an annual average of about 0.1 ppb to the existing level of about 20 ppb in the basin while expanding existing CGs will add about 0.05 ppb to the existing level. The impact of DG penetration is likely to be smaller if their emissions are offset by the decrease in boiler emissions if waste heat from the DGs is captured.

- The area near Central LA station will exceed the California NO_2 annual standard if any generating capacity is located in the area.

The secondary conclusions of this study are:

- The personal exposure due to both DGs and CGs is insensitive to the effective stack height. It increases with the increase of the power and the decrease of the mean wind speed. The personal exposure due to most individual CGs is at least a factor of twenty higher than that due to DGs because of much higher emissions from CGs.
- Waste heat recovery is likely to increase the maximum ground-level concentrations in the vicinity of a DG especially when the average winds are low. This conclusion is relevant to locating DGs in urban areas where wind speeds are typically low because of sheltering by buildings.

6.0 Conclusions and recommendations

6.1. Conclusions

This study on the interaction between DG plant characteristics and meteorology in determining ground-level concentrations results in the following major conclusions:

- The hourly averaged ground-level concentration and the grid maximum annually averaged ground-level concentrations are determined by the interaction of meteorology and the physical characteristics of the DG unit rather than only the total power output of the DG. A DG unit located in urban area emits its hot exhaust gases through relatively short stacks mounted on buildings that rarely exceed 10 m. The ground-level concentrations associated with the emissions are governed by plume rise of the buoyant exhaust, and the effects of the building wake on the emissions: these ground-level concentrations increase with wind speed because plume rise decrease and downwash effects increase with wind speed. Heat recovery from exhaust gases has the potential of magnifying these effects by decreasing plume buoyancy. Thus, ground-level concentrations do not necessarily increase with power plant capacity.
- Modeling the air quality impact of DGs requires careful considerations of a number of interacting processes such as building enhanced turbulent levels, building downwash, micrometeorology and exhaust gas characteristics, in addition to emissions.
- The maximum hourly and annually averaged concentrations from a DG unit increase with wind speeds. However, annually averaged increases of concentrations averaged over a grid cell are proportional to the total power output due to DG deployment in that grid cell.
- The maximum concentrations from the DG units considered in this study occur within hundred meters from the source.

The comparison of the relative impacts of distributed and centralized generation of electricity on local air quality yields the following major conclusions:

- Although the hourly maximum NO_x dilution from CGs is at least a factor of ten higher than that of DGs, the hourly maximum NO_x nominal concentration associated with most CGs is at least a factor of two higher than those of DGs because of the much higher emissions from CGs. The maximum impact on hourly concentrations in the basin can be reduced from 24.5 ppb to 6.0 ppb if DGs rather than CGs are used to generate power. This result is important in view of the recently promulgated 1 hour NO_2 standard.
- The grid averaged annual concentrations (long-term exposure from the DG scenario) are generally higher than those from the CG scenario over most of the basin. Over half of the basin, the annually air quality impact of the DG scenario is about a factor of two larger than that of the CG scenario. Future DG penetration into the SoCAB will add an annual average of about 0.1 ppb to the existing level of about 20 ppb in the basin while expanding existing CGs will add about 0.05 ppb to the existing level. The impact of DG penetration is likely to be smaller if their emissions are offset by the decrease in boiler emissions if waste heat from the DGs is captured.
- The area near Central LA station will exceed the California NO_2 annual standard if any generating capacity is located in the area.

The comparison of the relative impacts of distributed and centralized generation of electricity on local air quality also yields the following secondary conclusions:

- The personal exposure due to both DGs and CGs is insensitive to the effective stack height. It increases with the increase of the power and the decrease of the mean wind

speed. The personal exposure due to most individual CGs is at least a factor of twenty higher than that due to DGs because of much higher emissions from CGs.

- Waste heat recovery is likely to increase the maximum ground-level concentrations in the vicinity of a DG especially when the average winds are low. This conclusion is relevant to locating DGs in urban areas where wind speeds are typically low because of sheltering by buildings.

The EHP and PW2010 scenario studies yield the following hourly and annual concentrations of four primary criteria pollutants.

- After DGs are deployed, the maximum hourly averaged increase of CO is 117 ppb for both EHP and PW2010 scenarios occurring near Riverside. Those of NO_x, SO_2 and PM are 19 ppb, 0.5 ppb, and 8 $\mu g/m^3$ respectively for both scenarios occurring near Fontana.
- After DGs are deployed, the highest grid maximum annually averaged increases of CO, NO_x, SO_2 and PM are 13 ppb, 1.9 ppb, 47 ppt, and 0.7 $\mu g/m^3$ respectively for EHP scenario occurring close to Banning, and are 11 ppb, 1.6 ppb, 38 ppt and 0.6 $\mu g/m^3$ respectively for PW2010 scenario occurring close to Banning.
- After DGs are deployed, the maximum grid-averaged annually averaged increases of CO, NO_x, SO_2 and PM for both scenarios occur near Lynnwood where the highest increase of power is met by DG, and they are 6.1 ppb, 1.3 ppb, 34 ppt, and 0.5 $\mu g/m^3$ respectively for EHP scenario and 1.4 ppb, 0.3 ppb, 8 ppt and 0.1 $\mu g/m^3$ respectively for PW2010 scenario.
- The annual exposure level can be represented by grid averaged annual averages of pollutants. The highest resulting grid-averaged annual averages of NO_2 are 32.7 ppb for EHP and 32.0 ppb for PW2010 occurring near Pomona, where the 2007 level was 31.8 ppb. Areas near Central LA are above California annual NO_2 standard after DG being deployed, which were under the standard in 2007. The impacts of DG on PM_{10} are negligible because the grid maximum increases are much smaller than 2007 levels.

6.2. Recommendations

- The near field impact of a DG unit is governed by the interaction of plume rise with the flow fields induced by the building housing the generator as well by buildings in the vicinity of the DG. A recent paper by Olesen *et al*. (2009) indicates that current regulatory models perform poorly in estimating building effects. As far as we know, none of the models deal with the effects of multiple buildings on plume rise and dispersion. We recommend that adequate models be developed for such situations because of the regulatory concern with risks posed by emissions of toxics in urban areas.
- We recommend that future modeling improvements address concentrations at scales ranging from scales of few meters to hundreds of kilometers by combining large scale grid models with short range dispersion models, such as AERMOD. Although progress has been made in this area (Stein *et al*. 2007; Isakov *et al*. 2007), there are still unresolved issues related to combining concentrations and the associated chemistry at vastly different scales.

- The near source air quality impact of DG estimated in this study does not account for the replacing of boilers by CHP. We recommend that future work consider the impact of this replacement.

7.0 References

Allison, J. E. and Lents, J., (2002) Encouraging distributed generation of power that improves air quality: can we have our cake and eat it too? Energy Policy. 30(9):737-752.

Anderson, J.R., E.E. Hardy, J.T. Roach, and R.E. Witmer, 1976, A Land Use and Land Cover Classification System for Use with Remote Sensor Data, .S. Geological Survey Professional Paper 964 (ftp://nmdpow9.er.usgs.gov/public/lulcpp964).

AQMD, (2009a) 26 sites with AERMOD-ready meteorological data. South Coast Air Quality Management District, Diamond Bar, CA <http://www.aqmd.gov/smog/metdata/AERMOD.html>.

AQMD, (2009b) Historical data by year – 2007 Air quality data tables. South Coast Air Quality Management District, Diamond Bar, CA (http://www.aqmd.gov/smog/AQSCR2007/aq07card.pdf).

Briggs, G. A., (1875) Plume rise predictions. Lectures on Air Pollution and Environmental Impact Analysis. Haugen, D. A., American Meteorological Society, 59-111.

Briggs, G. A. (ed) (1984) Plume Rise and Buoyancy Effects. D., U. S. Dept. of Energy, 327-366.

Brode, R. W. (2002) Implementation and Evaluation of PRIME in AERMOD. The 12th Joint Conference on Applications of Air Pollution Meteorology with A&WMA, Norfolk, VA.

CARB, (2003) Quality assurance air monitoring site information. California Environmental Protection Agency, Air Resources Board, Sacramento, CA (http://www.arb.ca.gov/qaweb/sitelist_create.php).

CARB, (2010) California Ambient Air Quality Standards. California Environmental Protection Agency, Air Resources Board, Sacramento, CA (http://www.arb.ca.gov/research/aaqs/aaqs2.pdf)

Carreras, M., M. Medrano, G.S. Samuelsen, J. Brouwer, M. Rodriguez, and D. Dabdub, 2004, Urban air quality impacts of distributed generation, Proceedings of ASME Turbo Expo, 14-17 June, Vienna, Austria.

CEC, (2006) California distributed energy resources guide. California Energy Commission, Sacramento, CA (http://www.energy.ca.gov/distgen/index.html).

CEC, (2009) Database of California power plants (Excel spreadsheet of plants greater than 0.1 megawatt). California Energy Commission, Sacramento, CA (http://energyalmanac.ca.gov/powerplants/POWER_PLANTS.XLS).

Cimorelli A.J., Perry S.G., Venkatram A., Weil J.C., Paine R.J., Wilson R.J., Lee R.F. and Peters W.D. (1998), AERMOD –-Description of Model Formulation (Version 98314 (AERMOD and AERMET) and 98022 (AERMAP). USEPA, RTP, NC 27711, 113 pages.

Cimorelli, A. J., Perry, S. G., Venkatram, A., Weil, J. C., Paine, R., Wilson, R. B., Lee, R. F., Peters, W. D. and Brode, R. W. (2005) AERMOD: A Dispersion Model for Industrial Source Applications. Part I: General Model Formulation and Boundary Layer Characterization. Journal of Applied Meteorology. 44(5):682-693.

Cimorelli, A. J., Perry, S. G., Venkatram, A., Weil, J. C., Paine, R. J., Wilson, R. B., Lee, R. F., Peters, W. D., Brode, R. W. and Paumier, J. O. (2004) Aermod: Description of Model Formulation. U.S. Environmental Protection Agency Office of Air Quality Planning and Standards Emissions Monitoring and Analysis Division Research Triangle Park, North Carolina.

EPA, 2007. Criteria air pollutants inventory – Final 2002 NEI Version 3. US Environmental Protection Agency, Washington, DC (ftp://ftp.epa.gov/EmisInventory/2002finalnei/2002_final_v3_2007_summaries/point/allneicap_annual_11302007.zip) .

EPA, (2008) The emission and generation resource integrated database (eGrid2007 Version 1.1). US Environmental Protection Agency, Washington, DC (http://www.epa.gov/cleanenergy/documents/egridzips/eGRID2007_Version1-1.zip).

EPA, (2010) National Ambient Air Quality Standards. US Environmental Protection Agency, Washington, DC (http://www.epa.gov/air/criteria.html).

Heath, G.A., A.S. Hoats, and W.W. Nazaroff, 2003, Air pollutant exposure associated with distributed electricity generation, project report for California Air Resources Board, Contract No. 01-341.

Heath, G. A., Granvold, P. W., Hoats, A. S. and W Nazaroff, W. (2006) Intake fraction assessment of the air pollutant exposure implications of a shift toward distributed electricity generation. Atmospheric Environment. 40(37):7164-7177.

Heath, G. A. and W. W. Nazaroff, (2007) Intake-to-delivered-energy ratios for central station and distributed electricity generation in California. Atmospheric Environment. 41(39):9159-9172.

Iannucci, J., Horgan, S., Eyer, J. and Cibulka, L. (2000) AIr pollution emission impacts associated with economic market potential of distributed generation in California. California Air Resources Board Research Division. Contract NO. 97-326

Isakov, V., Venkatram, A., Touma, J. S., Koracin, D. and Otte, T. L. (2007) Evaluating the use of outputs from comprehensive meteorological models in air quality modeling applications. Atmospheric Environment. 41(8):1689-1705.

Jing, Q., Pankratz, D., Princevac, M. and Venkatram, A. (2009) Modeling Dispersion of Buoyant Releases in an Urban Area. 11th Conference on Atmospheric Chemistry in the 89th American Meteorological Society Annual Meeting, Phoenix, AZ.

Jing, Q., Venkatram, A., Princevac, M., Pankratz, D. and Qian, W., (2010) Modeling dispersion of buoyant emissions from a low level source in an urban area. 16th Conference on Air Pollution Meteorology in the 90th American Meteorological Society Annual Meeting, Atlanta, GA.

Medrano, M., Brouwer, J., Samuelsen, G. S., Carreras, M. and Dabdub, D. (2003) Urban Air Quality Impacts of Distributed Generation. Proceedings of ASME Turbo Expo 2003, Atlanta, Georgia, USA.

Olesen, H. R., and R. Berkowicz, and P. Løfstrøm, 2007, OML: Review of model formulation. NERI Technical Report No. 609.

Perry, S. G., Cimorelli, A. J., Paine, R. J., Brode, R. W., Weil, J. C., Venkatram, A., Wilson, R. B., Lee, R. F. and Peters, W. D. (2005) AERMOD: A Dispersion Model for Industrial Source Applications. Part II: Model Performance against 17 Field Study Databases. Journal of Applied Meteorology. 44(5):694-708.

Rodriguez, M. A., Carreras-Sospedra, M., Medrano, M., Brouwer, J., Samuelsen, G. S. and Dabdub, D. (2006) Air quality impacts of distributed power generation in the South Coast Air Basin of California 1: Scenario development and modeling analysis. Atmospheric Environment. 40(28):5508-5521.

Rawson, M. (2004) Distributed Generation Costs and Benefits Issue Paper. Public Interest Energy Research, California Energy Commission. 500-04-048

Samuelsen, S., D. Dabdub, J. Brouwer, M. Medrano, M. Rodriguez, and M. Carreras-Sosedra. 2005. Air quality impacts of distributed generation. California Energy Commission, PIER Energy-Related Environmental Research. CEC-500-2005-069-F.

Schulman, L. L. and Scire, J. S. (1980): Development of an air quality dispersion model for aluminium reduction plants. Environmental Research and Technology, Inc. Document P-7304 A.

Stein, A. F., Isakov, V., Godowitch, J. and Draxler, R. R. (2007) A hybrid modeling approach to resolve pollutant concentrations in an urban area. Atmospheric Environment. 41(40):9410-9426.

Tomashefsky, S. and Marks, M. (2002) Distributed Generation Strategic Plan. California Energy Commission. P700-02-002

U.S. Census Bureau, 2000, Unites States Census 2000, Summary File 1 (SF 1) & Summary File 3 (SF 3).

U.S. Geological Survey, 1990, USGeoData 1:250,000 and 1:100,000 Scale Land Use and Land Cover and Associated Maps Digital Data (Available from ftp://nmdpow9.er.usgs.gov/public/lulcguide)

Venkatram, A., Brode, R., Cimorelli, A., Lee, R., Paine, R., Perry, S., Peters, W., Weil, J. and Wilson, R. (2001) A complex terrain dispersion model for regulatory applications. Atmospheric Environment. 35(24):4211-4221.

Venkatram, Akula, (2008) Improvement of short-range dispersion models to estimate air quality impact of power plants in urban environments. California Energy Commission, PIER Energy-Related Environmental Research Program. CEC-500-2007-096.

8.0 Glossary

^{o}C	Celsius degree
AAC	Annually averaged and normalized concentration of DG units
AAC_Grid	Annually averaged nominal concentration of the 5km by 5km grid
AERMET	AERMOD's meteorology processor
AERMOD	A steady-state plume model
A_i	Area of land use category *i* over the whole domain
As_i	Average area for a stack of a LU category *i*
$Agrid_i$	Area of LU category *i* in the grid

AQMD	South Coast Air Quality Management District
CA	California
CACM	Caltech Atmospheric Chemical Mechanism
CAAQS	California Ambient Air Quality Standards
CARB	California Air Resources Board
CEC	California Energy Commission
CG	Central generation
CHP	Combined heat and power
C_{max}	Maximum ground-level concentration
CO	Carbon monoxide
C_p	Specific heat of the exhaust gases
$C(x,0)$	Ground-level concentration along the plume centerline
$C_{ex}(r)$	Average concentration that a person is exposed to in moving about in an area that is within a distance r from the source
$C_{av}(r)$	Long-term average concentration at a distance r from the source
DG	Distributed generation
EHP	Extra high penetration
EPA	Environmental Protection Agency
F_B	The buoyancy parameter
e_f	Emission factor
F_M	Momentum parameter
g	Acceleration due to gravity
g/MWh	grams per megawatt per hour
g/s	grams per second
GIRAS	Geographic Information Retrieval Analysis System
GIS	Geographical Information System
h_0	Height of the building
h_b	Effective stack height
h_{eff}	Effective stack height
h_s	Physical stack height
IF	Inhalation factor
K	Kelvin
km	kilometers
kg/day	kilograms per day
kg/s	kilograms per second
KW	Kilowatts
L	Monin-Obukhov length
LU	Land use

LULC	Land use and land cover
m	meter
mg/m^3	milligram per cubic meter
m/s	meters per second
MW	Megawatts
NAAQS	National Ambient Air Quality Standards
ng/m^3	nanograms per cubic meter
NO	Nitrogen oxide
NO_2	Nitrogen dioxide
NO_x	Nitrogen oxides
NWS	National Weather Service
OLM	Ozone limiting method
P_o	Output power
P	Population
PM	Particulate matter
$PM_{2.5}$	Particulate matter (less than 2.5 microns)
PM_{10}	Particulate matter (less than 10 microns)
ppb	parts per billion
ppm	parts per million
ppt	parts per trillion
PVMRM	Plume volume molar ratio Method
PW2010	Population weighted 2010
Q	Emission rate
Q_0	Surface kinematic heat flux
Q-Q	Quantile-quantile
r	Radial distance from the source
r_p	Radius of the plume
r_0	Initial radius of the plume
r_{0y}	horizontal radius of the plume
r_{0z}	Vertical radius of the plume
r_b	Ratio of h_b to h_0, is used to compute the,
R_i	Adoption rate of land use category i
r_s	Stack radius
SoCAB	South Coast Air Basin
SO_2	Sulfur dioxide
SO_3	Sulfur trioxide
SO_x	Sulfur oxides
t	Travel time, x/U

T_0	Surface temperature
T_a	Ambient temperature
tons/day	Tons per day
T_s	Exit gas temperature
u_*	Surface friction velocity
U	Mean wind speed
UCI	University of California at Irvin
UCR	University of California at Riverside
u_f	Free convection velocity scale
u_p	Wind speed at h_s
USGS	United States Geological Survey
UTM	Universal Transverse Mercator
VOC	Volatile organic compound
V_b	Breathing rate
v_s	Exit gas velocity
w	Vertical velocity of the rising plume
W/m^2	Watts per square meter
w_*	Convective velocity scale
x_f	The distance to plume stabilization
z	Plume rise
z_0	Roughness length
z_b	Plume rise at a distance of $2h_0$ downwind of the building
z_i	Mixed layer height
z_r	Height at which U is measured
□	Constant for maximum concentration
□	Entrainment parameter
□h	Plume rise associated with the buoyancy and momentum of the exhaust gases.
□	Angular spread of the plume
□	Overall efficiency of a power plant with heat recovery
□$_h$	Efficiency of heat recovery from the exhaust gases
□$_t$	Thermal efficiency
$\mu g/m^3$	Micrograms per cubic meter
$\mu s/m^3$	Microseconds per cubic meter
□$_e$	Density of the exhaust gases
□(r)	Population density of within a radial distance of r
σ_v	Standard deviations of the horizontal velocity fluctuations
σ_w	Standard deviations of the vertical velocity fluctuations

σ_{wt}	Turbulent plume spreads in the vertical directions
σ_{y}	Plume spreads in the horizontal direction
σ_{yp}	Plume contributions to the horizontal plume spreads
σ_{yt}	Turbulent plume spreads in the horizontal directions
σ_{z}	Plume spreads in the vertical directions
σ_{zp}	Plume contributions to the vertical plume spreads